MUSC Health
Medical University of South Carolina

Storm Eye Institute
Ophthalmology
167 Ashley Avenue, MSC 611
Charleston, SC 29425
Office 843-792-2020
Fax 843-792-1166
MUSChealth.org/eyes

Livia Hu, MS
Managing Editor, IJMS

RE: ijms-3802232-R2

September 3, 2025

Dear Ms. Hu,

Please see the enclosed resubmission of our manuscript "Evaluation of sex differences in laser-induced choroidal neovascularization: roles of estrogen and innate immunity in age-dependent sexual dimorphism." This is a second submission and is based on a few Editorial requests and Reviewer feedback requesting extensive statistical analyses.

The specific analyses requested by the Reviewer are not standard practice in the L-CNV model, but rather are more appropriate for clinical data. In the rebuttal, we reference the literature extensively to ensure that our data analysis practices are appropriate for the model and scientifically rigorous.

However, some of the Reviewer's points are well-taken, for example that protocols for qualitative analyses and exclusion criteria should be better-defined. We have now provided this information. The Reviewer also asked that we report numbers of excluded outliers for each exclusion criterion. In our original analyses of CNV phenotypic data, we did not record the reasons for which outliers were excluded. We thus re-analyzed these datasets in their entirety such that this information could be provided.

Cumulatively, we have added the following to the manuscript:

- Figures S1-S3: Representative images and descriptions for image quantification and exclusion criteria for fluorescein angiography (S1), OCT (S2), and flat mount (S3)
- Figure S4: Batch analysis to demonstrate consistency between independent repetitions
- Supplementary Tables 1-3: Experimental numbers for all L-CNV phenotypic experiments, including number of animals, number of lesions, and number of outliers
- Figures 1-3 and S5: OCT and flat mount data are now presented as individual value plots
- Raw data uploaded onto Harvard Dataverse such that all analyses can be reviewed if desired

Together, this has provided valuable protocol information for model standardization and significantly improved the manuscript's scientific rigor. We thank the Reviewer for their unique perspective.

We confirm that the manuscript is not under consideration by any other journal, in part or in full. All authors have read the revised manuscript and agree with its revisions and resubmission to IJMS. All authors have chosen to participate in the MDPI Open Review Process, and for reviewer and editorial correspondence to be published with the manuscript.

Sincerely,

Elizabeth Pearsall, PhD
Assistant Professor of Ophthalmology
843-792-5469
pearsale@musc.edu
167 Ashley Ave HA611 Charleston SC 29425

RESPONSE TO EDITORIAL COMMENTS AND REQUESTS

(I) Ensure all references are relevant to the content of the manuscript.

We apologize for overlooking this important point in the first resubmission. We have now removed the following references, with prior references numbers indicated:

14. Liu et al. 2017
19. Kato et al 2005
20. Kim et al. 2010
21. Holenkam et al. 2005
22. Carceres-del-carpio et al. 2016

We hope that we have now addressed this important point. However, should we have overlooked any other unnecessary references, please specify the references and/or topics that require further consideration, and we will be pleased to make these changes immediately.

(II) Highlight any revisions to the manuscript, so editors and reviewers can see any changes made.

Changes made to the first revision remain highlighted in red. Changes to the second revision are now highlighted in blue. The revised manuscript had to be submitted as an unformatted word document, as the LaTeX-formatted article did not allow us to change the references. We sincerely apologize for the inconvenience.

(III) Provide a cover letter to respond to the reviewers' comments and explain, point by point, the details of the manuscript revisions.

We have provided this.

(IV) If the reviewer(s) recommended references, critically analyze them to ensure that their inclusion would enhance your manuscript. If you believe these references are unnecessary, you should not include them.

In the first revision, Reviewer 3 asked that we cite two papers by Maltseve et al. related to serous choroidopathy (previously references 44 and 45). This has now been removed, as has the corresponding information related to these citations, which was previously following the sentence on page xx lines xx of the revised manuscript. (sentence: Females are also more likely to progress to wet AMD and develop CNV, the most sight-threatening AMD complication, which can progress to permanent central blindness if left untreated)

(V) If you found it impossible to address certain comments in the review reports, include an explanation in your appeal.

We sincerely appreciate the Editor's recognition that some comments cannot realistically be addressed.

The Reviewer asked for extensive statistical analyses. Some of these requests were appropriate and addressing them has improved the manuscript's rigor, as outlined in the cover letter and described in detail in the point-by-point rebuttal.

However, the specific analyses, for example the statistical modeling, seem more appropriate for clinical findings and are not consistent with standard practices for the L-CNV model. In these cases, we have provided a detailed explanation and referenced well-accepted and highly cited L-CNV protocol papers reporting standard data analysis practices in the model, which are consistent with those used in the present study. In the interest of impartiality, we have ensured that none of the referenced papers include any of the present manuscript's authors. Further, we reference highly-cited L-CNV research articles from multiple investigators. Cumulatively, we reference 10 independent PIs with studies spanning multiple decades to demonstrate that these practices are well-established across groups and considered standard for the model.

RESPONSE TO REVIEWER

The Reviewer's primary comments were related to statistical analyses. The specific analyses and statistical modeling requested by the Reviewer are not standard practice in the L-CNV model, but rather seem more appropriate for clinical data.

The specific analyses requested by the Reviewer are not standard practice in the L-CNV model, but rather are more appropriate for clinical data. In the rebuttal below, we reference the literature extensively to ensure that our data analysis practices are appropriate for the model and scientifically rigorous.

However, some of the Reviewer's points are well-taken, for example that protocols for qualitative analyses and exclusion criteria should be better-defined. The Reviewer also asked that we report numbers of excluded outliers for each exclusion criterion. In our original analyses of CNV phenotypic data, we did not record the reasons for which outliers were excluded. We thus re-analyzed these datasets in their entirety such that this information could be provided.

Cumulatively, we have added the following to the manuscript:

- Figures S1-S3: Representative images and descriptions for image quantification and exclusion criteria for fluorescein angiography (S1), OCT (S2), and flat mount (S3)
- Figure S4: Batch analysis to demonstrate consistency between independent repetitions
- Supplementary Tables 1-3: Experimental numbers for all L-CNV phenotypic experiments, including number of animals, number of lesions, and number of outliers
- Figures 1-3 and S5: OCT and flat mount data are now presented as individual value plots
- Raw data uploaded onto Harvard Dataverse such that all analyses can be reviewed if desired

Together, this has provided valuable protocol information for model standardization and significantly improved the manuscript's scientific rigor. We thank the Reviewer for their unique perspective.

Major Points

Major point 1: Pre-specify the primary endpoint and hypotheses.

Response 1: There is no single primary endpoint. However, we have specified the hypotheses for each experiment as below:

- CNV on Page 15 lines 18-19 and Page 15 line 1
- IHC on Page 18 lines 4-6, and
- Real-time PCR on Page 19 lines 20-21.

Major point 2: Reanalyse all outcomes using appropriate mixed-effects/ordinal/ count models with random effects for mouse (± eye) and batch.

Response 2: As detailed below, these analyses are more appropriate for clinical studies and are not considered standard practice for the L-CNV model. Please see the below point-by-point description for each analysis.

Major point 3: Control multiplicity as specified.

Response 3: As detailed below, these analyses are more appropriate for clinical studies and are not considered standard practice for the L-CNV model. Please see the below point-by-point description for each analysis.

Major Point 4: Provide full sensitivity analyses and updated figures/tables reflecting per-animal inference.

Response 4: As detailed below, per-animal interference is not reported in the L-CNV model.

Major point 5: Supply analysis code and a de-identified dataset sufficient to reproduce results.

Response 5: All analyses were conducted using publicly available code as is described in the methods section. All raw datasets are now provided on the Harvard Dataverse (doi:10.7910/DVN/H1TCLA).

Major point 6: Provide the methods used for assumptions assessment (normality, homoscedasticity)

Response 6: These analyses are not necessary or routinely conducted for animal data. Rather, they are more appropriate for clinical studies, as they are used to compensate for the variability between patients due to risk factors that are standardized in animals (age, smoking status, diet, BMI, etc).

Major point 7: Provide sample size calculation.

Response 7: Please refer to Page 19 lines 14-16.

Full Comments

Comment 1: Lesions have been treated as independent replicates despite multiple lesions per eye/mouse and repeated imaging. The proper unit is the animal, or lesions modelled within animals using hierarchical methods.

Response 1: In some animal models of choroidal/subretinal neovascularization, for example spontaneous genetic models that develop many lesions per eye, this is correct.[1,2] However, in L-CNV, only four lesions are present per eye.

We carefully reviewed L-CNV methods papers from four independent groups describing data analysis processes, all of which considered lesions as independent replicates in angiography, OCT, and flat-mount analyses.[3-6] Further, we did an in-depth search of the literature to find any potential research articles that used the Reviewer's suggested analyses, and to the best of our ability, were unable to find any papers that reported L-CNV findings in this manner. As a cross-section, we reference research articles from five well-established investigators spanning two decades, each with > 100 citations.[7-11]

Comment 2: Longitudinal structure (days 3/5/7/±14) is analysed with separate tests rather than a repeated-measures/mixed-effects framework accounting for within-mouse correlation.

Response 2: These practices would be more appropriate for clinical studies. This is not a common practice in the L-CNV model in longitudinal analyses of either OCT[4,6] or fluorescein angiography.[4] We were also unable to locate any L-CNV articles using these analyses in the literature.

Comment 3: FA leakage grades are ordinal and clustered; require ordinal mixed-effects (or GEE) models.

Response 3: Although this is standard practice for clinical findings, these analyses are not used for the L-CNV model according to well-cited protocol papers.[4,12] In our literature search, we also were unable to find any publications using these analyses for FA leakage.

Comment 4: OCT/flat-mount areas/volumes are skewed and clustered; require log-linear LMMs or appropriate GLMMs with random effects for mouse (± eye) and batch.

Response 4: This is not standard practice for either OCT or flat-mount analyses of L-CNV according to protocol papers. In our literature search, we also were unable to find any publications using these analyses for OCT or flat-mount data from L-CNV.

Comment 5: IHC counts require negative binomial (or over-dispersed Poisson) mixed models with offsets where appropriate

Response 5: We are unable to conduct these analyses in our current dataset, and they are not considered standard practice for this application. Although these in-depth analyses are necessary in clinical samples with multiple risk-modifying variables,[13] the experimental conditions in animal data are better standardized. Further, each lesion was imaged in a single field of view and CNV lesions are uniform, so spatial distribution is not a concern.

Comment 6: qPCR must be based on independent biological experiments, analysed on ΔCt/log2FC with experiment as a random effect; technical replicates should be averaged.

Response 6: We apologize for the confusion; data presented here are the averaged technical replicates for three independent biological replicates.

Comment 7: No declared primary endpoint and no control for multiple testing across endpoints/timepoints. Define a single primary endpoint and control the family-wise error (e.g., Holm) or FDR within families of outcomes.

Response 7: There is no single primary endpoint in this basic research study, as all outcomes were considered equally important experimentally speaking. For animal experiments, in all time points/disease parameters, age-matched male and female animals were compared. For in vitro experiments, untreated macrophages were the control group. This information was provided in the original methods.

Comment 8: Post-hoc outlier removal lacks a pre-specified rule and transparency. Provide a priori criteria, report numbers removed per group/timepoint, and show sensitivity analyses with and without these data.

Response 8: This point is well-taken. We now provide the below:

- Figure S1: Angiography lesion grading and exclusion criteria
- Figure S2: OCT lesion quantification and exclusion criteria
- Figure S3: Flat mount lesion quantification and exclusion criteria
- Table S1: Angiography experimental numbers, including number of experimental animals, lesions quantified, and excluded outliers (specific criteria) for each group and time point
- Table S2: OCT experimental numbers, including number of experimental animals, lesions quantified, and excluded outliers (specific criteria) for each group and time point
- Table S3: Flat mount experimental numbers, including number of experimental animals, lesions quantified, and excluded outliers (specific criteria) for each group and time point

Comment 9: Experiments performed across batches are not modelled; include batch/day/operator as random or blocking factors. Provide clear details on randomisation of surgical/imaging order and masking of grading and exclusion decisions; if not done, acknowledge and mitigate analytically.

Response 9: We have specified that experiments were performed by a single operator and provided details as to how surgical/imaging order were randomized. Please refer to Page 15 line 1, lines 6-8, and lines 10-12. We also provide a batch analysis in Figure S4 to show that findings were consistent between independent cohorts of animals subjected to L-CNV induction and imaging analyses in separate batches. All L-CNV experiments represent two independent repetitions, and in the raw data uploaded onto the Harvard dataverse, we provide a subgroup analysis for each experiment.

Comment 10: Report diagnostics (normality, variance, over-dispersion, proportional-odds where relevant). Provide 95% CIs; report effect sizes (differences, ratios, odds ratios) with CIs.

Response 10: We carefully reviewed L-CNV methods papers from four independent groups describing data analysis processes, and these diagnostics/analyses were not performed.[3-6] We were also unable to locate any L-CNV articles using these analyses in the literature.

Comment 11: Provide an animal-level justification for the primary endpoint (Resource Equation Method)

Response 11: The Resource Equation Method was not necessary as our prior experience in the model ensured that we could be relatively confident in the anticipated standard deviation.

Comment 12: Show per-animal data (dot/violin plots), state exact n (mice) per group/timepoint in every panel, and provide CONSORT-style counts for included/excluded lesions per group.

Response 12: We carefully reviewed L-CNV methods papers from four independent groups describing data analysis processes, and none recommended reporting data in this way.[3-6] We were also unable to locate any L-CNV articles using this data presentation style. However, in the raw data, statistical outlier calculations and data ± outliers can be accessed. Please refer to Page 20 lines 8-9.

Comment 13: Distinguish clearly between biological and technical replicates.

1. Joyal JS, Sun Y, Gantner ML, Shao Z, Evans LP, Saba N, Fredrick T, Burnim S, Kim JS, Patel G, et al. Retinal lipid and glucose metabolism dictates angiogenesis through the lipid sensor Ffar1. *Nat Med*. 2016;22:439-445. doi: 10.1038/nm.4059
2. Hasegawa E, Sweigard H, Husain D, Olivares AM, Chang B, Smith KE, Birsner AE, D'Amato RJ, Michaud NA, Han Y, et al. Characterization of a spontaneous retinal neovascular mouse model. *PLoS One*. 2014;9:e106507. doi: 10.1371/journal.pone.0106507
3. Lambert V, Lecomte J, Hansen S, Blacher S, Gonzalez ML, Struman I, Sounni NE, Rozet E, de Tullio P, Foidart JM, et al. Laser-induced choroidal neovascularization model to study age-related macular degeneration in mice. *Nat Protoc*. 2013;8:2197-2211. doi: 10.1038/nprot.2013.135
4. Ragauskas S, Kielczewski E, Vance J, Kaja S, Kalesnykas G. In Vivo Multimodal Imaging and Analysis of Mouse Laser-Induced Choroidal Neovascularization Model. *J Vis Exp*. 2018. doi: 10.3791/56173
5. Gong Y, Li J, Sun Y, Fu Z, Liu CH, Evans L, Tian K, Saba N, Fredrick T, Morss P, et al. Optimization of an Image-Guided Laser-Induced Choroidal Neovascularization Model in Mice. *PLoS One*. 2015;10:e0132643. doi: 10.1371/journal.pone.0132643
6. Giani A, Thanos A, Roh MI, Connolly E, Trichonas G, Kim I, Gragoudas E, Vavvas D, Miller JW. In vivo evaluation of laser-induced choroidal neovascularization using spectral-domain optical coherence tomography. *Invest Ophthalmol Vis Sci*. 2011;52:3880-3887. doi: 10.1167/iovs.10-6266
7. Espinosa-Heidmann DG, Suner I, Hernandez EP, Frazier WD, Csaky KG, Cousins SW. Age as an independent risk factor for severity of experimental choroidal neovascularization. *Invest Ophthalmol Vis Sci*. 2002;43:1567-1573.
8. Sakurai E, Taguchi H, Anand A, Ambati BK, Gragoudas ES, Miller JW, Adamis AP, Ambati J. Targeted disruption of the CD18 or ICAM-1 gene inhibits choroidal neovascularization. *Invest Ophthalmol Vis Sci*. 2003;44:2743-2749. doi: 10.1167/iovs.02-1246
9. Qiu F, Meng T, Chen Q, Zhou K, Shao Y, Matlock G, Ma X, Wu W, Du Y, Wang X, et al. Fenofibrate-Loaded Biodegradable Nanoparticles for the Treatment of Experimental Diabetic Retinopathy and Neovascular Age-Related Macular Degeneration. *Mol Pharm*. 2019;16:1958-1970. doi: 10.1021/acs.molpharmaceut.8b01319

10. Bora PS, Hu Z, Tezel TH, Sohn JH, Kang SG, Cruz JM, Bora NS, Garen A, Kaplan HJ. Immunotherapy for choroidal neovascularization in a laser-induced mouse model simulating exudative (wet) macular degeneration. *Proc Natl Acad Sci U S A*. 2003;100:2679-2684. doi: 10.1073/pnas.0438014100
11. Shi X, Semkova I, Muther PS, Dell S, Kociok N, Joussen AM. Inhibition of TNF-alpha reduces laser-induced choroidal neovascularization. *Exp Eye Res*. 2006;83:1325-1334. doi: 10.1016/j.exer.2006.07.007
12. Hoerster R, Muether PS, Vierkotten S, Schroder S, Kirchhof B, Fauser S. In-vivo and ex-vivo characterization of laser-induced choroidal neovascularization variability in mice. *Graefes Arch Clin Exp Ophthalmol*. 2012;250:1579-1586. doi: 10.1007/s00417-012-1990-z
13. Wilson CM, Ospina OE, Townsend MK, Nguyen J, Moran Segura C, Schildkraut JM, Tworoger SS, Peres LC, Fridley BL. Challenges and Opportunities in the Statistical Analysis of Multiplex Immunofluorescence Data. *Cancers (Basel)*. 2021;13. doi: 10.3390/cancers13123031

MUSC Health
Medical University of South Carolina

Storm Eye Institute
Ophthalmology
167 Ashley Avenue, MSC 611
Charleston, SC 29425
Office 843-792-2020
Fax 843-792-1166
MUSChealth.org/eyes

Livia Hu, MS
Managing Editor, IJMS
RE: ijms-3802232-R3

October 22, 2025

Dear Ms. Hu,

Please see the enclosed third resubmission of our manuscript "Evaluation of sex differences in laser-induced choroidal neovascularization: roles of estrogen and innate immunity in age-dependent sexual dimorphism." Although the manuscript was deemed satisfactory for publication after rigorous peer review from three independent reviewers in early September, we are now in our second round of revision to address additional concerns of the Guest Editor, which are related primarily to statistical concerns.

We thank the Editorial Office for extra time to submit the revision, as it has allowed us to dedicate necessary additional effort to unresolved concerns. We have realized that they could be related in part to fundamental misunderstandings between the first and senior authors, who are basic scientists, and the Guest Editor, Dr. Georgios Panos, a vitreoretinal surgeon with a remarkable publication track record of 134 peer-reviewed articles, most of which report clinical and surgical outcomes, contributing to disease management.

We have studied the overarching themes of Dr. Panos's research, and also common approaches used for longitudinal analyses of imaging findings. We also sought additional input from our co-author Dr. Peter Tang, a vitreoretinal surgeon and physcician-scientist, who has published multiple senior-author clinical papers, including outcomes-based studies.[1-10] Further, we consulted his trainee Dr. Dimitrios C. Arhontoulis, who is a contributing author to the present study and two of Dr. Tang's clinical studies.[2,3] Together, this has allowed us to:

- Appreciate why standard data analysis practices for L-CNV, for example treating individual lesions as independent replicates, although well-accepted by basic scientists in the field, lack scientific rigor.
- Develop new analyses to treat animals as biological replicates and lesions within the same animal as technical replicates for FA, OCT, and FM. This allows us to not only improve scientific rigor of the present study, but also use the manuscript as a platform to address this important issue, hopefully educating other basic scientists in the field.
- Improve our understanding of the Editor's other statistical concerns and make better-informed responses using appropriate language and terminology to improve clarity.
- Research advanced tools available for analysis of human AMD data, for example algorithms used to detect/predict severe disease, and conduct literature searches to determine their availability for mouse data.

We also hope that our new approach will allow the editor to better understand the nature of our datasets and efforts undertaken to mitigate concerns raised. We hope that our collective responses and alterations to the manuscript will help establish the following:

- In the mouse L-CNV model, we can tightly control and mitigate most potential confounders, such as animal age, housing conditions, genetic background, diet, lack of comorbidities and identical disease etiologies. Therefore, the resulting data are reasonably simple with less variability and evenly distributed standard deviations.
- Due to the comparatively simplistic nature of L-CNV data, complex analyses used to compensate for biological variables and heterogenous disease etiology in human cohorts are in some cases not necessary,

or potentially possible, in mouse L-CNV data.

- We have attempted, in earnest, to be as responsive as possible to concerns, which are well-taken, and have undertaken a significant amount of work to do so, within the inherent limitations of our dataset. We hope that the additional analyses and information provided in the rebuttal will be helpful.

In the revised manuscript, Editor-requested changes are indicated by red font. Some excerpts are shown in blue font used to highlight content that was already present in the prior resubmission but is mentioned in the rebuttal to clarify specific points.

We hope that our new overall perspective and additional analyses will address the Editor's concerns and resolve misunderstandings between both parties. If not, we wonder if a direct conversation with the Editor (if this is permitted) could help clarify additional points that are sometimes difficult to communicate in formal written correspondence.

I confirm that the manuscript is not under consideration with any other journal, in part or in full, and that all contributing authors have read and approved the revised resubmission to *IJMS*. All authors have agreed to the transparent review process, such that all correspondence will be made public.

Sincerely,

Elizabeth Pearsall, PhD
Assistant Professor of Ophthalmology
843-792-5469
pearsale@musc.edu
167 Ashley Ave HA611 Charleston SC 29425

Cohort-based study design

Before directly addressing the Editor's comments, we would like clarify that live-animal imaging readouts are cohort-based, so each time point contains a new cohort of animals. Thus, none of the live-animal imaging studies repeatedly image the same lesions over time. This confusion was due to a clerical error in the manuscript (detailed below) for which we sincerely apologize.

Below is a schematic summarizing experimental design:

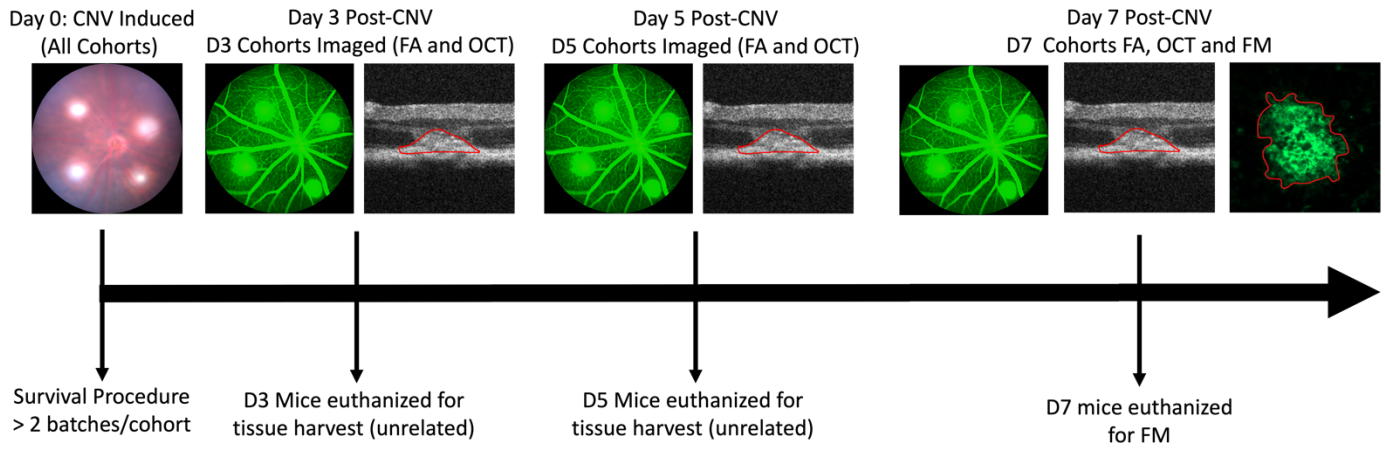

Reviewer-only Figure 1: Experimental design schematic. On Day 0, laser-induced choroidal neovascularization (CNV) was induced in at least two separate batches on separate days for each cohort. On Day 3 post-CNV, the Day 3 (D3) cohorts were imaged for fluorescein angiography (FA) and optical coherence tomography (OCT). The animals were subsequently euthanized for tissue harvest, with tissue used for an unrelated study. Similarly, on Day 5 post-CNV, D5 cohorts were imaged and subsequently euthanized for tissue harvest. On Day 7 post-CNV, D7 cohorts were imaged with OCT and FA, then subsequently euthanized for histological measurement of lesion size using choroidal flat mount (FM).

Thus, although the longitudinal modeling suggested by the Editor would be insightful, it is not possible to conduct these analyses with the current datasets. Fortunately, longitudinal analyses in the same animals are also not as important in L-CNV mice as in clinical studies, or in more complex animal models such as non-human primates. In rodent models, confounding variables are minimized by using animals with identical genetic backgrounds directly purchased from the vendor to prevent genetic drift, matching ages, identical housing conditions, identical and simplified disease etiology, and means to minimize interbatch variations. This also prevents any artifacts caused by repeated imaging at very short intervals (every two days) in a longitudinal design.

Most L-CNV studies, even those in high-impact journals, routinely report only Day 7 post-CNV, which is the most common experimental endpoint. Data reported only at this time point is thus considered sufficient to demonstrate a reported phenotype. However, in my research program, I routinely grade disease severity and conduct mechanistic analyses at three time points (Day 3, Day 5, Day 7). Inflammatory processes are more active in early-stage disease, and intriguingly, I have found that some diseases processes are biphasic, with opposite effects in early- versus mid-/late-stage disease.

In other published studies that report live animal imaging findings at multiple time points, it is common to use a cohort-based approach with different animals at each time point, as animals are frequently euthanized directly after live animal imaging is complete, such that tissues can be harvested for histological CNV quantification or mechanistic analyses. Therefore, an additional cohort of animals must be used for subsequent time points.

Source of confusion for study design and subsequent corrections/clarifications

The manuscript incorrectly stated that the study was longitudinal due to a clerical error, for which we sincerely apologize. Below is the incorrect passage, with relevant error highlighted (page 3-4):

> Lesion leakage was measured using fluorescein angiography (FA), in which the leakage of fluorescein dye from CNV lesions is assessed in blinded images using an established grading system [21]. Optical coherence tomography (OCT) was used to measure lesion size in live animals, which reflects not only the extent of vascular outgrowth, but also lesion edema [22]. Finally, choroids were flat-mounted and vessels la-belled histologically to measure the size of neovessels that comprise L-CNV lesions [23]. These distinct but interrelated parameters allowed us to determine the effects of ex-perimental variables on different aspects of L-CNV pathology, and live-animal imaging allowed longitudinal assessment of disease severity across timepoints.

We have now altered this paragraph as quoted below; for clarity we left changed text in red font.

> On Days 3, 5, and 7 post-CNV, lesion leakage was measured using fluorescein angiography (FA), in which the leakage of fluorescein dye from CNV lesions is assessed in blinded images using an established grading system [11]. On days 3, 5, and 7 post-CNV, optical coherence tomography (OCT) was used to measure lesion size in live animals, which reflects not only the extent of vascular outgrowth, but also lesion edema [12]. Choroids from animals on Day 7 post-CNV were flat-mounted and vessels labelled histologically to measure the size of neovessels that comprise L-CNV lesions [13]. These distinct but interrelated parameters allowed us to determine the effects of experimental variables on different aspects of L-CNV pathology.

We have further clarified this point in the Methods section on Page 14, section 4.7, quoted below and in the revised manuscript highlighted in red:

> The data are cohort-based and not longitudinal, with each post-CNV time point consisting of completely different mice. This was because animals subjected to live-animal imaging at early time points were euthanized for tissue harvest and subsequent mechanistic analyses for unrelated studies. Experimental numbers for each datapoint are specified in figure legends, and a full summary of statistical analyses is available in Supplementary Tables 1-4.

EDITOR FEEDBACK

Dear Authors,

Thank you for the revision and response letter. After re-examining both, the manuscript is not yet suitable for publication on statistical grounds. The analyses do not match the structure of the data, and several essentials are missing. A further, substantive revision is required. Please address the following points in full and reflect all changes in the manuscript, figures, tables, and supplements.

Comment 1: Treat the animal as the unit of inference. If retaining lesion-level data, reanalyse with mixed-effects models that account for lesions within eye and mouse; do not treat lesions as independent.

Response 1: The model standard for L-CNV is to treat each lesion as an independent replicate, partly because the lesions are surgically induced, and some investigators argue that this introduces within-animal variation that is greater than between-animal variation.

However, we agree with the Editor that this logic is flawed and that the approach lacks scientific rigor. We have thus incorporated per-animal data into all analyses and provide a direct comparison between lesion-level and animal-level data. We describe below the analytic procedures and findings for angiography, OCT, and flat-mount.

We first introduce this discrepancy in the beginning of the Results section as shown below and highlighted in red on Page 3, Section 2.1:

> We analyzed FA, OCT, and FM data at a lesion-based level, where each lesion was considered an independent replicate, which is the standard data analysis practice in the L-CNV model.
>
> However, individual lesions could also be considered technical, rather than biological replicates. Therefore, we also conduced per-animal data analyses in parallel, where all lesions in a single animal were considered technical replicates, and averaged prior to further analyses. We then considered individual animals as biological replicates, which were used to determine statistical significance. Our statistical findings were similar between approaches, but in the interest of scientific rigor and model standardization, we addressed this important point. The calculations used for animal-level analyses can be found in Materials and Methods Section 4.3 (FA), 4.4 (OCT) and 4.5 (FM).

In the methods section, we describe the calculations used to obtain per-animal data as shown below and highlighted in the revised manuscript. Below, we also provide figures and tables with side-by-side comparisons of each analytic approach.

1.1. Fluorescein Angiography

Means for lesion-level and animal-level data analyses are described in materials and methods (Page 12, Section 4.3 continued, last paragraph, highlighted in red):

> To determine the statistical significance of lesion-level data, in which lesions from all animals in each cohort were pooled and considered independent replicates, we conducted a contingency analysis (CI 95%) with each lesion grade (0, 1, 2A, 2B) considered a separate outcome, and χ^2 $p < 0.05$ considered statistically significant. To generate animal-level data, the bilateral percent of clinically significant (2B) lesions per mouse was calculated, with each individual lesion in a single mouse thus considered a technical replicate. The mean % 2B lesions/mouse was thus considered a biological replicate, and a two-tailed unpaired Student's t-test used to determine statistical significance, with $p < 0.05$ considered significant. Statistical findings (significant or non-significant) were similar between approaches (Figure S2, Table S1).

Findings from each type of analysis are shown in Supplementary Table 1:

Experimental Conditions				Experimental Findings			Experimental Numbers		
Fig Panel	**Age (wk)**	**Sex**	**Post-CNV**	**Cohort M v F χ^2 (All Lesion Grades)**	**Cohort % 2B Lesions**	**Per-Mouse % 2B**	**No. Mice**	**Lesions /Mouse**	**Cohort Lesions**
1A	8	M	3D	0.71	44.9	48.8 ± 9.1	10	7.2	83
	8	F	3D		41.8	36.2 ± 7.1	9	7.4	69
1C	8	M	5D	0.68	44.3	39.8 ± 9.2	10	6.2	67
	8	F	5D		34.7	32.6 ± 6.2	10	7.1	77
2A	8	M	7D	0.30	43.6	41.6 ± 6.7	9	6.7	59
	8	F	7D		27.9	29.9 ± 7.2	9	6.9	74
3A	26	M	3D	< 0.0001	17.1	16.1 ± 5.7	11	6.9	78
	26	F	3D		71.6	75.0 ± 7.9	11	7.3	83
3C	26	M	5D	0.01	41.2	22.3 ± 5.7	10	7.5	70
	26	F	5D		62.1	56.1 ± 5.8	10	7.1	67
4A	26	M	7D	0.005	22.4	18.0 ± 5.4	10	6.7	72
	26	F	7D		43.9	50.7 ± 10.6	10	7.5	68

Supplementary Table 1: Fluorescein Angiography (FA) experimental conditions, findings, and numbers. **Experimental Conditions: "**Fig. Panel" refers to the main-text figure panel in which data are presented. "Post-CNV" refers to the time in days (D) following CNV induction. **Experimental Findings: "**Cohort M v F χ^2" refers to the p-value from contingency testing of all lesion grades (0, 1, 2A, 2B) between M vs. F animals in each condition, with all lesions from each cohort combined and each lesion considered to be an independent variable. "Cohort %2B lesions" refers to the total lesions graded "2B" relative to total lesions assigned any other grade (0, 1, or 2A). This percentage represents combined lesions from all animals in the cohort. "Per mouse % 2B" refers to the percent of lesions graded as 2B within each experimental animal (% 2B lesions/mouse ± SEM). "Per-Mouse M v F t-test" refers to the p-value in male vs. female mice in each experimental condition. Each mouse is considered a biological replicate, and lesions within each mouse (averaged prior to statistical analyses) are considered technical replicates. **Experimental Numbers:** "No Mice" refers to the number of experimental animals (biological replicates) in each cohort, and "Lesions/mouse" refers to the mean number of lesions (technical replicates) used to calculate Per-Mouse % 2B. "Cohort Lesions" refers to the total number of analyzed lesions for each cohort (all lesion grades, combined from all animals) prior to exclusions.

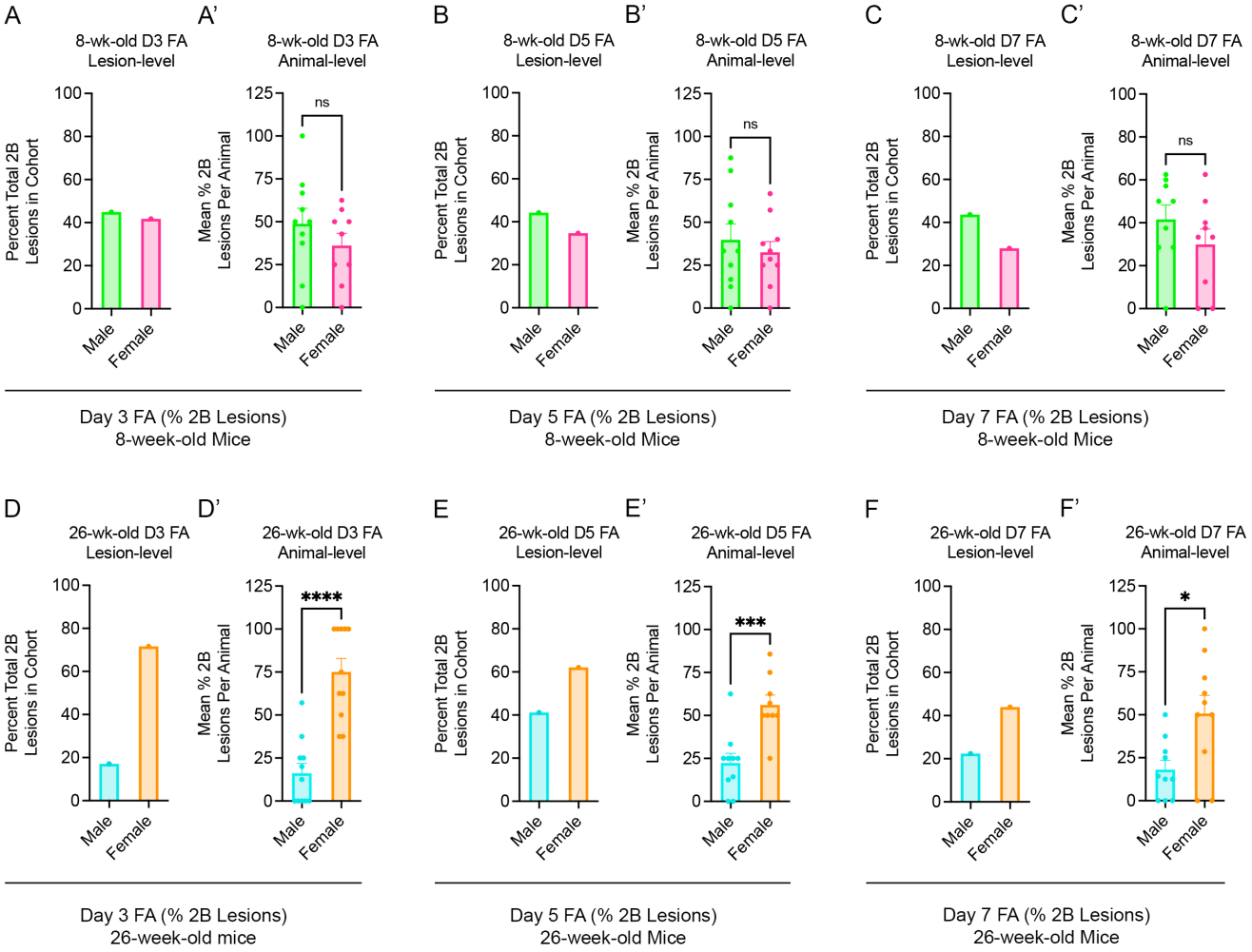

Supplementary Figure 2: Animal-level and Lesion-level fluorescein angiography analyses. Relevant to materials and methods, Figures 1-4. **(A)** Total percentage of clinically-significant 2B lesions from 8-week-old Day 3 FA mice (Male n = 83, female n = 69 lesions/group). **(A')** Mean % 2B lesions per mouse in the same cohort. Individual mice are considered biological replicates, while individual lesions used to calculate % 2B lesions/mouse are considered technical replicates. (Male n = 10 mice, Avg 7.2 lesions/mouse; Female n = 9 mice, mean 7.4 lesions/mouse). There was no significant difference between male and female mice (t-test p = 0.29) consistent with the contigency analysis of pooled lesion grades from the same cohort (χ^2 p = 0.71, shown in Fig. 1A). **(B)** Total percentage of 2B lesions from 8-week-old Day 5 FA mice (Male n = 67, Female n = 77 lesions/group). **(B')** Mean % 2B lesions per mouse in the same cohort. (Male n = 10 mice, Female n = 10 mice). Statistical analyses of both mouse-level % 2B lesions/mouse (t-test p = 0.52) and a lesion-level contingency analysis (χ^2 p = 0.68, shown in Fig. 1C) did not detect significant differences between sexes. **(C)** Total percentage of 2B lesions from 8-week-old Day 7 FA mice (Male n = 59, Female n = 74 lesions/group). **(C')** Mean % 2B lesions per mouse in the same cohort. (Male n = 10 mice, Female n = 10 mice). Statistical analyses of both mouse-level % 2B lesions/mouse (t-test p = 0.30) and a lesion-level contingency analysis (χ^2 p = 0.30, shown in Fig. 2A) did not detect significant differences between sexes. **(D)** Total percentage of 2B lesions from 26-week-old Day 3 FA mice (Male n = 78, Female n = 83 lesions/group). **(D')** Mean % 2B lesions per mouse in the same cohort. (Male n = 11 mice, Female n = 11 mice). Statistical analyses of both mouse-level % 2B lesions/mouse (t-test p < 0.0001) and a lesion-level contingency analysis (χ^2 p < 0.0001, shown in Fig. 3A) detected significantly increased lesion leakage in female mice. **(E)** Total percentage of 2B lesions from 26-week-old Day 5 FA mice (Male n = 70, Female n = 67 lesions/group). **(E')** Mean % 2B lesions per mouse in the same cohort. (Male n = 10 mice, Female n = 10 mice). Statistical analyses of both mouse-level % 2B lesions/mouse (t-test p = 0.0006) and a lesion-level contingency analysis (χ^2 p = 0.01, shown in Fig. 3C) detected significantly increased lesion leakage in female mice. **(F)** Total percentage of 2B lesions from 26-week-old Day 7 FA mice (Male n = 72, Female n = 68

lesions/group). **(E')** Mean % 2B lesions per mouse in the same cohort. (Male n = 10 mice, Female n = 10 mice). Statistical analyses of both mouse-level % 2B lesions/mouse (t-test p = 0.01) and a lesion-level contingency analysis (χ^2 p = 0.005, shown in Fig. 4A) detected significantly increased lesion leakage in female mice.

1.2. Optical Coherence Tomography (OCT)

Means for calculating lesion-level and animal-level data are described in the Materials and Methods Section (Page 13, final paragraph of continued Section 4.4; highlighted in red):

> To evaluate the statistical significance of lesion-level data, we pooled lesions from all animals of each cohort, and considered each lesion to be an independent replicate. To determine the statistical significance of mouse-level data, we calculated the mean volume of all lesions measured in each mouse (with each lesion considered a technical replicate), and used the mean lesion volume per mouse for further statistical analyses, with each mouse then considered a biological replicate. Statistical findings (significant or non-significant) were similar between approaches (Figure S4, Table S2).

Findings from each type of analysis are shown in Supplementary Table 2:

Experimental Conditions				**Experimental Findings**				**Numbers**	
Fig Panel	**Age (Wk)**	**Sex**	**Post-CNV**	**Cohort lesion size**	**Cohort t-test**	**Mouse lesion size**	**Mouse t-test**	**No. Mice**	**No. Lesions**
1B	8	M	3D	18.54 ± 0.74	0.09	18.69 ± 1.19	0.53	8	45
	8	F	3D	17.0 ± 0.48		17.65 ± 0.48		7	41
1D	8	M	5D	13.41 ± 0.53	0.07	13.37 ± 0.56	0.46	10	44
	8	F	5D	15.13 ± 0.84		15.84 ± 1.25		10	48
2B	8	M	7D	12.08 ± 0.65	0.49	12.01 ± 0.90	0.09	10	47
	8	F	7D	12.70 ± 0.59		12.73 ± 0.71		10	63
3B	26	M	3D	12.28 ± 0.71	0.0015	12.48 ± 0.79	0.0043	10	47
	26	F	3D	15.58 ± 0.73		16.70 ± 1.02		10	59
3D	26	M	5D	17.74 ± 0.81	0.0001	17.74 ± 1.14	0.0004	9	56
	26	F	5D	33.27 ± 0.78		23.54 ± 0.59		9	61
4B	26	M	7D	14.59 ± 0.58	<0.0001	15.76 ± 0.83	<0.0001	9	46
	26	F	7D	21.49 ± 0.60		22.12 ± 0.68		10	56

Supplementary Table 2: Optical coherence tomography (OCT) experimental conditions, findings and numbers. **Experimental Findings:** "Cohort lesion size" refers to the mean lesion size of all lesions in the cohort, with all animals combined (Mean ± SEM, μm^2), and "Cohort t-test" refers the M v F t-test for each experimental condition, with each lesion considered an independent replicate. "Mouse Lesion Size" refers to the average size of all lesions within each separate mouse (Mean ± SEM, μm^2), while "Mouse t-test" refers to the M v F t-test for each experimental condition, with individual mice considered biological replicates, and individual lesions in each mouse (averaged for statistical analyses) considered technical replicates **Numbers: "**No. Mice" refers to the number of experimental animals (biological replicates) for each cohort. "No. Lesions" refers to the lesion number in the cohort.

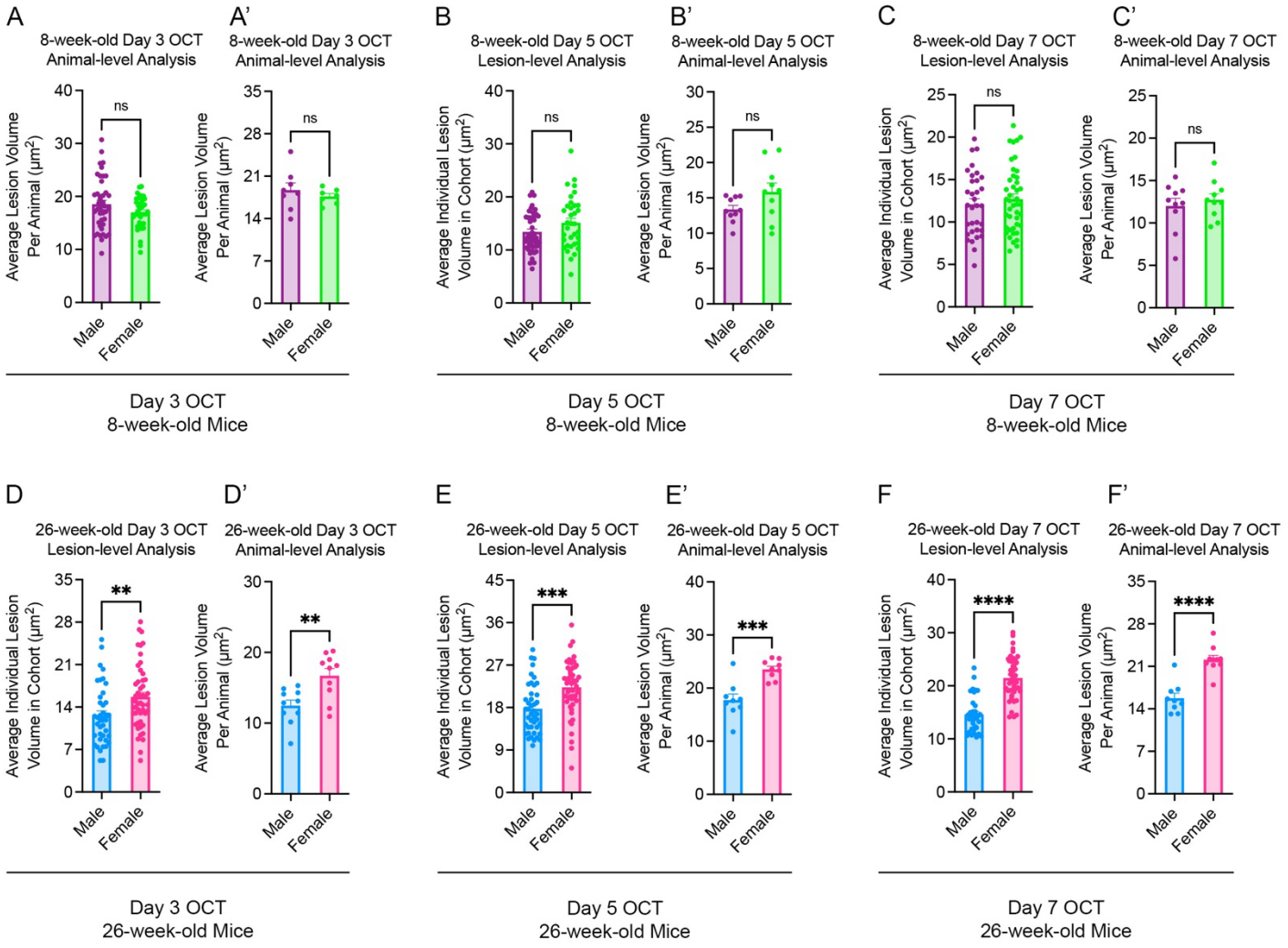

Supplementary Figure 4: Lesion-level and animal-level optical coherence tomography quantification. Relevant to materials and methods, figures 1-4. **(A)** Lesion-level quantification of cross-sectional lesion volume in 8-week-old D3 OCT mice, with lesions from all animals in each cohort pooled and considered independent replicates (Male n = 45, Female n = 41 lesions/group). **(A')** Animal-level quantification of cross-sectional lesion volume in 8-week-old D3 OCT mice, with cross-sectional volumes of all lesions in each mouse averaged (serving as technical replicates), and data expressed as mean cross-sectional lesion volume per animal (biological replicate). (Male n = 8 mice, mean of 5.38 lesions/mouse; Female n = 7 mice, mean of 5.43 lesions/mouse). **(B)** Lesion-level quantification of cross-sectional lesion volume in 8-week-old D5 OCT mice, with lesions from all mice of each cohort pooled and considered independent replicates (Male n = 44, Female n = 48 lesions/group). **(B')** Animal-level quantification of cross-sectional lesion volume in the same cohort, expressed as mean size of all lesions measured (technical replicates) per each mouse (biological replicate). (Male n = 10 mice, Female n = 10 mice). **(C)** Lesion-level quantification of cross-sectional lesion volume in 8-week-old D7 OCT mice (Male n = 47, Female n = 63 lesions/group). **(C')** Animal-level quantification in the same cohort (Male n = 10 mice, Female n = 10 mice). **(D)** Lesion-level quantification of cross-sectional lesion volume in 26-week-old D3 OCT mice (Male n = 47, Female n = 59 lesions/group). **(D')** Animal-level quantification of cross-sectional lesion volume in 26-week-old D3 OCT mice, expressed as mean of all lesions measured (technical replicate) in each mouse, which represents an independent biological replicate. (Male n = 10 mice, Female n = 10 mice). Both metrics identified a statistically significant increase in cross-sectional lesion volume in female mice with acceptable sensitivities (D p = 0.0015, D' p = 0.0043, Student's t-test). **(E)** Lesion-level quantification of cross-sectional lesion volume in 26-week-old D5 OCT mice (Male n = 56, Female n = 61 lesions/group). **(E')** Animal-level analysis of cross-sectional lesion volume in 26-week-old D5 OCT mice (Male n = 9 mice, Female n = 9

mice). Both metrics identified a significant increase in female mice with acceptable sensitivities (D p = 0.0001, D' p = 0.0004, Student's t-test). **(F)** Lesion-level quantification of cross-sectional lesion volume in 26-week-old D7 OCT mice (Male n = 46, Female n = 56 lesions/group). **(E')** Animal-level analysis of cross-sectional lesion volume in 26-week-old D7 OCT mice (Male n = 9 mice, Female n = 10 mice). Both metrics identified a significant increase in female mice, with the same p-value readout ($p < 0.0001$, Student's t-test).

1.3. Choroidal Flat Mount (FM)

Means for lesion-level and animal-level quantification of FM data are described in Materials and Methods (Page 13, Section 4.5, highlighted in red):

> To evaluate the statistical significance of lesion-level data, we pooled lesions from all animals of each cohort and considered each lesion to be an independent replicate for statistical analyses. To determine the statistical significance of animal-level data, we calculated the mean volume of all lesions measured in each mouse (with each lesion considered a technical replicate), and used the mean lesion volume per mouse for further statistical analyses, with each mouse then considered a biological replicate. Statistical findings (significant or non-significant) were similar between approaches (Figure S6, Table S3).

Findings from each type of analysis are shown in Supplementary Table 3:

Experimental Conditions				**Experimental Findings**				**Numbers**	
Fig. Panel	**Age (Wk)**	**Sex**	**Post-CNV**	**Cohort Lesion Size**	**Cohort t-test**	**Per-Mouse Lesion Size**	**Per-Mouse t-test**	**No. Mice**	**Cohort Lesions**
2C	8	M	7D	18.26 ± 0.81	0.42	18.38 ± 0.74	0.73	9	43
	8	F	7D	19.28 ± 0.98		18.87 ± 1.19		8	36
4C	26	M	7D	13.7 ± 0.44	<0.0001	13.93 ± 0.49	<0.0001	10	75
	26	F	7D	21.64 ± 0.56		22.92 ± 0.86		10	78

Supplementary Table 3: Flat Mount experimental conditions, findings and numbers. **Experimental Findings:** "Cohort lesion size" refers to the mean size of all lesions in the cohort, with all animals combined (Mean ± SEM, μm^2), and "Cohort t-test" refers the M v F t-test for each experimental condition, with each lesion considered an independent replicate. "Per-Mouse Lesion Size" refers to the average size of all lesions within each separate mouse (Mean ± SEM, μm^2), while "Per-mouse t-test" refers to the M v F t-test for each experimental condition, with individual mice considered biological replicates, and individual lesions in each mouse (averaged prior to statistical analyses) considered technical replicates. **Numbers: "**No. Mice" refers to the total number of experimental animals (biological replicates) for each cohort. "No. Lesions" refers to the total number of lesions.

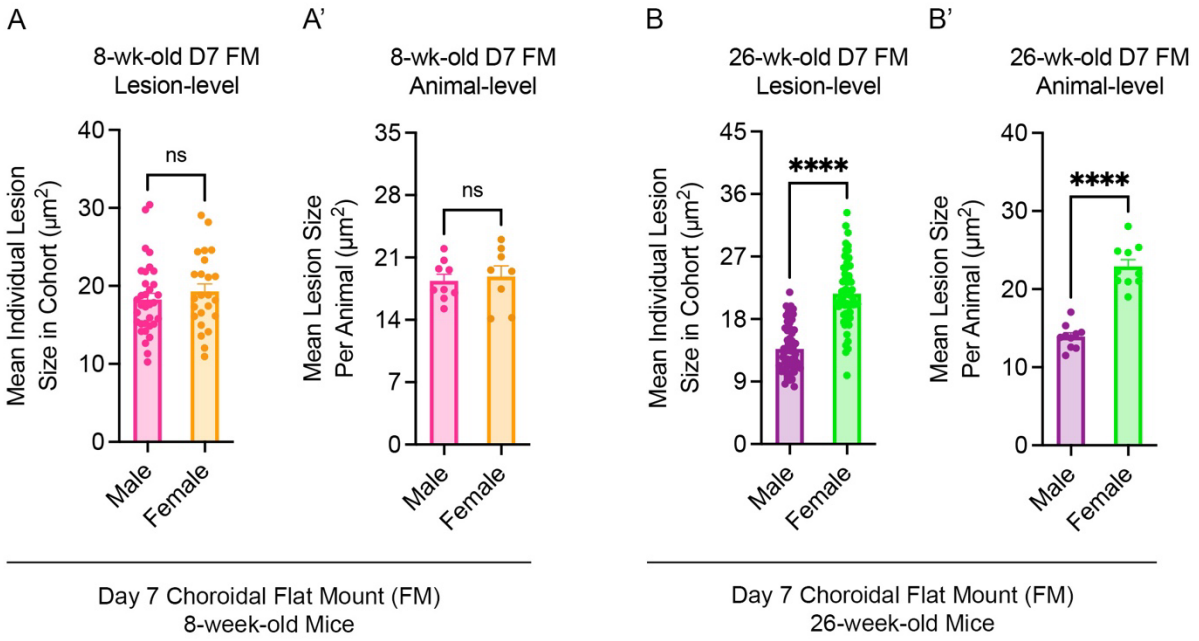

Supplementary Figure 6: Lesion- and Animal-level choroidal flat mount (FM) quantification. Relevant to materials and methods, Figure 2, Figure 4. **(A)** Lesion-level analysis of Day 7 FMs from 8-week-old mice, with lesions from all animals in the experimental cohorts pooled and considered to be independent replicates in statistical analyses (Male n = 53, Female n = 36 lesions/group). **(A')** Animal-level analysis of the same cohorts, with sizes of all lesions in each mouse averaged (serving as technical replicates), and data expressed as mean lesion size per animal (biological replicate). (Male n = 9 mice, Female n = 8 mice). Neither metric identified significant differences between sexes **(B)** Lesion-level analysis of Day 7 FMs from 26-week-old mice with each lesion considered an independent replicate (Male n = 75, Female n = 78 lesions/group). **(B')** Animal level analysis of Day 7 FMs from 26-week-old mice, with sizes of all lesions in each mouse averaged (serving as technical replicates), and data expressed as mean lesion size per animal (biological replicate). (Male n = 10 mice, Female n = 10 mice). Both metrics identified significantly increased lesion size in female mice with the same detectable sensitivity ($p < 0.0001$, unpaired two-tailed Student's t-test).

Comment 2: Model the repeated measures across days using an appropriate mixed-effects/repeated-measures framework (include time and its interactions, with random effects for mouse ± eye).

Response 2: As described above, the datasets are cohort-based, and not longitudinal. Therefore, each time point contains new animals, and repeated measures of images across days cannot be conducted. Fortunately, the relative simplicity of the mouse L-CNV model and easily standardized experimental variables allow for more consistent per-lesion metrics across experiments, such that longitudinal imaging of the same animals/lesions is not as necessary as in patients or more complex animal models such as non-human primates. We also performed all procedures, including surgical CNV induction and live animal imaging, in at least two separate batches per cohort, and conducted statistical analyses to detect potential interbatch variation, which was not found (Supplementary Tables 1-3).

Comment 3: Match models to outcomes: ordinal (FA grades), count (IHC; use negative binomial/over-dispersed Poisson), and skewed continuous (OCT/flat-mount; use transformed LMM or suitable GLMM).

Response 3: We will address each of these requests individually below.

<u>3.1. Ordinal response analysis of FA grades:</u> Lesions were graded on an ordinal scale well-established in the L-CNV model.[14]

Please see the below-quoted excerpt from the materials and methods section of Mizutani et al. 2013, which describes the same grading system and criteria used in the present study. The only difference is that what we refer to as "2A" lesions are categorized as "2" lesions, and what we refer to as "2B" lesions are categorized as "3."

> "Briefly, the lesions were graded on an ordinal scale based on the spatial and temporal evolution of fluorescein leakage as follows; 0 (nonleaky) = no leakage, faint hyperfluorescence, or mottled fluorescence without leakage; 1 (questionable leakage) = hyperfluorescent lesion with no progressive increase in size or intensity; 2 (leaky) = hyperfluorescence increasing in intensity but not in size, no definite leakage; 3 (pathologically significant leakage) = hyperfluorescence increasing in intensity and size, definite leakage."
>
> [Excerpt quoted directly from Mizutani et al.[14] to clarify that the ordinal grading scheme of the present study is commonly used by other groups].

However, the advanced algorithms and AI-based approaches used for advanced ordinal response analyses of FA data in clinical studies[15] are not available for L-CNV. Therefore, we are unable to perform the automated and predictive analyses available in clinic.

We carefully searched the literature for L-CNV data analysis platforms that could provide insights of this type. We did find an L-CNV study that used the area of lesion leakage in FA to automate assessment of lesion leakage and provided computational information for this analysis.[16] However, we captured only two images during FA imaging (early- and late-stage) so were unable to subject our data to posthoc analyses using this platform. Moreover, we have previously attempted to use these techniques to quantify the leakage area and found that it is not as consistent between animals as is ordinal grading.

3.2. Negative binomial/over-dispersed Poisson analyses of IHC counts: Our current dataset is not sufficiently powered for these analyses, and the IHC counts are a relatively minor point of the study. Moreover, the analyses used here are well-accepted in animal data from basic research studies, as data are much less complex due to the ability to standardize most confounders such as disease-modifying biological variables and tissue preparation. Also, each lesion was imaged in a single field of view and CNV lesions are uniform, so spatial distribution is not a concern, as it would be in cross-sections with localization to different retinal layers or pathological features.

Contrastingly, histology data from clinical samples are affected by counfounders such as multiple risk-modifying variables and sample preparation effects, and often include a panel of markers. These complex datasets thus require higher statistical powering and more in-depth analyses, such as those suggested by the Editor, to produce reliable findings.[17] This absolutely is required for scientific rigor in clinical histology data, but for the present study, this would be considered overkill.

3.3. Use transformed LMM or suitable GLMM to analyse OCT/FM data: Many of these models require longitudinal data so cannot be conducted on our cohort-based datasets. However, even non-longitudinal models of these types are most often used for complex multivariate analyses that do not appear to fit the outcomes measured in our study. Further, these analyses are most appropriate for data with unevenly distributed standard deviations, which is not the case for our findings.

However, we have made a good faith effort to accommodate this request. We conducted an extensive literature search and were unable to find any rodent L-CNV studies that used LMM/GLMM, and therefore cannot identify the appropriate parameters to conduct these analyses. We would very much appreciate if the Editor could provide a citation describing use of LMM/GLMM in cohort-based data in the L-CNV mouse model, as it could inform these analyses and allow us to address the Editor's request. Otherwise, we are unsure of how to do this and sincerely apologize. We hope also to have mitigated some of these concerns by providing greater clarity.

Comment 4: Specify a single primary endpoint and contrast a priori and control multiplicity for secondary endpoints/time-points (Holm or Benjamini–Hochberg).

Response 4: We wonder if this comment could be based on our failure to clearly communicate the objectives of the study and nature of our experimental findings.

Because this is a basic research study, its purpose is not to investigate overall disease outcome, so no single primary endpoint can be considered to have priority over others. For example, all time points post-CNV are considered equally important, as we wanted to identify potential time-dependent effects.

Similarly, the three measured parameters of disease severity (FA, OCT, FM) provide interrelated but pathophysiologically distinct phenotypic information:

- FA: lesion leakage determines the permeability of neovesels
- OCT: reflects not only size of neovessels, but also lesion edema
- FM: Histological analysis allows quantification of neovessles

Although these parameters generally follow the same trend, as in the present study, one of our group's most important findings to date is that an experimental treatment has opposing effects on these parameters, simultaneously increasing lesion leakage and decreasing lesion size measured by OCT and FM. Its effects are also disease-stage dependent. We are still investigating the basis and expect it to yield high-impact findings. This is an example of how study design of exploratory basic research often cannot and should not identify a single readout or time point, as all parameters could reveal important information.

Our data are cohort-based rather than longitudinal, so physiologic interference introduced by earlier time points is less important. For example, if we were to image the same animals every two days following L-CNV induction (Days 3, 5, 7), we could reasonably expect this to affect disease pathology/image quality in later timepoints. However, in our case, the only analysis conducted following any live-animal imaging is choroidal flat mount, and the stable histologic readout of neovessel size is not likely to be affected by imaging conducted minutes prior to euthanasia.

Comment 5: Replace post-hoc outlier deletion with a pre-specified rule plus sensitivity analyses or use robust methods; include batch/day/operator as a random/blocking factor; state randomisation steps and confirm masking.

Response 5: This point is well-taken. We will thus address each of these components separately below.

5.1. Transparent application of exclusion criteria: This was also a concern in our first round of feedback from the Editor, and we undertook significant effort to address it:

- In our original data analysis, we did not note the reason for image exclusion. Therefore, to provide this information for the resubmission, we re-analyzed all CNV phenotypic data. This included 198 FA images, 613 OCT images, and 232 FM images.
    - This information, including the number of excluded lesions and reason for exclusion, is now provided in supplementary tables 1-3. Very few lesions are excluded from any given cohort due to the relatively simplistic nature of L-CNV data as compared to clinical data.
- Provided supplementary figures (1, 3, and 5 in the revised manuscript) describing lesion quantification and providing descriptions of exclusion criteria with examples of lesions that were excluded from analysis.

5.2. Animal-level randomization and masking: Ordinarily we conduct this as described by the Editor, but in this study faced inherent limitations due to the experimental variables to be tested.

Animal randomization: We were unable to randomize animals into treatment groups, as the experimental variables themselves (age and sex) were the biological characteristics of the animals. Other than this, all experimental animals were subjected to L-CNV, and there were no other treatments, for example experimental drugs.

This is now included on Page 11, section 4.1 and is highlighted in red:

> Animals were not randomized into treatment groups prior to beginning, as their biological characteristics determined the treatment group, and all animals were subjected to L-CNV.

Animal masking: Similarly, it was impossible to mask the operator to experimental group during disease induction and live animal imaging, as the experimental variables of age and sex were visibly apparent. This is indicated in blue on Page 11, section 4.2:

> During the LPC procedure, alternating mice between groups were operated sequentially. Masking groups during the procedure was not possible, as the differences between groups (animal age and sex) were visually apparent.

> As animals were imaged, we alternated between groups sequentially. Masking groups during the procedures was not possible, as the differences between groups (animal age and sex) were visually apparent.

5.3. Masking of image analysis and assessment of pre-determined exclusion criteria: We believe that some concerns regarding exclusion criteria could be due in part to misunderstanding and apologize if we have not provided sufficient clarity. Exclusion criteria for each parameter were determined prior to beginning the study. They have been published and well-described by multiple groups and are biologically justified.[12,18-20] . We describe our process for image analysis masking and assessment of pre-determined criteria for each parameter:

5.3.1. Angiography: Image masking, blinded lesion grading and identification of exclusion criteria, and data analyses were conducted as described below.

FA image masking is described on page 12, section 4.3, as quoted below and highlighted in red:

> All images were blinded prior to any analyses, including evaluation of pre-determined exclusion criteria. First, a separate investigator coded image file names with a random number, such that the assessor was unable to determine the image's experimental group when grading severity of lesion leakage and identifying lesions that met pre-determined exclusion criteria.

FA image grading and blinded application of pre-determined exclusion criteria are described on page 12, section 4.3. Below, we leave the text color-coded to indicate new additions (red) and prior information highlighted for clarity (blue).

> Lesion leakage severity was then graded in blinded images according to a previously established grading scheme, and lesions were excluded from analyses according to the predetermined exclusion criteria of being either overburnt or fused (Figure S1C, D). In Figure S1, we provide examples and descriptions of lesion grading and exclusion, and in Table S1, we provide total numbers of graded and excluded lesions per group.

> …. After grading was complete and outliers identified, images were decoded and data were analyzed.

FA data analyses are quoted below and described on Page 12, section 4.3 (continued), highlighted in red:

> To determine the statistical significance of lesion-level data, in which lesions from all animals in each cohort were pooled and considered independent replicates, we conducted a contingency analysis (CI 95%) with each lesion grade (0, 1, 2A, 2B) considered a separate outcome, and χ^2 $p < 0.05$ considered statistically significant. To generate animal-level data, the percent of clinically significant (2B) lesions per mouse was calculated, with each individual

lesion in a single mouse thus considered a technical replicate. The mean % 2B lesions/mouse was thus considered a biological replicate, and a two-tailed unpaired Student's t-test used to determine statistical significance, with $p < 0.05$ considered significant. Statistical findings (significant or non-significant) were similar between approaches (Figure S2, Table S1).

5.3.2. Optical Coherence Tomography (OCT): Image masking, blinded assessment of pre-determined exclusion criteria, and data analyses were conducted as described below.

OCT image masking is described below and highlighted in red on page 12, Section 4.4:

All images were blinded prior to analyses, including determining whether images met pre-determined exclusion criteria. First, a separate investigator coded image file names with a random number, such that the assessor was unable to determine the image's experimental group when identifying images that met pre-determined exclusion criteria and quantifying lesion size.

OCT quantification and application of exclusion criteria are descried on Page 13, Paragraph 1. Below, we leave the text color-coded to distinguish new additions (red) from prior text that has been highlighted for clarity (blue).

Pre-determined exclusion criteria included overburnt lesions (Figure S2C), fused images (Figure S2D), and insufficient lesion quality for quantification, for example poor image focus (Figure S2E) or failure to include the entire lesion on the scan (Figure S2F). After quantification was complete and outliers identified, images were decoded and data were analyzed.

OCT data analyses at the per-lesion and per-animal levels were performed as described below and on Page 13, Paragraph 2, highlighted in red.

To evaluate the statistical significance of lesion-level data, we pooled lesions from all animals of each cohort, and considered each lesion to be an independent replicate. To determine the statistical significance of mouse-level data, we calculated the mean volume of all lesions measured in each mouse (with each lesion considered a technical replicate) and used the mean lesion volume per mouse for further statistical analyses, with each mouse then considered a biological replicate. Statistical findings (significant or non-significant) were similar between approaches (Figure S4, Table S2).

5.3.3. Flat mount (FM): Image masking, blinded image quantification and assessment of pre-determined exclusion criteria, and data analyses were conducted as described below.

FM image masking was conducted as quoted below and described on Page 13, Section 4.5, highlighted in red:

All images were blinded prior to analyses. First, a separate investigator coded image file names with a random number, such that the assessor was unable to determine the image's experimental group when identifying images that met pre-determined exclusion criteria and quantifying lesion size.

FM quantification and application of exclusion criteria are descried on Page 13, Section 4.5. Below, we leave the text color-coded to distinguish new additions (red) from prior text that has been highlighted for clarity (blue).

Lesion size was quantified using FIJI software (Version 2.9.0). Lesion borders were traced to quantify the lesion size (Figure S3A,B). Pre-determined exclusion criteria included overburnt lesions (Figure S3C), fused lesions (Figure S3D), and for Day 14 post-CNV, resorbed lesions (Figure S3E). After quantification was complete and outliers identified, images were decoded and data were analyzed.

FM data analyses are quoted below and described on Page 13, last paragraph, highlighted in red:

To evaluate the statistical significance of lesion-level data, we pooled lesions from all animals of each cohort and considered each lesion to be an independent replicate for statistical analyses. To determine the statistical significance of animal-level data, we calculated the mean volume of all lesions measured in each mouse (with each lesion considered a technical replicate) and used the mean lesion volume per mouse for further statistical analyses, with each mouse then considered a biological replicate. Statistical significance was determined with a two-tailed, unpaired Student's t-test, with $p < 0.05$ considered statistically significant. Statistical findings (significant or non-significant) were similar between approaches (Figure S6, Table S3).

5.4. Operator effects: These potential effects were mitigated as now indicated on Page 11, section 4.2 in red:

All LPC was performed by a single operator (EAP) who was extensively trained in the procedure and had demonstrated proficiency in masked positive control experiments prior to beginning the studies.

LPC was performed on at least two separate days for each experimental group, and during the procedure, animals for each treatment group were alternated (Page 11, section 4.2, paragraph 1, blue):

During the LPC procedure, alternating mice between groups were operated sequentially. Masking groups during the procedure was not possible, as the differences between groups (animal age and sex) were visually apparent.

5.5. Batch and day effects: Protocols to mitigate these effects and monitor for interbatch variation are quoted below and described on Page 11, section 4.2, last paragraph, highlighted in red:

All surgical and imaging procedures were performed in at least two separate batches on two separate days for each cohort, which were at least one week apart. We used statistical analyses to identify significant differences in experimental readouts between batches and did not detect interbatch variations in any of our findings (Supplementary Tables 1-3).

Comment 6: Add a pre-study sample size justification for the animal experiments. The resource-equation method is acceptable only where a power analysis is genuinely not feasible.

Response 6: To approximate pre-study sample sizes, we utilize prior template data from L-CNV mice injected with Eylea, the standard of care for CNV in humans. These results are shown below in Supplementary Table 4.

We have also added this information in the manuscript text, quoted below and shown on Page 14, Section 4.7 highlighted in red:

To calculate the predicted sample size for CNV studies, we use template data from a prior study of CNV mice injected with VEGF-neutralizing antibody (aflibercept), the standard of care for CNV, with Power Value = 0.99, p = 0.01 (Supplementary Table 4).

Parameter	Ctrl Lesion Size (Mean ± SD, μm^2)	Eylea Lesion Size (Mean ± SD, μm^2)	Predicted No. Lesions/Group	Predicted No. Mice/Group
Day 3 OCT	19.66 ± 4.79	17.43 ± 5.83	86	11
Day 5 OCT	15.40 ± 5.71	13.51 ± 3.41	66	9
Day 7 OCT	14.69 ± 4.9	11.72 ± 3.84	71	9
Flat Mount	20.52 ± 4.99	16.10 ± 5.72	73	10

Supplementary Table 4. Power analysis for sample size prediction. To calculate approximate number of animals required for experiments, we use prior template data from CNV mice injected with 1 µl sham (sterile saline) or Eylea (40 mg/mL aflibercept) as optimized previously[21] with Power Value = 0.99, p = 0.01. Predicted

sample size refers to the number of lesions, while the predicted number of mice assumes 8 total lesions/animal, with 4 lesions/eye.

REFERENCES CITED

1. Wagley S, Belin PJ, Dollar JJ, Harbour JW, Maltry AC, Mruthyunjaya P, Schefler AC, Tang PH. Multiple Genetically Distinct Uveal Melanomas Arise in the Same Eye of Two Patients with Melanosis Oculi. *Am J Ophthalmol*. 2022;234:1-5. doi: 10.1016/j.ajo.2021.06.037
2. Mellencamp EA, Arhontoulis DC, DiBona SC, Baxley DE, Yannuzzi NA, Tang PH. Novel Gore-Tex Scleral Fixation Technique for Dual-Eyelet Intraocular Lenses. *Ophthalmic Surg Lasers Imaging Retina*. 2025;56:202-204. doi: 10.3928/23258160-20241216-05
3. Hill C, Arhontoulis DC, Bui H, DeVaro SM, Tang PH. Bilateral Sterile Granulomatous Uveitis Caused by Intravitreal Injections of Faricimab. *J Vitreoretin Dis*. 2025:24741264251330339. doi: 10.1177/24741264251330339
4. Nazari H, Emerson G, Tang PH. Intractable Pain and Diplopia after Scleral Buckle Surgery. *Retin Cases Brief Rep*. 2023;17:41-43. doi: 10.1097/ICB.0000000000001104
5. Prairie ML, Rubino SM, Tang PH. Resolution of Lipemia Retinalis With Lifestyle Modification. *J Vitreoretin Dis*. 2024;8:728-730. doi: 10.1177/24741264241275285
6. Adams OE, Sodhi GS, Vagaggini T, Haq Z, Curran CD, Prairie ML, Montezuma SR, Koozekanani DD, Ryan EH, Parke DW, 3rd, et al. Clinical Outcomes of Acute Endophthalmitis after Intravitreal Delivery of Vascular Endothelial Growth Factor Inhibitors Versus Steroids. *Retina*. 2023;43:947-954. doi: 10.1097/IAE.0000000000003748
7. Curran CD, Masters TC, Engel KC, Lee MS, Davies JB, Ryan EH, Parke DW, 3rd, Mittra RA, Dev S, Tang PH. Advanced Diabetic Retinopathy May Promote Ocular Neovascularization after Central Retinal Artery Occlusion. *Ophthalmol Retina*. 2023;7:932-933. doi: 10.1016/j.oret.2023.06.018
8. Curran CD, Adams OE, Vagaggini T, Sodhi GS, Prairie ML, Baker MJ, Sastry A, Ryan EH, Parke DW, 3rd, Mittra RA, et al. Prophylactic Treatment of Lattice Degeneration in Fellow Eyes after Repair of Uncomplicated Primary Rhegmatogenous Retinal Detachment. *Retina*. 2024;44:63-70. doi: 10.1097/IAE.0000000000003908
9. Adams OE, Vagaggini T, Groth SL, Curran CD, Prairie ML, Sastry A, Ryan EH, Parke DW, Mittra RA, Dev S, et al. Evaluation of Outcomes of Acute Cataract Surgery-Related Endophthalmitis Using a Novel Management Algorithm Based on Presenting Risk Factors. *Semin Ophthalmol*. 2023;38:648-655. doi: 10.1080/08820538.2023.2194985
10. Mundae R, Velez A, Sodhi GS, Belin PJ, Kohler JM, Ryan EH, Tang PH. Trends in the Clinical Presentation of Primary Rhegmatogenous Retinal Detachments During the First Year of the COVID-19 Pandemic. *Am J Ophthalmol*. 2022;237:49-57. doi: 10.1016/j.ajo.2021.11.017
11. Marneros AG, She H, Zambarakji H, Hashizume H, Connolly EJ, Kim I, Gragoudas ES, Miller JW, Olsen BR. Endogenous endostatin inhibits choroidal neovascularization. *FASEB J*. 2007;21:3809-3818. doi: 10.1096/fj.07-8422com
12. Giani A, Thanos A, Roh MI, Connolly E, Trichonas G, Kim I, Gragoudas E, Vavvas D, Miller JW. In vivo evaluation of laser-induced choroidal neovascularization using spectral-domain optical coherence tomography. *Invest Ophthalmol Vis Sci*. 2011;52:3880-3887. doi: 10.1167/iovs.10-6266
13. Hasegawa E, Inafuku S, Mulki L, Okunuki Y, Yanai R, Smith KE, Kim CB, Klokman G, Bielenberg DR, Puli N, et al. Cytochrome P450 monooxygenase lipid metabolites are significant second messengers in the resolution of choroidal neovascularization. *Proc Natl Acad Sci U S A*. 2017;114:E7545-E7553. doi: 10.1073/pnas.1620898114
14. Mizutani T, Ashikari M, Tokoro M, Nozaki M, Ogura Y. Suppression of laser-induced choroidal neovascularization by a CCR3 antagonist. *Invest Ophthalmol Vis Sci*. 2013;54:1564-1572. doi: 10.1167/iovs.11-9095
15. Parmar UPS, Arora A, Agarwal A, Gangaputra S, Agrawal R, Gupta V. Detection and quantification of fluorescein angiography leakage: From manual grading to advances in machine learning. *Surv Ophthalmol*. 2025. doi: 10.1016/j.survophthal.2025.08.015
16. Toma HS, Barnett JM, Penn JS, Kim SJ. Improved assessment of laser-induced choroidal neovascularization. *Microvasc Res*. 2010;80:295-302. doi: 10.1016/j.mvr.2010.05.011

17. Wilson CM, Ospina OE, Townsend MK, Nguyen J, Moran Segura C, Schildkraut JM, Tworoger SS, Peres LC, Fridley BL. Challenges and Opportunities in the Statistical Analysis of Multiplex Immunofluorescence Data. *Cancers (Basel)*. 2021;13. doi: 10.3390/cancers13123031
18. Lambert V, Lecomte J, Hansen S, Blacher S, Gonzalez ML, Struman I, Sounni NE, Rozet E, de Tullio P, Foidart JM, et al. Laser-induced choroidal neovascularization model to study age-related macular degeneration in mice. *Nat Protoc*. 2013;8:2197-2211. doi: 10.1038/nprot.2013.135
19. Ragauskas S, Kielczewski E, Vance J, Kaja S, Kalesnykas G. In Vivo Multimodal Imaging and Analysis of Mouse Laser-Induced Choroidal Neovascularization Model. *J Vis Exp*. 2018. doi: 10.3791/56173
20. Gong Y, Li J, Sun Y, Fu Z, Liu CH, Evans L, Tian K, Saba N, Fredrick T, Morss P, et al. Optimization of an Image-Guided Laser-Induced Choroidal Neovascularization Model in Mice. *PLoS One*. 2015;10:e0132643. doi: 10.1371/journal.pone.0132643
21. Ichiyama Y, Matsumoto R, Obata S, Sawada O, Saishin Y, Kakinoki M, Sawada T, Ohji M. Assessment of mouse VEGF neutralization by ranibizumab and aflibercept. *PLoS One*. 2022;17:e0278951. doi: 10.1371/journal.pone.0278951

MUSC Health
Medical University of South Carolina

Storm Eye Institute
Ophthalmology
167 Ashley Avenue, MSC 611
Charleston, SC 29425
Office 843-792-2020
Fax 843-792-1166
MUSChealth.org/eyes

Prof. Dr. Marizio Battino
Editor-in-Chief
International Journal of Molecular Sciences

RE: ijms-3802232-R4: Appeal to EiC

24th October 2025

Dear Prof. Dr. Battino,

Thank you for considering this appeal for our manuscript "Evaluation of sex differences in laser-induced choroidal neovascularization: roles of estrogen and innate immunity in age-dependent sexual dimorphism." This manuscript has already been rigorously reviewed by three peer reviewers, who were satisfied with its subsequent revision, recommending that it be accepted for publication. The manuscript has been under consideration for a special edition, "Advances in the Pathophysiology and Treatment of Eye Diseases." We are now in our third round of revisions with the Guest Editor (fourth overall), and **it remains in conflict because the Guest Editor requires advanced clinical statistical analyses that cannot be conducted in our mouse datasets.**

This manuscript reports findings in the mouse laser-induced choroidal neovascularization (L-CNV) model, a common animal model of age-related macular degeneration **(Figure 1)**, where CNV lesions are surgically induced using a laser beam to disrupt the membrane that partitions the retina from the choroid vascular bed at the back of the eye **(Fig. 1a-c)**. This is the most common animal model of wet AMD and has significant preclinical utility, but the artificially-induced lesions are robust and homogenous in shape (Fig 1d), unlike the structurally complex and relatively subtle CNV lesions that develop in AMD patients, as shown in a representative image from Pfau et al. **(Fig. 1e)**.[1] Therefore, the L-CNV model and its image-based phenotypic readouts are similar to human CNV, but much more simplistic.

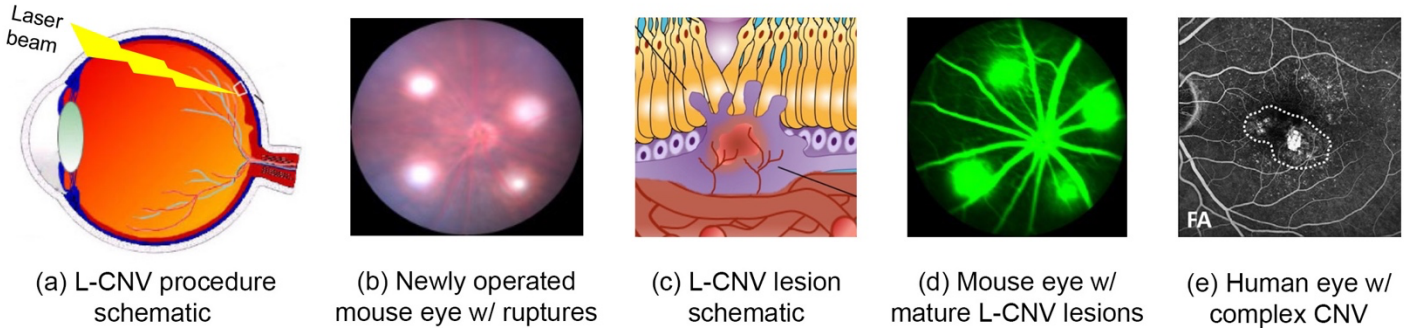

Figure 1: Laser-induced choroidal neovascularization (L-CNV) model. (a-b) To induce L-CNV, a laser beam is used to rupture a membrane in the back of the eye that separates the retina from the choroid vascular bed. **(c)** This disruption allows blood vessels from the choroid to invade the outer retina, forming CNV lesions. **(d)** Mature L-CNV lesions are quite robust, with a homogenous simplistic morphology. **(e)** Comparatively, human CNV lesions are much more subtle and complex. Image from Pfau et al. 2020.

The Guest Editor, Dr. Georgios Panos, is an esteemed vitreoretinal surgeon with a remarkable publication track record of 134 peer-reviewed articles, most of which report clinical outcomes and are geared towards disease management in ophthalmology. The Guest Editor's demonstrable knowledge in biostatistics and best practices for rigorous analysis and reporting of clinical findings have driven his primary concerns with the manuscript, which are statistical. His suggestions are in theory excellent and addressing them to the extent possible has

improved the manuscript's rigor and even informed ongoing efforts towards improving L-CNV data analyses to be more rigorous.

However, the expectation to treat mouse data exactly as one would clinical findings is not feasible; the advanced analytics recommended by the Guest Editor are paramount for robust analysis of complex clinical data but require algorithms and large image databases that are not available for mice. These metrics are also not as essential for animal data, as experimental variables can be tightly controlled, negating the need to compensate for disease-modifying variables such as heterogenous disease origin and duration, age, genetic risk factors, smoking status, BMI, and other comorbid conditions, as in patient data.

We have attempted to (a) respond to all concerns to the best of our ability, within the limitations of our experimental datasets and available analytic tools, (b) explain the infeasibility of analyses that are not possible, and (c) ask for exemplary citations using the requested analyses in L-CNV mice in case we are mistaken, and the tools are indeed available. The Guest Editor has recognized our efforts, although stating that they are insufficient, and has not acknowledged our responses regarding feasibility or requests for exemplary citations.

We respect that it is common for different scholars to hold varying perspectives on the same matter and contend that this difference in perspectives arises from the intersection between a clinical ophthalmologist and basic researchers, which is common in the eye research field. Because the eye is a small field and considered a niche, it is common for clinicians and basic scientists to review one another's work.

This cross-pollination can be beneficial. Review from clinicians helps ensure that basic research is clinically relevant and statistically rigorous. When I personally am asked to review clinical work, my perspective as an exploratory basic researcher can be helpful, but I must also conduct a significant amount of research to ensure my conclusions are accurate. For this intersection to be productive, both parties must ultimately reach an understanding that there are fundamental differences between basic research and clinical studies.

In this case, addressing the Guest Editor's points have indeed improved the rigor of the paper. They have in fact identified valid concerns regarding the scientific rigor of L-CNV data analysis practices that are, to our knowledge, ubiquitous to the field. Thus, we also use the manuscript as a platform to point out this discrepancy, as highlighted in Comment 1 below.

However, we have now addressed the Guest Editor's concerns to the greatest extent possible and cannot do anything further with existing analytic tools. The L-CNV data analyses and statistics are now more rigorous than even very high-impact papers using the model, a point that we raise in the revised manuscript. We hope the EiC can make an arbitration that balances technically accurate statistical concerns with the limitations of existing analytics and what would be considered reasonable for animal data.

Sincerely,

Elizabeth Pearsall, PhD
Assistant Professor of Ophthalmology
Medical University of South Carolina
pearsale@musc.edu
843-792-5469
167 Ashley Ave HA611 Charleston SC 29425

Revision 4 (Round 3 from Guest Editor)

Received: 23rd October 2025

Guest Editor Summary: Thank you for the latest revision and your response to comments. I acknowledge the additional detail on cohort structure, the inclusion of per-animal summaries alongside lesion-level plots, and clearer reporting of exclusions. However, the principal statistical issues remain unresolved. The manuscript's conclusions continue to rely on analyses that do not align with the data structure or outcome types. Please address the following points in full; each requires changes to both the methods and the results, with revised figures/tables and, where relevant, supplementary material.

Response: Many of the complex analyses requested by the Guest Editor are not possible with our datasets and available analytics for mouse data, so these requests cannot be met. This is why the manuscript decision remains in conflict.

We have thoroughly explained this in prior revisions and in the below rebuttal, but the Guest Editor has not acknowledged these responses. We have also asked the Guest Editor to provide examples of the requested analyses in the animal model in case we misunderstood what was being asked and it was indeed possible. However, these requests on our part have not been acknowledged.

That said, we have been as responsive as is possible to the peer review process, and addressing the practice of analyzing per-animal data raises an important point that we have addressed and highlighted in the revised manuscript, as detailed below in Comment 1 and Comment 15. Although out of the present study's scope, we will continue to further revise best practices for L-CNV data analysis, especially in considering variability between lesions versus variability between animals. We feel that this ongoing work will be important in model standardization for L-CNV, but developing new algorithms requires years of work, and a line must be drawn.

We hope to have established a reasonable middle ground that the Editor-in-Chief can evaluate to make a recommendation.

Comment 1: Treat the animal as the experimental unit. If analysing lesion data, use hierarchical models that account for lesions nested within eye and mouse, and report intraclass correlations.

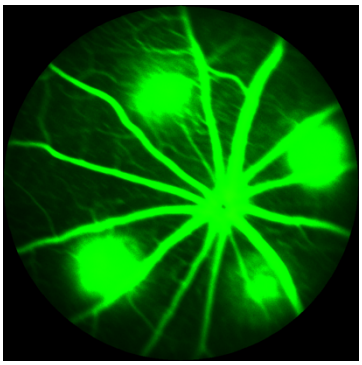

Response 1: A primary concern of the Guest Editor is that data in the L-CNV model are analyzed at a per-lesion level, with all lesions from experimental animals in each group pooled and treated as independent replicates. For example, in the image of L-CNV lesions pictured at left, each individual lesion would be considered a separate replicate for statistical analyses based on the commonly held belief that variations caused by surgical inconsistencies create greater variation within a single animal (or eye) than between different animals of the same treatment group.

Although this is considered the standard practice for the model and is regularly published in high-impact journals, we recognized the concern with scientific rigor, and developed new analyses to present data at both per-lesion level (standard) and per-animal, where all lesions within one animal are averaged, and the mean lesion size in each animal used to assess statistical significance. In this way, surgically created lesions within one animal serve as technical replicates, and individual animals serve as biological replicates, which is more appropriate.

The new data analysis schema we use to address this concern are oversimplified, and Guest Editor is correct that hierarchical modeling will be important in distinguishing variations between lesions from variations between animals. However, hierarchical models used in clinic rely on large image databases and neural network analyses that are presently unavailable for mouse data.[2,3] Although the Guest Editor's suggestions are excellent in theory

and address limitations in our current analytic approach, we have been unable to communicate their present infeasibility.
That said, we are grateful for this feedback, and hope that the manuscript can be impactful to the field by pointing out this inherent weakness. In fact, we have placed significant emphasis on this point in the revised manuscript, as outlined below:

The discussion now contains the below addition, shown on Page 9, section 3.2, highlighted in red:

> An additional consideration raised in the manuscript's review was the standard practice of treating individual CNV lesions as independent replicates for statistical analyses. Although this practice is, to the authors' knowledge, nearly ubiquitous in the L-CNV model, an individual lesion is a questionable biological replicate.
>
> We therefore present data in the standard per-lesion format alongside new calculations to generate per-animal data. For OCT and FM, we calculated the mean lesion size per animal, then subjected the mean values to statistical analyses, and presented these data as dot plots (Figure S4, S6). This allowed the lesions within each animal to serve as technical replicates, and the individual animals to serve as biological replicates. We found that the consensus (significant or non-significant) for t-tests conducted on individual lesion sizes versus mean lesion size per animal was the same for all experiments. For FA, we calculated the percent 2B lesions per animal, which was considered representative of each animal, and subjected these values to Student's t-tests for pairwise comparisons (Figure S2). Per-lesion data, which is considered categorical, was analyzed with contingency (χ^2) testing so these two statistical metrics were not directly comparable, but we found that all datasets were identified as being either significant or non-significant by both metrics.
>
> In the future, we will further evaluate the relative merit of each approach, or potentially identify new schema for statistical analyses that account for variability between lesions and between animals, for example hierarchical models. Although beyond the scope of the present study, further developing best practices for L-CNV data analyses will be an important contribution to model standardization.

The Results section now contains the below addition, shown on Page 3, Section 2.1, highlighted in red:

> We analyzed FA, OCT, and FM data at a lesion-based level, where each lesion was considered an independent replicate, which is the standard data analysis practice in the L-CNV model.
>
> However, individual lesions could also be considered technical, rather than biological replicates. Therefore, we also conduced per-animal data analyses in parallel, where all lesions in a single animal were considered technical replicates, and averaged prior to further analyses. We then considered individual animals as biological replicates, which were used to determine statistical significance. Our statistical findings were similar between approaches, but in the interest of scientific rigor and model standardization, we addressed this important point. The calculations used for animal-level analyses can be found in Materials and Methods Section 4.3 (FA), 4.4 (OCT) and 4.5 (FM). Side-by-side comparisons of per-lesion versus per-animal data can be found in Supplementary Figure 2 (FA), Supplementary Figure 4 (OCT), and Supplementary Figure 6 (FM).

Comment 2: Base all inferential claims on animal-level results (or mixed models that yield animal-level contrasts). Keep lesion-level plots for illustration only.

Response 2: This request was addressed in Revision 3. Please refer to Supplemental Figures 2, 4, and 6.

Comment 3: FA leakage: replace $\chi 2$ on pooled lesions and t-tests on per-mouse percentages with an ordinal (cumulative-logit) model at the mouse level. If using a threshold (e.g., $\geq$2A), fit a binomial model with the number of affected lesions out of lesions induced.

Response 3: We did not use threshold grading, but instead used ordinal grading.

The model used for ordinal grading was addressed as below Revision 3, Response 3.1. It is summarized in brief below, and in the revision document, the full response is highlighted in purple:

> Lesions were graded on an ordinal scale well-established in the L-CNV model.[4] However, the advanced algorithms and AI-based approaches used for advanced ordinal response analyses of FA data in clinical settings[5] are not available for L-CNV. Therefore, we are unable to perform the automated and predictive analyses available in clinic.

Comment 4: OCT and flat-mount: address right-skew by analysing on a log scale with linear models at the mouse level or use an appropriate GLM/GLMM. Include planned interactions (e.g., sex × age).

Response 4: In L-CNV, only four lesions per eye (eight per mouse) are generated surgically. Data are thus not sufficiently powered to analyze with linear scales at the mouse level.

GLM/GLMM approaches have not ever been used to analyze mouse L-CNV data to our knowledge; we have carefully searched the literature and been unable to identify any such studies. Therefore, we are unsure of how this could be conducted at present. We also asked the Guest Editor to provide an exemplary citation of these analyses in case we were mistaken, but this request was not acknowledged.

The simplistic nature of our datasets is in general not well-suited to GLM/GLMM modeling and compensation for the potential interactions mentioned by the Guest Editor:

- All comparisons in the paper are pairwise, comparing disease severity of male and female mice of the same age, but not between ages.
- There are no disease-modifying biological variables to incorporate (age, smoking status, genetic risk factors, BMI), as would be the case in clinical data.
- Unlike human data, disease etiology and duration is identical.
- Data are not longitudinal; although different time points are shown, they are in separate animal cohorts and do not assess the same lesions over time, so time-based changes cannot be incorporated into any such modeling, as would be the case in most clinical studies.

Comment 5: IHC counts: use negative binomial (or over-dispersed Poisson) models at the mouse level; include an offset for sampled area/field where relevant.

Response 5: This was addressed in Revision 3, Response 3.2:

> Our current dataset is not sufficiently powered for these analyses, and the IHC counts are a relatively minor point of the study. Moreover, the analyses used here are well-accepted in animal data from basic research studies, as data are much less complex due to the ability to standardize most confounders such as disease-modifying biological variables and tissue preparation. Also, each lesion was imaged in a single field of view and CNV lesions are uniform, so spatial distribution is not a concern, as it would be in cross-sections with localization to different retinal layers or pathological features.
>
> Contrastingly, histology data from clinical samples are affected by confounders such as multiple risk-modifying variables and sample preparation effects, and often include a panel of markers. These complex datasets thus require higher statistical powering and more in-depth analyses, such as those suggested by the Guest Editor, to produce reliable findings.[6] This absolutely is required for scientific rigor in clinical histology data, but for the present study, this would be considered overkill.

Comment 6: Declare a single primary endpoint and primary contrast a priori. Treat all other endpoints/time-points as secondary and apply error-rate control (Holm or Benjamini–Hochberg within clearly defined families).

Response 6: This was addressed in Revision 3, Response 4:

> We wonder if this comment could be based on our failure to clearly communicate the objectives of the study and nature of our experimental findings.

Because this is a basic research study, its purpose is not to investigate overall disease outcome, so no single primary endpoint can be considered to have priority over others. For example, all time points post-CNV are considered equally important, as we wanted to identify potential time-dependent effects.

Similarly, the three measured parameters of disease severity (FA, OCT, FM) provide interrelated but pathophysiologically distinct phenotypic information:

- FA: lesion leakage determines the permeability of neovessels
- OCT: reflects not only size of neovessels, but also lesion edema
- FM: Histological analysis allows quantification of neovessels

Although these parameters generally follow the same trend, as in the present study, one of our group's most important findings to date is that an experimental treatment has opposing effects on these parameters, simultaneously increasing lesion leakage and decreasing lesion size measured by OCT and FM. Its effects are also disease-stage dependent. We are still investigating the basis and expect it to yield high-impact findings. This is an example of how study design of exploratory basic research often cannot and should not identify a single readout or time point, as all parameters could reveal important information.

Comment 7: Replace post-hoc outlier removal (e.g., ROUT at 90%) with a pre-specified rule plus sensitivity analyses (with and without exclusions), or use robust methods that down-weight extreme values without deleting data.

Response 7: This concern has been newly raised in the third round of comments from the Guest Editor, so we newly address it as below:

The ROUT test is considered an acceptable means for outlier removal in this data structure. All quantitative findings were subjected to the same test, and as shown in Supplementary Figures 1-3, very few if any outliers were removed from the datasets.

The pre-exclusion data, which are still statistically significant, are available in the raw data files, uploaded onto the Harvard Dataverse: https://doi.org/10.7910/DVN/H1TCLA Please note that the datasets have only been updated to the third submission, and will be updated to reflect the final dataset if the manuscript is accepted.

As quoted below and stated in the manuscript on Page 15-16, Section 4.8 (highlighted in blue font for clarity):

Statistical outliers were identified using the ROUT test (CI 90%) and were excluded from final analyses. Outlier calculations and data sets ± outliers can be found in supporting raw data files.

Comment 8: Include batch/day/operator in the model (random or fixed effects as appropriate) rather than relying on separate checks. Report estimates to show their impact.

Response 8: Because the model is surgical, the Guest Editor was concerned about effects introduced by different operators, procedure days, and batches. These have been addressed in prior rounds of revision to the Guest Editor's satisfaction. Each experiment was conducted in two independent batches and when findings were compared statistically, described as "separate checks" above, no differences were identified (Supplementary Tables 1-3). Incorporating the above comment would require GLM or GLMM.

Comment 9: State exactly what was randomised (laser order, eye selection, imaging order, cage allocation) and confirm masking for grading and exclusion decisions.

Response 9: This has been addressed in prior rounds of revision as stated below:

9.1. Animal randomisation: This was addressed as below in Revision 3, Comment 5.2:

> Ordinarily we conduct this as described by the Guest Editor, but in this study faced inherent limitations due to the experimental variables to be tested.
>
> We were unable to randomize animals into treatment groups, as the experimental variables themselves (age and sex) were the biological characteristics of the animals. Other than this, all experimental animals were subjected to L-CNV, and there were no other treatments, for example experimental drugs.
>
> This is now included on Page 12, section 4.1, highlighted in red:
>
> > Animals were not randomized into treatment groups prior to beginning, as their biological characteristics determined the treatment group, and all animals were subjected to L-CNV, without any other experimental manipulation.

9.2. Laser and imaging order: These points were addressed in Revision 2, Response 9, highlighted in purple in the revision document:

> We provided details as to how surgical/imaging order were randomized. Please refer to Page 12, Section 4.2, highlighted in red.
>
> > Page 12, Section 4.2, Paragraph 1:
> >
> > > During the LPC procedure, alternating mice between groups were operated sequentially.
> >
> > Page 12, Section 4.2, Paragraph 2:
> >
> > > As animals were imaged, we alternated between groups sequentially.

9.3. Masking for grading and exclusion decisions: This was addressed as below in Revision 3, Response 5.3.1:

> FA image masking is described on page 13, section 4.3 (top of page), as quoted below and highlighted in red:
>
> > All images were blinded prior to any analyses, including evaluation of pre-determined exclusion criteria. First, a separate investigator coded image file names with a random number, such that the assessor was unable to determine the image's experimental group when grading severity of lesion leakage and identifying lesions that met pre-determined exclusion criteria.
>
> FA image grading and blinded application of pre-determined exclusion criteria are described on page 12, section 4.3. Below, we leave the text color-coded to indicate new additions (red) and prior information highlighted for clarity (blue).
>
> > Lesion leakage severity was then graded in blinded images according to a previously established grading scheme, and lesions were excluded from analyses according to the predetermined exclusion criteria of being either overburnt or fused (Figure S1C, D). In Figure S1, we provide examples and descriptions of lesion grading and exclusion, and in Table S1, we provide total numbers of graded and excluded lesions per group.
> >
> > …. After grading was complete and outliers identified, images were decoded and data were analyzed.

Comment 10: Report mean ± SD for descriptive summaries and 95% confidence intervals for effect estimates (odds ratios, ratios of geometric means, rate ratios) on the analysis scale.

Response 10: Because all data are in dot-plot format, our understanding is that mean ± SEM is considered acceptable. However, if requested by the Editor-in-chief, we will make this update. The 95% confidence intervals would only apply to the linear modelling requested.

Comment 11: Provide the exact number of animals contributing to each panel/table at each time-point, and add a concise CONSORT-style table of inclusions and exclusions (animals and lesions) with reasons.

Response 11: We originally provided this information in Revision 2, and further updated it in Revision 3. It is shown in Supplementary Tables 1-3.

Comment 12: Define precisely how "cross-sectional lesion volume" is derived. If based on the largest B-scan, justify this choice; where feasible, provide a volumetric measure or a pre-specified time summary (e.g., area-under-the-curve).

Response 12: This concern has been newly raised in the third round of comments from the Guest Editor, so we newly address it as below:

Cross-sectional lesion volume was based on the largest B-scan, which was determined visually by a blinded investigator. The lesion area was then measured using Image J software.

Comment 13: Supply an animal-level sample size calculation for the primary endpoint: state α, target power, minimally important difference on the analysis scale, variance source, and attrition allowance. Do not convert lesion counts into "effective" animal numbers. Use the resource-equation method only if a power analysis is genuinely not possible, showing the residual degrees of freedom for the planned model.

Response 13: In the above comment, the Guest Editor refers to the dataset used for power analyses to predict sample size. We used previous per-lesion datasets, as this was the analysis practice we used at the time of study design. When designing future studies, we can now use our new per-animal datasets for predictive analyses.

Comment 14: Provide analysis code and a de-identified dataset (animal-level table plus lesion-level table if used), with clear model formulas (fixed effects, random effects, link functions) and planned contrasts, to permit reproduction.

Response 14: Raw data were uploaded beginning at Revision 2: https://doi.org/10.7910/DVN/H1TCLA. This is not updated to include new calculations conducted in subsequent revisions, but if the manuscript is accepted, the dataset will be updated to its final form.

Comment 15: Update the methods, results, figures and tables to reflect the revised models, primary endpoint, multiplicity plan, handling of batch/day, outlier strategy, and the complete accounting of exclusions; revise the discussion accordingly.

Response 15: This is addressed as below:

- Primary endpoint, and multiplicity plan: not included for reasons stated above.
- Revised models: see Comment 1 above, which outlines significant revisions to the Results and Discussion section
- Handling of batch/day: Page 12, section 4.2
- Outlier Strategy and complete accounting of exclusions for each metric of disease severity is presented as follows:
    - Fluorescein angiography: Section 4.3, Supplementary Figure 1, Supplementary Table 1
    - Optical coherence tomography: Section 4.4, Supplementary Figure 3, Supplementary Table 2
    - Choroidal flat mount: Section 4.5, Supplementary Figure 5, Supplementary Table 3

- General handling of statistical outliers: Section 4.8

Comment 16: Data distribution and homoscedasticity:

16a) For continuous outcomes, examine distributions and justify transformations (e.g., log) where appropriate; present residual plots and normal Q–Q plots for fitted models.

R: We did not conduct these analyses as discussed above in Comment 4.

16b) Test and report heteroscedasticity (e.g., Levene's or Brown–Forsythe at the group level; residual vs fitted diagnostics for models). Use Welch's tests or variance-modelled LMM/GLM if variances differ.

R: We did not conduct these analyses as discussed above in Comment 4.

16c) For count data, assess over-dispersion and zero-inflation; choose negative binomial where dispersion exceeds Poisson.

R: We did not conduct these analyses as discussed above in Comment 5.

16d) For ordinal models, check proportional-odds assumptions; if violated, use partial proportional-odds or an alternative suitable model.

R: We did not conduct these analyses as discussed above in Comment 3.

1. Pfau M, Moller PT, Kunzel SH, von der Emde L, Lindner M, Thiele S, Dysli C, Nadal J, Schmid M, Schmitz-Valckenberg S, et al. Type 1 Choroidal Neovascularization Is Associated with Reduced Localized Progression of Atrophy in Age-Related Macular Degeneration. *Ophthalmol Retina*. 2020;4:238-248. doi: 10.1016/j.oret.2019.09.016
2. Shao A, Liu X, Shen W, Li Y, Wu H, Pan X, Yang Z, Xu Y, Zhu T, Wang Y, et al. Generative artificial intelligence for fundus fluorescein angiography interpretation and human expert evaluation. *NPJ Digit Med*. 2025;8:396. doi: 10.1038/s41746-025-01759-z
3. Han J, Choi S, Park JI, Hwang JS, Han JM, Lee HJ, Ko J, Yoon J, Hwang DD. Classifying neovascular age-related macular degeneration with a deep convolutional neural network based on optical coherence tomography images. *Sci Rep*. 2022;12:2232. doi: 10.1038/s41598-022-05903-7
4. Mizutani T, Ashikari M, Tokoro M, Nozaki M, Ogura Y. Suppression of laser-induced choroidal neovascularization by a CCR3 antagonist. *Invest Ophthalmol Vis Sci*. 2013;54:1564-1572. doi: 10.1167/iovs.11-9095
5. Parmar UPS, Arora A, Agarwal A, Gangaputra S, Agrawal R, Gupta V. Detection and quantification of fluorescein angiography leakage: From manual grading to advances in machine learning. *Surv Ophthalmol*. 2025. doi: 10.1016/j.survophthal.2025.08.015
6. Wilson CM, Ospina OE, Townsend MK, Nguyen J, Moran Segura C, Schildkraut JM, Tworoger SS, Peres LC, Fridley BL. Challenges and Opportunities in the Statistical Analysis of Multiplex Immunofluorescence Data. *Cancers (Basel)*. 2021;13. doi: 10.3390/cancers13123031

MUSC Health
Medical University of South Carolina

Storm Eye Institute
Ophthalmology
167 Ashley Avenue, MSC 611
Charleston, SC 29425
Office 843-792-2020
Fax 843-792-1166
MUSChealth.org/eyes

Livia Hu, MS
Managing Editor, IJMS

RE: ijms-3802232

November 12, 2025

Dear Ms. Hu,

Thank you extending the original submission deadline of November 10. We would also like to thank you for your hard work and diligence during the revisions process.

Please see the enclosed resubmission of our manuscript "Evaluation of sex differences in laser-induced choroidal neovascularization: roles of estrogen and innate immunity in age-dependent sexual dimorphism." This is responsive to the EiC's final arbitration.

We have addressed the EiC's minor requests, as outlined in the below point-by-point rebuttal, included ARRIVE documentation in the Supplementary Files, and updated our raw dataset to include additional analyses requested by the GE during the revision. In the revised manuscript, additions made per the EiC are highlighted in red font, while additions made to clarify adherence to ARRIVE guidelines are highlighted in blue font.

We thank the EiC for his thoughtful arbitration, and the GE for feedback that has both improved this manuscript's scientific rigor and highlighted an important methodological issue for further consideration in the field.

We confirm that the manuscript is not under consideration by any other journal, in part or in full. All authors have read the revised manuscript and agree with its revisions and resubmission to IJMS.

Sincerely,

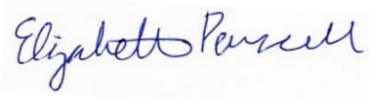

Elizabeth Pearsall, PhD
Assistant Professor of Ophthalmology
843-792-5469
pearsale@musc.edu
167 Ashley Ave HA611 Charleston SC 29425

RESPONSE TO EDITOR-IN CHIEF

EiC Summary: Thank you for your patience during the extended review process of your manuscript "Evaluation of sex differences in laser-induced choroidal neovascularisation: roles of oestrogen and innate immunity in age-dependent sexual dimorphism." I have now completed my independent review of the file, including all correspondence, the Guest Editor's comments and your detailed appeal. I appreciate the considerable effort you have invested in revising and documenting your analyses. Your responses have been careful, constructive and transparent, and the additional per-animal data and open access to your raw datasets have greatly strengthened the paper. Having considered both positions, I am satisfied that your analyses are scientifically sound and that the data support your conclusions. The Guest Editor's concerns about statistical modelling are valid in principle, but I believe that the methods you have used are appropriate for this model and dataset. Your revised manuscript now meets the journal's requirements for scientific validity and transparency. Before the paper can be accepted, I ask only that you make three minor textual additions to acknowledge the points raised… [See below text for point-by point responses].

These additions require no new analysis but will enhance clarity and ensure full transparency for readers. Once these minor revisions have been made, the manuscript will be ready for acceptance. I would also like to thank Dr Panos for his rigorous input, which has highlighted an important methodological issue for future consideration within the field.

Summary Response: We thank the EiC for their thoughtful review of the manuscript and its revisions. We have made the requested textual additions, as described point-by-point below. We have also responded to editorial requests by providing a full summary of the ARRIVE guidelines, uploaded all documents onto the submission site, and updated our raw dataset on the Harvard Dataverse to include the additional analyses requested by the GE in the revisions process.

Addition 1: Add a short statement in the Methods or Discussion noting that lesions within an eye or animal are not wholly independent and that mixed-effects models could, in principle, account for this structure, but that such approaches are not yet established for the L-CNV mouse model.

Response 1: Please see the Discussion section on Page 9, Section 2.3 with new addition highlighted in red font, as quoted below:

> Because lesions within an eye or animal are not wholly independent due to the joint contributions of both biological differences and surgical variability, mixed-effects models could, in principle, account for this structure.
>
> However, for the purposes of this study, we address this consideration by expressing data in the standard per-lesion format alongside new calculations to generate per-animal data, even though these schemas do not account for mixed-effects variability.

Addition 2: Confirm in the Statistical Analysis or Discussion section that your procedures conform to ARRIVE 2.0 reporting principles and that animals were treated as the biological unit, with all data made publicly available.

Response 2: Please refer to page 16, second paraph, highlighted in red font and quoted below:

> All procedures conformed to ARRIVE 2.0 principles, and animals were treated as the biological unit. All data are publicly available: https://dataverse.harvard.edu/dataset.xhtml?persistentId=doi:10.7910/DVN/H1TCLA

Addition 3: Add a brief comment recognising that future standardisation of the L-CNV model may incorporate hierarchical or mixed-effects methods as analytic tools become validated for small datasets. These additions require no new analysis but will enhance clarity and ensure full transparency for readers.

Response 3: We have made the following addition to the manuscript, highlighted in red font on page 9, last paragraph, and quoted below:

> As analytic tools are validated for smaller datasets, hierarchical or mixed-effects methods could become an important component of standardizing the L-CNV model.

EiC Conclusion: I would also like to thank Dr Panos for his rigorous input, which has highlighted an important methodological issue for future consideration within the field.

Response: We also thank the Dr. Panos for his valuable feedback. In fact, we are already working with a retina specialist and biostastician to develop some of the analysis platforms suggested, so this truly is a case where rigorous review has affected meaningful scientific improvements with implications beyond the current manuscript.

International Journal of
Molecular Sciences

MDPI

Article

Evaluation of Sex Differences in Laser-Induced Choroidal Neovascularization: Roles of Estrogen and Innate Immunity in Age-Dependent Sexual Dimorphism

Rui Cheng [1,†], Kamala Sundararaj [2,†], Atiyabanu Nagingar [2], Dimitrios Arhontoulis [2], Jiyang Cai [3], Peter Hao Tang [2], Kip M. Connor [4,5] and Elizabeth A. Pearsall [2,4,*]

[1] Department of Biochemistry, Wake Forest University School of Medicine, Winston-Salem, NC 27175, USA; rcheng@wakehealth.edu
[2] Department of Ophthalmology, Medical University of South Carolina, Charleston, SC 29425, USA; sundarak@musc.edu (K.S.); nagingar@musc.edu (A.N.); arhontou@musc.edu (D.A.); tanghao@musc.edu (P.H.T.)
[3] Department of Biochemistry & Physiology, Dean McGee Eye Institute, University of Oklahoma Health Sciences Center, Oklahoma City, OK 73126, USA; jiyang-cai@ouhsc.edu
[4] Angiogenesis Laboratory, Department of Ophthalmology, Massachusetts Eye & Ear, Harvard Medical School, Boston, MA 02114, USA
[5] Neuroscience and Disease Area Stronghold (DAS), Johnson & Johnson, Cambridge, MA 02142, USA; kconnor6@its.jnj.com
* Correspondence: pearsale@musc.edu
† These authors contributed equally to this work.

Abstract

Age-related macular degeneration (AMD) progresses through two phases: a non-exudative "dry" stage that compromises vision but does not involve angiogenesis, and an angiogenic "wet" phase characterized by choroidal neovascularization (CNV), where pathological neovessels originating from the choroid invade the macula. Laser-induced (L-CNV) is a surgical model and is considered the gold-standard model for wet AMD/CNV. Although AMD is an aging-related disease, most L-CNV studies are conducted in young animals, and the effects of other biological variables such as sex are not well-characterized. The present study evaluated the single and combined effects of biological sex and animal age in L-CNV. In young (8-week-old) mice, L-CNV severity did not differ between male and female mice. However, in even moderately older mice (26 weeks), L-CNV was more severe in females. Considering the immune etiology of AMD and well-documented sexual dimorphism in immunity, we determined if sex affected the innate immune response in L-CNV. On CNV lesions, M2 macrophages, which exacerbate CNV, were more prevalent in females, while M1 macrophages, which promote disease resolution, were decreased in females. In cultured macrophages, estrogen repressed M1- and promoted M2-like phenotypes, suggesting sex hormones could contribute to pro-angiogenic macrophage reprogramming in this context.

Keywords: age-related macular degeneration; AMD; choroidal neovascularization; CNV; sex differences; sexual dimorphism; inflammation; innate immune response; macrophage; M1 macrophage; M2 macrophage; macrophage reprogramming; estrogen; estrogen receptor-alpha

Academic Editor(s): Name

Received: 22 July 2025
Revised: 9 September 2025
Accepted: date
Published: date

Citation: Cheng, R.; Sundararaj, K.; Nagingar, A.; Arhontoulis, D.; Cai, J.; Tang, P.H.; Connor, K.M.; Pearsall, E.A. Evaluation of Sex Differences in Laser-Induced Choroidal Neovascularization: Roles of Estrogen and Innate Immunity in Age-Dependent Sexual Dimorphism. *Int. J. Mol. Sci.* **2025**, *26*, x. https://doi.org/10.3390/xxxxx

Copyright: © 2025 by the authors. Submitted for possible open access publication under the terms and conditions of the Creative Commons Attribution (CC BY) license (https://creativecommons.org/licenses/by/4.0/).

1. Introduction

Age-related macular degeneration (AMD) is a leading cause of blindness in the elderly population. AMD has two phases, the early non-exudative (dry) phase, characterized by retinal pigment epithelium (RPE) atrophy, accumulation of toxic lipid deposits in the subretinal space, and cell death in the neural retina [1,2]. In advanced disease, dry AMD converts to wet (exudative) AMD, in which compensatory but ultimately pathological neovessels originating from the choroid vascular plexus invade the outer retina in the process of choroidal neovascularization (CNV), which can cause irreversible central blindness [3,4].

Age-adjusted clinical data demonstrate increased AMD severity in female patients, consistently identifying female sex as a risk factor for developing multiple aspects of advanced disease [5]. Advanced dry AMD pathologies associated with conversion to wet AMD are more common in female patients [6–8]. Moreover, females are more likely to develop CNV, the most sight-threatening AMD pathology [5,9–12]. Despite robust clinical evidence of sexual dimorphism, clinical management of AMD is not sex-specific, and the underlying biological processes and molecular mechanisms for sexual dimorphism are incompletely understood. Delineating the operative physiological processes and molecular mechanisms of AMD sexual dimorphism could lay the groundwork for new therapeutic approaches. Additionally, because the mechanisms for this robust and clinically significant phenomenon are largely unknown, these studies could identify paradigm-shifting disease mechanisms that are impactful to the AMD field.

To meet these goals, it is necessary to determine if sex differences are present in animal models of AMD, and if so, to identify the pathophysiological and molecular underpinnings. No presently available animal models fully recapitulate the process of AMD in humans, including CNV [13,14]. Laser-induced CNV (L-CNV) is a very common and well-accepted CNV/wet AMD model. In this surgically-induced model, laser photocoagulation is used to rupture the Bruch's membrane, causing neovessels originating from the choroid to invade the outer retina, forming CNV lesions [15]. L-CNV is considered a gold-standard model for CNV secondary to wet AMD [13], and was used to develop anti-VEGF therapy, the standard of care for CNV patients, supporting its relevance to human disease [16,17]. In fact, L-CNV is considered a standard pre-requisite for wet AMD clinical trials [15,18].

The clinical importance and widespread use of the L-CNV model emphasizes the need to identify biological variables that affect disease etiology and severity. Although AMD is an aging-related disease, L-CNV can be surgically induced at any age, and young animals (~6–8 weeks) are used routinely, and recommended as an optimal age [19]. The importance of age as a biological variable is underscored by prior studies demonstrating that L-CNV is more severe in senescent animals (64 weeks) [20].

Sex is not well-standardized as a potential biological variable in the L-CNV model, and increased disease severity in female AMD patients prompted us to thoroughly investigate the effect of animal sex in the model. Further, because L-CNV is affected by age [20], we sought to determine whether animal age affected any potential sexual dimorphism. To address these experimental questions, we induced L-CNV in young (8-week-old) and middle-aged (26-week-old) animals of both sexes and measured multiple parameters of disease severity, including lesion leakage in live animals, cross-sectional lesion volume in live animals, and neovessel size using histology.

On Days 3, 5, and 7 post-CNV, lesion leakage was measured using fluorescein angiography (FA), in which the leakage of fluorescein dye from CNV lesions is assessed in blinded images using an established grading system [21]. On days 3, 5, and 7 post-CNV, optical coherence tomography (OCT) was used to measure lesion size in live animals, which reflects not only the extent of vascular outgrowth, but also lesion edema [22]. Choroids from animals on Day 7 post-CNV were flat-mounted and vessels labelled

histologically to measure the size of neovessels that comprise L-CNV lesions [23]. These distinct but interrelated parameters allowed us to determine the effects of experimental variables on different aspects of L-CNV pathology.

Macrophages, part of the innate immune response, play central roles in AMD, with dynamic phenotype- and context-specific effects that can either suppress or exacerbate disease [24,25]. Environmental stimuli polarize macrophages into two broadly-defined theoretical phenotypes, with M1-like macrophages promoting inflammation and M2-like macrophages suppressing inflammation, although macrophage populations are much more heterogenous than this simplified linear paradigm suggests [26]. Macrophages are central regulators of angiogenesis with phenotype-dependent effects; in most contexts M1-like macrophages are anti-angiogenic, while M2-like macrophages are generally pro-angiogenic [27]. Prior studies suggest that in some contexts, M1-like macrophage populations suppress [28,29], while M2-like macrophages promote [30–32], L-CNV. Further, in patient samples, M2-like macrophages and the M2/M1 ratio are increased in neovascular AMD [33,34].

Many aspects of the immune response are sexually dimorphic, and in most contexts, the innate and adaptive immune responses are much more robust in females [35]. Females are more subject to immune dysfunction and autoimmunity [36], prompting the hypothesis that this could be responsible in part for increased AMD severity in females. We thus examined macrophage polarization in male and female L-CNV mice by quantifying M1- and M2-like macrophages on CNV lesions. Female sex hormones, especially estrogen, play a prominent role in female immune dysfunction. In macrophages, estrogen suppresses M1-like macrophage polarization and promotes M2-like macrophage polarization [37–39]. We therefore determined whether estrogen affected experimental M1- and M2-like macrophage polarization in vitro.

Together, these studies provide valuable information for (a) standardizing the widely-used L-CNV model, (b) determining the individual and combined effects of biological variables in this experimental system, and (c) the physiological and molecular underpinnings of AMD sexual dimorphism.

2. Results

2.1. L-CNV Was Not Sexually Dimorphic in Young Mice

To determine if CNV was sexually dimorphic in young mice, L-CNV was induced in 8-week-old male and female animals, and disease severity was measured at multiple time points. FA was used to measure lesion leakage, OCT was used to measure cross-sectional lesion volume, and histological analyses of choroidal FMs were used to measure the size of neovessels. We analyzed FA, OCT, and FM data at a lesion-based level, where each lesion was considered an independent replicate, which is the standard data analysis practice in the L-CNV model.

However, individual lesions could also be considered technical, rather than biological replicates. Therefore, we also conduced per-animal data analyses in parallel, where all lesions in a single animal were considered technical replicates, and averaged prior to further analyses. We then considered individual animals as biological replicates, which were used to determine statistical significance. Our statistical findings were similar between approaches, but in the interest of scientific rigor and model standardization, we addressed this important point. The calculations used for animal-level analyses can be found in Materials and Methods Section 4.3 (FA), 4.4 (OCT) and 4.5 (FM). Side-by-side comparisons of per-lesion versus per-animal data can be found in Supplementary Figure 2 (FA), Supplementary Figure 4 (OCT), and Supplementary Figure 6 (FM).

The early-stage L-CNV response did not differ between sexes in 8-week-old mice. Neither Day 3 nor Day 5 lesion leakage, as measured by FA in the forms of both contingency analysis of combined lesions (Figure 1a, 1c) and per-animal data, expressed as average % 2B lesions/mouse (Figure S2a, S2b) differed between male and female mice. (Figure 1a, 1c, S2a, S2b). Cross-sectional lesion volume, as measured by OCT, did not differ on Day 3 or Day 5 at the per-lesion (Figure 1b, 1d) or per-animal levels (Figure S4a, S4b).

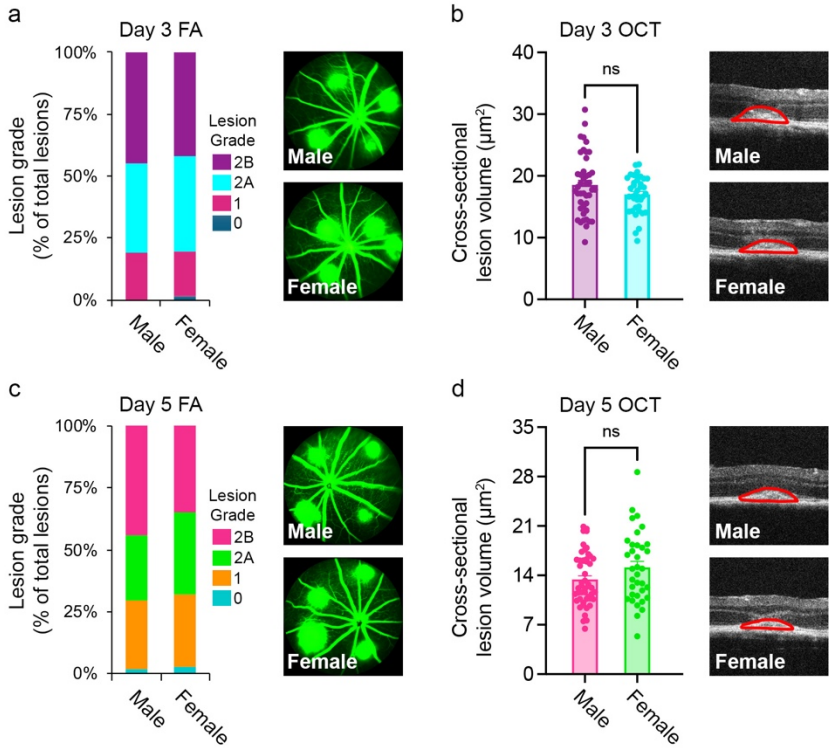

Figure 1. In young mice, sex did not affect the early-stage L-CNV disease response. Eight-week-old male and female mice were subjected to L-CNV, and disease severity measured in animals Day 3 and Day 5 post-CNV. (a) In Day 3 mice, lesion leakage, as measured by fluorescein angiography (FA) was similar in young male and female mice (Male n = 9 mice, 78 lesions; Female = 10 mice, 67 lesions, χ^2 p = 0.71). (b) On Day 3, cross-sectional lesion volume, as measured by optical coherence tomography (OCT), was similar in male and female mice (Male n = 8 mice, 43 lesions; Female n = 7 mice, 38 lesions; ns, p = 0.09). (c) On Day 5, lesion leakage was similar in male and female mice (Male n = 10 mice, 61 lesions; Female = 10 mice, 72 lesions; χ^2 p = 0.68). (d) On Day 5, cross-sectional lesion volume was similar in young male and female mice (Male n = 10 mice, 49 lesions; Female n = 10 mice, 35 lesions; ns, p = 0.07). Statistical significance was determined using contingency analyses (a, c) or two-tailed unpaired Student's t-tests (b, d).

Similarly, mid-stage disease severity was not sexually dimorphic in 8-week-old animals. Day 7 lesion leakage (FA) did not differ between males and females at per-lesion or per-animal levels (Figure 2a, S2c), nor did OCT cross-sectional lesion volume (Figure 2b, S4c). Neovascular lesion area, as measured by isolectin labelling of neovessels on choroidal FM, did not differ between young male and female mice on Day 7 at per-lesion or per-animal levels (Figure 2c, S6a).

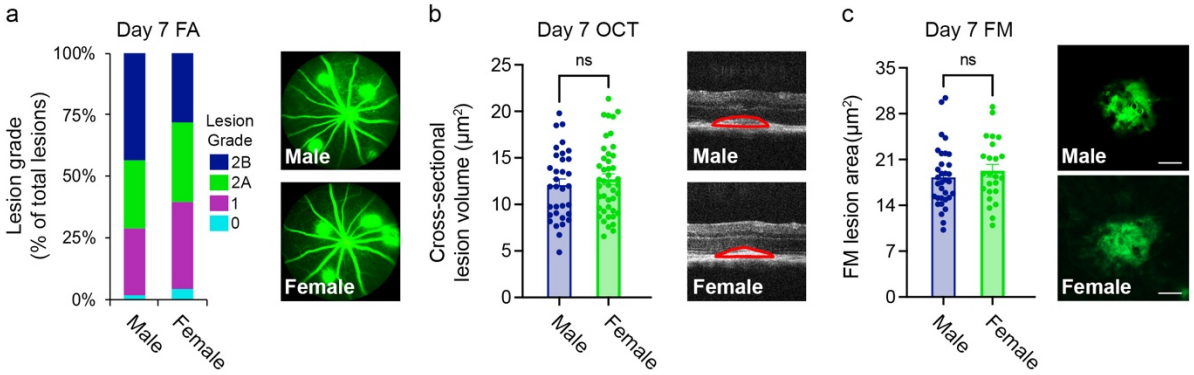

Figure 2. In young mice, mid-stage L-CNV severity did not differ between sexes. Eight-week-old male and female mice were subjected to L-CNV, and disease severity measured Day 7 post-CNV. (a) Lesion leakage was unchanged between young Day 7 male and female L-CNV mice (Male $n = 9$ mice, 55 lesions; Female $n = 10$ mice, 68 lesions, χ^2 $p = 0.30$). (b) Cross-sectional lesion volume was similar in male and female mice on Day 7 (Male $n = 10$ mice, 33 lesions; Female $n = 10$ mice, 43 lesions; ns, $p = 0.49$). (c) Neovessel lesion area, as measured histologically by choroidal flat mount (FM), was comparable in Day 7 male and female L-CNV mice (Male $n = 10$ mice, 33 lesions; Female $n = 8$ mice, 24 lesions; ns, $p = 0.42$). Scale bar, 50 μm. Statistical significance was determined using contingency analyses (a) or two-tailed unpaired Student's t-tests (b, c).

2.2. Female Sex Exacerbated L-CNV in Middle-Aged Mice

To determine if age affected sex differences, L-CNV was induced in 26-week-old animals, and multi-parameter disease severity measured in both sexes and across time points as described above.

In contrast to young animals, the early-stage L-CNV response was more severe in 26-week-old female mice relative to age-matched males. Day 3 lesion leakage (FA) was increased in females at both the per-lesion and per-animal levels (Figure 3a, S2d), and cross-sectional lesion volume (OCT) was significantly larger at both per-lesion and per-animal levels (Figure 3b S4d). Day 5 lesion leakage was also more severe in females (Figure 3c, S2e), and Day 5 cross-sectional lesion volume was larger (Figure 3d, S4e). Mid-stage L-CNV was also sexually dimorphic at 26 weeks, with significantly increased lesion leakage identified by contingency analysis (Figure 4a) and an increase that did not reach statistical significance using the metric of %2B lesions (Figure S2F). All metrics of lesion size were significantly increased with larger cross-sectional lesion volume via OCT (Figure 4b, S4f), and larger lesion area in female mice via FM (Figure 4c, S6b).

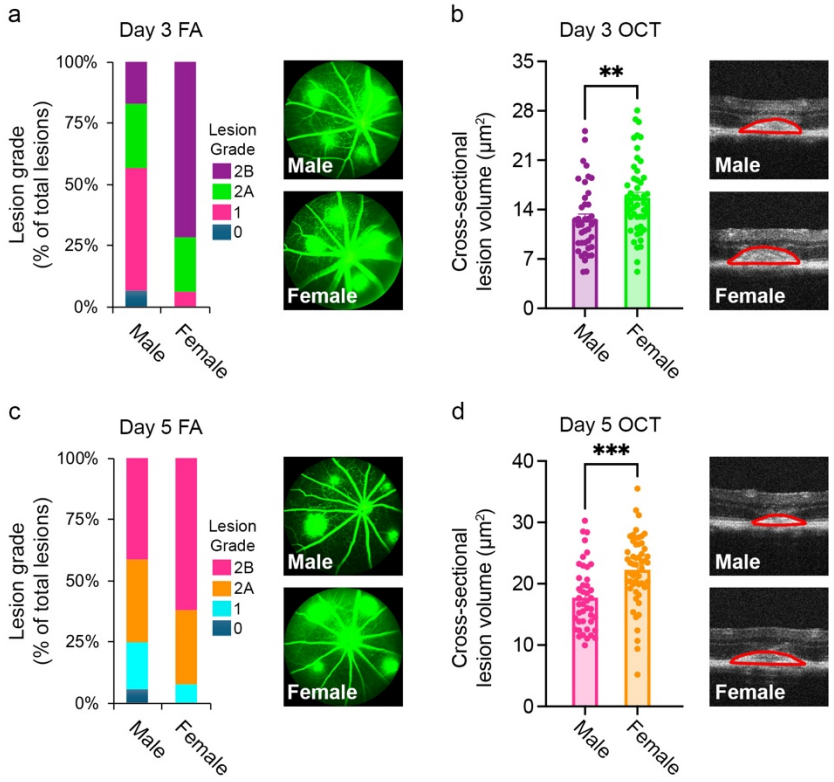

Figure 3. Female sex exacerbated the early-stage L-CNV disease response in middle-aged animals. Twenty-six-week-old male and female mice were subjected to L-CNV, and disease severity measured in cohorts Day 3 and Day 5 post-CNV. (a) Day 3 lesion leakage was more severe in aged female mice relative to age-matched males (Male n = 11 mice, 76 lesions; Female n = 11 mice, 81 lesions; χ^2 $p < 0.0001$). (b) Day 3 cross-sectional lesion volume was increased in aged female mice relative to male (Male n = 10 mice, 40 lesions; Female n = 10 mice, 50 lesions; ** $p = 0.0052$). (c) Day 5 lesion leakage was more severe in aged female mice (Male n = 10 mice, 68 lesions; Female n = 9 mice, 66 lesions; χ^2 $p = 0.01$). (d) Day 5 OCT cross-sectional lesion volume was increased in aged female mice relative to male (Male n = 10 mice, 43 lesions; Female n = 10 mice, 53 lesions; *** $p = 0.0001$;). Statistical significance was determined using contingency analyses (a, c) or two-tailed unpaired Student's t-tests (b, d).

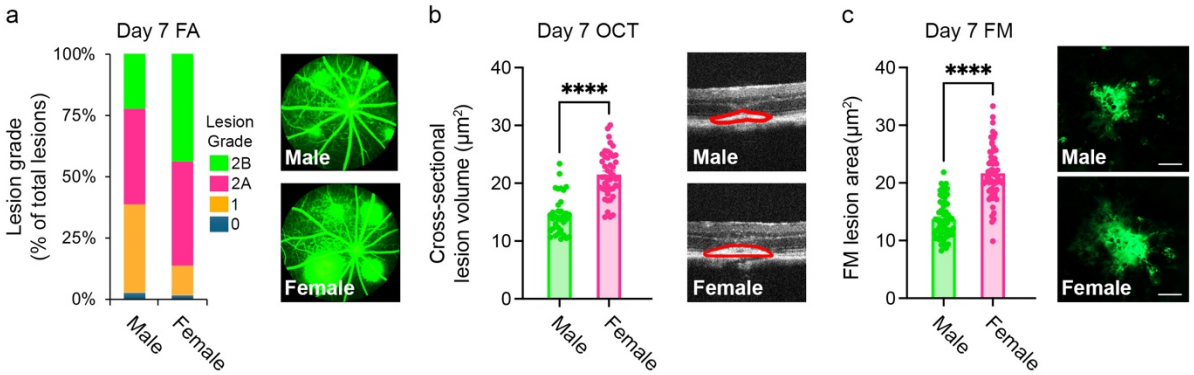

Figure 4. Mid-stage L-CNV was more severe in middle-aged female animals relative to age-matched males. Twenty-six-week-old male and female mice were subjected to L-CNV, and disease severity measured on Day 7. (a) Day 7 lesion leakage was more severe in aged female mice than in age-matched male mice (Male n = 10 mice, 67 lesions; Female n = 10 mice, 66 lesions; χ^2 $p = 0.005$). (b) Day 7 cross-sectional lesion volume was larger in aged female mice than in male (Male n = 9 mice, 34 lesions; Female n = 10 mice, 44 lesions; **** $p < 0.0001$). (c) FM lesion size was larger in aged female

mice relative to male. Scale bar, 50 μm. (Male n = 10 mice, 59 lesions; Female n = 10 mice, 63 lesions; **** $p < 0.0001$). Statistical significance was determined using contingency analyses (a) or two-tailed unpaired Student's t-tests (b, c).

2.3. Anti-Inflammatory Macrophage Phenotype in Female L-CNV Mice

Immunohistochemistry was utilized to determine if female sex affected macrophage phenotype in L-CNV. Histological analyses of choroidal flat-mounts from 26-week-old CNV mice revealed that both Iba1$^+$ (pro-inflammatory) and CD86$^+$ (anti-inflammatory) macrophages were present on Day 7 CNV lesions (Figure 5a). Pro-inflammatory Iba1$^+$ macrophages were decreased in female animals relative to males (Figure 5b), while anti-inflammatory CD86$^+$ macrophages were increased in females (Figure 5c).

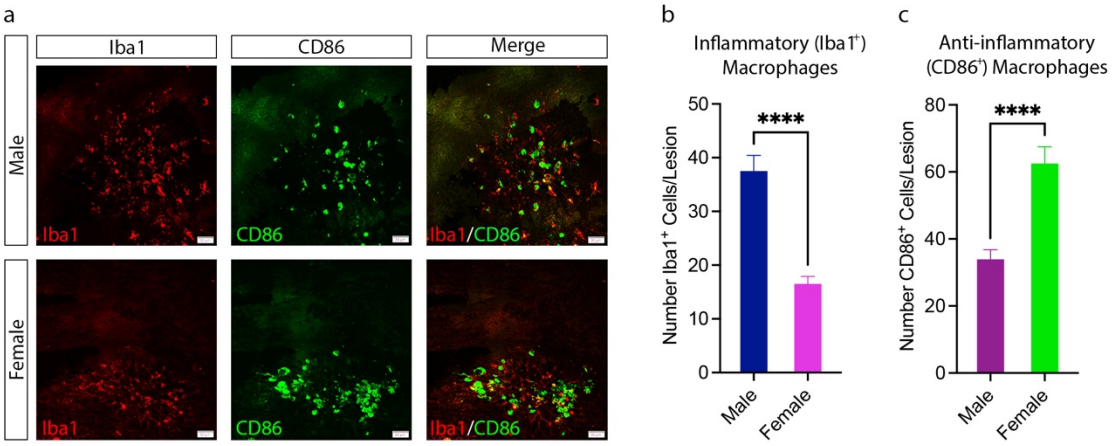

Figure 5. Anti-inflammatory phenotype of L-CNV lesion-localized macrophages in female mice. (a) Choroidal flat-mounts of male and female L-CNV mice were co-stained with pro-inflammatory macrophage marker Iba1 and anti-inflammatory macrophage marker CD86. (b,c) Iba1$^+$ and CD86$^+$ cells were counted on each lesion, revealing that (b) Inflammatory (Iba1$^+$) macrophages were decreased in females and (c) Anti-inflammatory (CD86$^+$) macrophages were increased in females. **** $p \leq 0.0001$, unpaired two-tailed Student's t-test.

2.4. Estrogen Suppressed M1-Like and Promoted M2-Like Macrophage Phenotypes

To determine if estrogen affected macrophage polarization, RAW 264.7 cells were M1-skewed ± co-treatment with 17β-estradiol (estrogen, E2) or the estrogen receptor-alpha (ERα) agonist Propyl pyrazole triol (PPT), and mRNA levels of M1-like markers Inducible nitric oxide synthase (iNOS) and Interleukin-6 (IL-6) measured. M1 skewing upregulated *inos* and *il-6* mRNA levels, which was partially inhibited by co-treatment with estrogen or ERα agonist PPT (Figure 6a,b). This suggested that estrogen suppressed M1-like macrophage phenotypic reprogramming, potentially via ERα.

To determine effects of estrogen on anti-inflammatory macrophage phenotypes, RAW 264.7 cells were M2-skewed ± estrogen or PPT co-treatment, and mRNA levels of M2-like markers Arginase-1 (Arg-1) and Interleukin-10 (IL-10) measured. M2 skewing upregulated *arg-1* and *il-10* mRNA levels, which was further augmented by estrogen and PPT co-treatment (Figure 6c,d), suggesting that estrogen/ERα promoted M2-like macrophage phenotypic reprogramming.

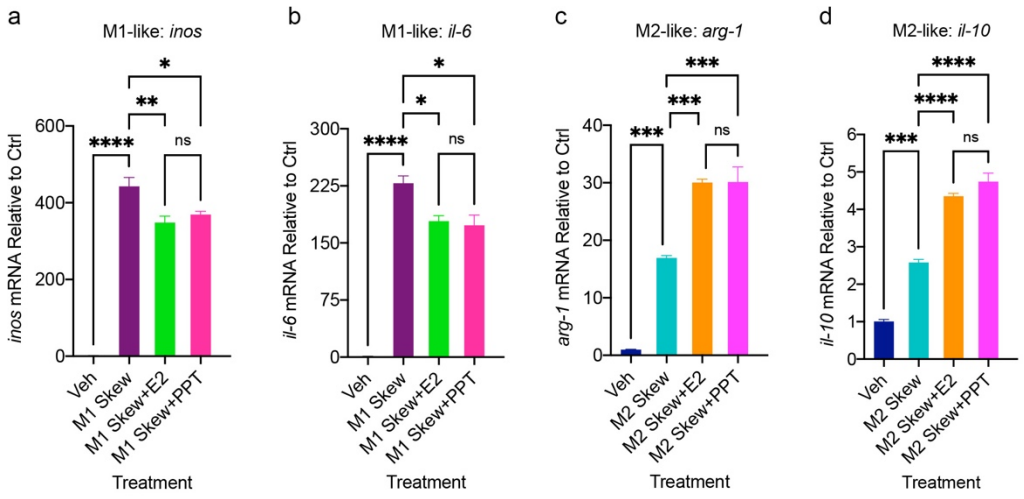

Figure 6. 17β-Estradiol and an estrogen receptor-alpha agonist promoted anti-inflammatory macrophage programming. (a,b) M1 skewing of RAW 264.7 macrophages with LPS + IFNγ up-regulated mRNA levels of M1-like macrophage markers (a) *inos* and (b) *il-6*, which was attenuated by co-treatment with 17β-Estradiol (E2) or estrogen receptor-alpha (ERα) agonist Propyl pyrazole triol (PPT). (c,d) M2 skewing with Il-4 + Il-10 + Il-13 up-regulated M2-like macrophage markers (c) *arg-1* and (d) *il-10,* which was further augmented by co-treatment with E2 or PPT. * $p \leq 0.05$, ** $p \leq 0.01$, *** $p \leq 0.001$, **** $p \leq 0.0001$, One-way ANOVA with Tukey's post-hoc comparison.

3. Discussion

In the present study, we identified age-dependent sexual dimorphism in L-CNV, in which disease was much more severe in aged female mice relative to age-matched males, but did not differ between young male and female mice. Further, we determined that macrophage polarization was sexually dimorphic in this context, with decreased M1-like and increased M2-like macrophages in female animals. Consistently, estrogen suppressed experimental M1-like polarization and augmented M2-like polarization. These findings have important implications for (1) future clinical disease management and treatment, (2) identification of relevant biological variables in the L-CNV model, and (3) the potential role of macrophages and female sex hormones in AMD sexual dimorphism.

3.1. Future Clinical Implications

Clinical data consistently demonstrate that disease is more severe in female AMD patients, and that female sex is an age-adjusted risk factor for advanced disease [5,6]. Females with AMD are more likely to develop advanced dry AMD pathologies such as drusen accumulation and geographic atrophy [5,7,8]. Females are also more likely to progress to wet AMD and develop CNV, the most sight-threatening AMD complication, which can progress to permanent central blindness if left untreated [9,10]. Despite robust clinical evidence of sexual dimorphism in AMD/CNV, the physiological and molecular underpinnings of this phenomenon remain unknown.

Clinical data prompted us to assess sex differences in L-CNV, the most commonly used animal model of wet AMD. We identified age-dependent sexual dimorphism, in which L-CNV was more severe in aged female mice relative to age-matched males, but did not differ between sexes in young mice. This underscores the biological relevance of the L-CNV model and suggests that it can be used to further investigate the bases of clinical AMD sexual dimorphism.

Further studies into the physiological and molecular mechanisms of sex differences in AMD could lay the groundwork for improved clinical management and new approaches to treatment. For example, understanding the presentation and risk factors for

advanced disease in females could better inform disease monitoring and screening, allowing earlier identification of disease progression in at-risk patients and eliminating excessive monitoring of patients at decreased risk. Because AMD sexual dimorphism is well-established clinically, new therapeutics targeting the operative physiological and molecular mechanisms are likely to have significant translational potential.

3.2. L-CNV Biological Variables and Model Standardization

We newly identified that the effects of biological sex in L-CNV are age-dependent. L-CNV was more severe in moderately-aged female animals (26 weeks) but did not differ between sexes in young animals (8 weeks), demonstrating the age-dependency of sexual dimorphism. This is highly relevant to the rigor and repeatability of L-CNV studies, as young animals (6–8 weeks) are used routinely for the model, and are recommended as an optimal age [19]. Thus, even if sex is considered as a biological variable, studies conducted in young animals could still fail to detect clinically relevant sex differences in experimental outcomes.

In fact, the first iteration of this work assessed the effects of sex on L-CNV phenotype and severity in only young (8-week-old) animals, as this is considered a standard age for the model [19]. In a 2022 pre-print, we reported the lack of sex differences in young mice as a negative data study [40]. However, stringent peer review of this work prompted us to examine sex differences in older animals. Addressing this invaluable feedback both corrected an oversight and newly identified the combined effects of age and sex on L-CNV, which is highly important to rigor/reproducibility in the model and will be helpful to other investigators in the field. This also facilitated mechanistic studies that yielded new insights into the regulatory mechanisms of CNV.

An additional consideration raised in the manuscript's review was the standard practice of treating individual CNV lesions as independent replicates for statistical analyses. Although this practice is, to the authors' knowledge, nearly ubiquitous in the L-CNV model, an individual lesion is a questionable biological replicate. Because lesions within an eye or animal are not wholly independent due to the joint contributions of both biological differences and surgical variability, mixed-effects models could, in principle, account for this structure.

However, for the purposes of this study, we address this consideration by expressing data in the standard per-lesion format alongside new calculations to generate per-animal data, even though these schemas do not account for mixed-effects variability. For OCT and FM, we calculated the mean lesion size per animal, then subjected the mean values to statistical analyses, and presented these data as dot plots (Figure S4, S6). This allowed the lesions within each animal to serve as technical replicates, and the individual animals to serve as biological replicates. We found that the consensus (significant or non-significant) for t-tests conducted on individual lesion sizes versus mean lesion size per animal, was the same for all experiments. For FA, we calculated the percent 2B lesions per animal, which was considered representative of each animal, and subjected these values to Student's t-tests for pairwise comparisons (Figure S2). Per-lesion data, which is considered categorical, was analyzed with contingency (χ^2) testing so these two statistical metrics were not directly comparable. Further, because we were subjecting a categorical variable to a mean percentage calculation, this metric was not as sensitive as that used for OCT and FM, which calculated the mean of numerical values. This suggests the ordinal grading of FA data would especially benefit from hierarchical and mixed-effects modeling.

In the future, we will further evaluate the relative merit of each approach, or potentially identify new schema for statistical analyses that account for variability between lesions and between animals, for example hierarchical models. Although beyond the scope of the present study, further developing best practices for L-CNV data analyses will be an

important contribution to model standardization. As analytic tools are validated for smaller datasets, hierarchical or mixed-effects methods could become an important component of standardizing the L-CNV model.

3.3. Effects of Aging Versus Pubertal Maturation on CNV Sexual Dimorphism

By 26 weeks of age, disease was more severe in female animals than in males. However, this is the human life stage equivalent of ~30 years, and menopausal/perimenopausal changes have not yet begun [41]. At 8 weeks of age, when L-CNV is not sexually dimorphic, mice are able to reproduce, but are the life stage equivalent of an adolescent human [42]. This suggests that the age-dependent phenotype could be related to pubertal maturation rather than true animal aging.

Although able to reproduce, ovulation and estrous cycles become more robust in the following 4–8 weeks, and animals do not reach full adult sexual maturity until approximately 12–16 weeks of age [43]. This timeline also correlates with development of the estrous cycle, so is consistent with the role of estrogen. Although serum estrogen begins to increase by approximately 6 weeks of age, levels fluctuates significantly with estrous cycle, ranging from 5–35 pg/mL in mature adult females [44]. Estrogen levels are highest during the proestrus and estrus phases of the estrous cycle [45], and as animals reach pubertal maturation, these cycles lengthen and become more pronounced [43]. Consistent with the timeline of pubertal maturation, a recent study found that in 12-week-old mice, macrophage recruitment to CNV lesions is more robust in females [46]. Further, a laser photocoagulation methodology study suggested that L-CNV is more robust in females by 16 weeks of age [19]. This is sustained through old age (64 weeks), with more-severe L-CNV in post-menopausal female mice relative to age-matched male controls [47].

Importantly, pubertal maturation and aging processes are highly variable by mouse strain and are also affected by environment. The above-referenced studies, as well as the present study, were all conducted in C57BL/6 mice. The age of onset for sexual dimorphism is likely to vary by strain, so animal age should be optimized for each strain.

3.4. Potential Role of Estrogenic Macrophage Phenotypic Reprogramming in Sexual Dimorphism

AMD is increasingly recognized as an autoimmune disease [48], and indeed, the most significant genetic risk factors for AMD are mutations that cause overactivation of the complement system, a central regulator of innate immunity, resulting in pathological overactivation of the innate immune response [49]. Immunity is highly sex-dependent, and the innate immune response to tissue damage is much more robust in females, including that of ocular tissue [50]. Estrogen signaling promotes increased macrophage activation in response to tissue damage, so the early inflammatory response is more robust in females versus males [39]. However, estrogen also accelerates resolution of the inflammatory response by stimulating the M1-M2 transition [39], which represses inflammation and stimulates reparative anti-inflammatory macrophages [51,52]. Its effects on inflammation are thus biphasic, but ultimately induce a pro-angiogenic macrophage phenotype.

In many contexts, M1-like macrophages are pro-inflammatory and anti-angiogenic, while M2-like macrophages are anti-inflammatory and pro-angiogenic [27]. Considering the generalized bias towards M2-like phenotypes in females, we assessed macrophage polarization in our model, identifying that on L-CNV lesions, M1-like macrophages were decreased, while M2-like macrophages were increased, in female mice. Consistently, prior studies suggest that some M1-like macrophage populations suppress L-CNV [28,29], while some M2-like populations exacerbate L-CNV [30–32]. We thus postulate that the M2 phenotypic shift in female L-CNV mice could contribute to sexual dimorphism. Importantly, the linear M1/M2 paradigm is grossly over-simplified; in CNV, ocular macrophages are comprised of at least 12 subpopulations with distinct and in some cases

paradoxical functions [46,53]. We expect that further studies with high-resolution phenotypic analyses, such as single-cell transcriptomics, will yield more insight into the role of macrophage sexual dimorphism in AMD and L-CNV.

Estrogen plays a prominent role in autoimmune disease, and estrogen supplementation exacerbates L-CNV [47]. We postulated that this could be due in part to estrogenic regulation of macrophage polarization. Consistently, we found that estrogen suppressed M1- and promoted M2-like macrophage polarization. ERα is responsible for many of estrogen's immunomodulatory effects, and consistent with this notion, treatment with an ERα agonist had similar effects to that of estrogen. Future studies in the laboratory will further dissect the roles of estrogen and its receptors in immunomodulation of CNV and determine the relative contribution of estrogen to sexual dimorphism in this context. Because macrophages and other immune cells comprise only a minority of the choroid, we will utilize flow cytometric and single-cell transcriptomic approaches in future studies. We will also examine inflammation-independent effects of estrogen on CNV, for example via direct interaction with endothelial cell estrogen receptors [54].

4. Materials and Methods

4.1. Experimental Animals

C57BL6/J mice purchased from Jackson Labs (Bar Harbor, ME) were used for all studies. Mice were purchased at 7 or 25 weeks of age and allowed to acclimate for one week prior to L-CNV induction. Mice were kept in specific pathogen-free conditions and provided with standard laboratory diet and tap water ad libitum. After the acclimation period of one week, CNV was induced and image analyses conducted as described below [19,22]. Animals were not randomized into treatment groups prior to beginning, as their biological characteristics determined the treatment group, and all animals were subjected to L-CNV, without any other experimental manipulation. All animal husbandry, handling and experimental procedures were approved by the appropriate Institutional Animal Care and Use Committees prior to initiating experiments (Massachusetts Eye & Ear approval no. 14-067; University of Oklahoma Health Sciences Center approval no. 24-071; Medical University of South Carolina approval no. IACUC-2024-01804). All procedures were in accordance with the NIH Guidelines for the Care and Treatment of Laboratory Animals and the ARVO Statement for the Use of Animals in Ophthalmic and Vision Research. Animals were euthanized by cervical dislocation while under confirmed deep anesthesia, which was consistent with the recommendations of the AVMA guidelines for the euthanasia of animals.

4.2. Laser Photocoagulation and L-CNV Induction

L-CNV studies were undertaken to test the hypothesis that L-CNV severity could differ between ages and sexes using the readouts of lesion leakage (angiography), lesion cross-sectional volume (OCT), and lesion neovessel area (flat mount). Laser photocoagulation (LPC) was used to induce L-CNV as described previously [55]. LPC was performed in anesthetized mice using a 532 nm laser (Oculight GLx Laser System, IRIDEX; Mountain View, CA, USA) attached to a slit lamp. To visualize the ocular posterior pole, the cornea was applanated by applying a coverslip containing a drop of 2.5% Goniosol (HUB Pharmaceuticals, Rancho Cucamonga, CA, USA) to the ocular surface. Four lesions (100 µm spot size) were placed around the optic nerve at 2, 5, 8 and 11 o'clock using 100 mW power with a 0.1 s pulse duration. All LPC was performed by a single operator (EAP) who was extensively trained in the procedure and had demonstrated proficiency in masked positive control experiments prior to beginning the studies. During the LPC procedure, alternating mice between groups were operated sequentially. Masking groups during the procedure was not possible, as the differences between groups (animal age and sex) were visually apparent.

Mice were subjected to live animal imaging procedures described below on days 3, 5, 7, and 14 post-LPC to quantify lesion volume and leakage in live animals. As animals were imaged, we alternated between groups sequentially. Masking groups during the procedures was not possible, as the differences between groups (animal age and sex) were visually apparent. For this study, animals were euthanized at 7 days post-LPC and eyes collected for choroidal flat mount. Tissues were collected from experimental animals at earlier time points for other ongoing mechanistic studies. All surgical and imaging procedures were performed in at least two separate batches on two separate days for each cohort, which were at least one week apart. We used statistical analyses to identify significant differences in experimental readouts between batches and did not detect interbatch variations in any of our findings (Supplementary Tables 1-3).

4.3. Fluorescein Angiography and Grading of Lesion Leakage Severity

Fluorescein angiography was used to visualize blood leakage from L-CNV lesions as described previously [55]. Mice were deeply anesthetized, and subsequently injected intraperitoneally with 100 µL 2% fluorescein sodium (Akorn, Lake Forest, IL, USA). Pupils were dilated using 5% phenylephrine and 0.5% tropicamide prior to capturing fluorescein images with a Micron IV Retinal Imaging Microscope (Phoenix Research Laboratories, Pleasanton, CA, USA) equipped with Streampix software (Version 9.0). To capture images, corneas were covered with Goniosol and then placed in direct contact with the Micron IV lens. Early phase images were captured 3–5 min following fluorescein injection, and late-phase images were captured 7–10 min following fluorescein injection. Mice were subjected to FA analysis once, on either day 3, 5, or 7 post-LPC.

All images were blinded prior to any analyses, including evaluation of pre-determined exclusion criteria. First, a separate investigator coded image file names with a random number, such that the assessor was unable to determine the image's experimental group when grading severity of lesion leakage and identifying lesions that met pre-determined exclusion criteria. Lesion leakage severity was then graded in blinded images according to a previously established grading scheme, and lesions were excluded from analyses according to the predetermined exclusion criteria of being either overburnt or fused (Figure S1C, D). In Figure S1, we provide examples and descriptions of lesion grading and exclusion, and in Table S1, we provided total numbers of graded and excluded lesions per group. Lesions were graded by comparing early- and late-stage images and according to a previously established grading scheme, and were assigned grades of "0" for minimal leakage, "1" for debatable leakage, "2A" for definite leakage, and "2B" for clinically significant leakage [55]. Lesions were graded as "0" if little to no dye perfusion was present in early-stage images, and very faint fluorescence was present in late-stage images (Figure S1A). Lesions were graded as "1" if faint dye perfusion was present in early-stage images, and only modest fluorescence was present in late-stage images (Figure S1A). Lesions were graded as "2A" if hyperfluorescence was present in late-stage images, with increased fluorescence intensity but not size between early-and late-stage images (Figure S1B). Lesions were graded as "2B" if robust hyperfluorescence was present in late-stage images, with increased fluorescence intensity and size between early- and late-stage images (Figure S1B). After grading was complete and outliers identified, images were decoded and data were analyzed. Using these schemas, we were able to obtain good repeatability between batches, with no statistically significant differences identified between batches of the same treatment group/time point (Table S1).

For all experiments, age-matched males were considered the control group, while female sex was considered the experimental variable. Data were analyzed with Graph Pad Prism (V. 10). To determine the statistical significance of lesion-level data, in which lesions from all animals in each cohort were pooled and considered independent replicates, we conducted a contingency analysis (CI 95%) with each lesion grade (0, 1, 2A, 2B) considered a separate outcome, and χ^2 $p < 0.05$ considered statistically significant. To generate animal-level data, the percent of clinically significant (2B) lesions per mouse was calculated, with each individual lesion in a single mouse thus considered a technical replicate. The mean % 2B lesions/mouse was thus considered a biological replicate, and a two-tailed unpaired Student's t-test used to determine statistical significance, with $p < 0.05$ considered significant. Because this methodology calculated the average prevalence of a categorical variable, it was not as sensitive as the analyses we used for OCT and FA, in which the average of numerical values could be calculated to represent each biological replicate.

4.4. Optical Coherence Tomography

Spectral domain-optical coherence tomography (SD-OCT) was used to measure cross-sectional lesion volume in live mice. Imaging was conducted as previously using a

Bioptigen system [22]. Mice were anesthetized and pupils dilated using 5% phenylephrine and 0.5% tropicamide before being placed on a freely rotating cassette platform customized for optimal ocular alignment. AB-scans (1.4 × 1.4 mm) were captured using 100 horizontal, raster, and consecutive B-scan lines, each comprised of 1000 A-scans. Cross sectional lesion images were captured at the consecutive B-scan line with the largest lesion size. Mice were subjected to OCT analysis once, on either day 3, 5, or 7 post-LPC.

All images were blinded prior to analyses, including determining whether images met pre-determined exclusion criteria. First, a separate investigator coded image file names with a random number, such that the assessor was unable to determine the image's experimental group when identifying images that met pre-determined exclusion criteria and quantifying lesion size. Cross-sectional lesion volume was quantified using FIJI software (Version 2.9.0). For quantification, the posterior border was defined as the intraretinal space, and the anterior border was defined as the lesion edge protruding into the retina (Figure S2A,B). Pre-determined exclusion criteria included overburnt lesions (Figure S2C), fused images (Figure S2D), and insufficient lesion quality for quantification, for example poor image focus (Figure S2E) or failure to include the entire lesion on the scan (Figure S2F). After quantification was complete and outliers identified, images were decoded and data were analyzed. Using these schemas, we were able to obtain good repeatability between batches, with no statistically significant differences identified between batches of the same treatment group/time point (Table S2). Total numbers of quantified and excluded lesions are shown in Table S2.

For all experiments, age-matched males were considered the control group, while female sex was considered the experimental variable. To evaluate the statistical significance of lesion-level data, we pooled lesions from all animals of each cohort, and considered each lesion to be an independent replicate. To determine the statistical significance of mouse-level data, we calculated the mean volume of all lesions measured in each mouse (with each lesion considered a technical replicate) and used the mean lesion volume per mouse for further statistical analyses, with each mouse then considered a biological replicate. Statistical significance was determined with a two-tailed, unpaired Student's t-test, with $p < 0.05$ considered statistically significant. Statistical findings (significant or non-significant) were similar between approaches (Figure S4, Table S2). All data were analyzed using Graph Prad Prism (Version 10).

4.5. Choroidal Flat Mounts

Lesion size was measured histologically using chordal flat mounts (FMs) as previously [55]. After euthanasia, mouse eyes were enucleated 7 days post L-CNV induction and fixed in 4% PFA at room temperature for 2 h. The sclera (eyecup) was then isolated, and subsequently permeabilized in 2% BSA/10% Triton X for 5 h at room temperature or overnight at 4 °C. Vessels were labelled by incubating eyecups overnight at 4 °C with a 1:100 dilution of Alexa Fluor 488-conjugated isolectin (Invitrogen/ThermoFisher; Waltham, MA, USA). Eyecups were then flat-mounted with lesions facing up using Perma-Fluor aqueous mount (Thermo Scientific; Waltham, MA, USA). Flat mount images were captured at 20X using a Zeiss AxioCam MRm camera and Zeiss AxioObserver (Z1) microscope. The operator was blinded to treatment group while capturing images.

All images were blinded prior to further analyses. First, a separate investigator coded image file names with a random number, such that the assessor was unable to determine the image's experimental group when identifying images that met pre-determined exclusion criteria and quantifying lesion size. Lesion size was quantified using FIJI software (Version 2.9.0). Lesion borders were traced to quantify the lesion size (Figure S3A,B). Pre-

determined exclusion criteria included overburnt lesions (Figure S3C), fused lesions (Figure S3D), and for Day 14 post-CNV, resorbed lesions (Figure S3E). After quantification was complete and outliers identified, images were decoded and data were analyzed. Using these schemas, we were able to obtain good repeatability between batches, with no statistically significant differences identified between batches of the same treatment group/time point (Table S3).

For all experiments, age-matched males were considered the control group, while female sex was considered the experimental variable. To evaluate the statistical significance of lesion-level data, we pooled lesions from all animals of each cohort and considered each lesion to be an independent replicate for statistical analyses. To determine the statistical significance of animal-level data, we calculated the mean volume of all lesions measured in each mouse (with each lesion considered a technical replicate) and used the mean lesion volume per mouse for further statistical analyses, with each mouse then considered a biological replicate. Statistical significance was determined with a two-tailed, unpaired Student's t-test, with $p < 0.05$ considered statistically significant. Statistical findings (significant or non-significant) were similar between approaches (Figure S6, Table S3). All analyses were conducted using Graph Pad Prism (V. 10).

4.6. Immunohistochemistry of CNV Lesions

Immunohistochemistry (IHC) studies were conducted to test the hypothesis that macrophage phenotype could be sexually dimorphic by comparing the numbers of lesion-proximal M1-like and M2-like macrophages between age-matched male and female animals. After euthanasia, mouse eyes were enucleated 7 days post L-CNV induction and fixed in 4% PFA at room temperature for 2 h. The sclera (eyecup) was then isolated, and subsequently permeabilized in 2% BSA/10% Triton X for 5 h at room temperature or overnight at 4 °C. Eyecups were then incubated with primary antibodies against Iba-1 (Rabbit, Wako 01919741) or Cd86 (Rat, Invitrogen MA1-10299) in blocking solution overnight at 4 °C, followed by incubating with secondary antibody for 3 h (Alexa Fluor 594-conjugated Donkey Anti-rabbit, Alexa Fluor 488-conjugated Donkey Anti-rat; Jackson Immunoresearch labs). Choroids were then flat-mounted on slides with DAPI-containing Hard-Set Antifade Mounting Medium (Vector Laboratories). Digital images of CNV lesions were taken using a Biotek Cytation1 microscope as previously [56], with one high-power field (HPF) per CNV lesion. Operator was blinded to treatment group while capturing images. Numbers of $Iba1^+$ and $CD86^+$ cells/lesion were quantified in blinded images using FIJI software (Version 2.9.0), and the number of cells/lesion was compared between age-matched males and females. After quantification was complete and outliers identified, images were decoded and data were analyzed with Graph Prad Prism (Version 10). Statistical outliers were identified using the ROUT test (CI 90%) and were excluded from final analyses. No statistical outliers were identified in these studies. A student's t-test was used to assess statistical significance, with $p < 0.05$ considered statistically significant.

4.7. Animal Experimental Numbers and Exclusion Criteria

To calculate the predicted sample size for CNV studies, we use template data from a prior study of CNV mice injected with VEGF-neutralizing antibody (aflibercept), the standard of care for CNV, with Power Value = 0.99, $p = 0.01$ (Supplementary Table 5). Experiments were conducted at minimum in duplicate, beginning with $n = 5$ mice/group for each repetition, although our final numbers were sometimes lower if animals did not survive anesthesia or had to be euthanized due to endpoint criteria including: clinical signs of illness such as inactivity and hunched posture, visible inflammation or damage to the ocular surface, or conjunctivitis. The data sets are cohort-based and not longitudinal,

with each post-CNV time point consisting of completely different mice. This was because animals subjected to live-animal imaging at early time points were euthanized for tissue harvest and subsequent mechanistic analyses for unrelated studies. Experimental numbers for each datapoint are specified in figure legends, and a full summary of statistical analyses is available in Supplementary Tables 1-5.

4.8. Statistical Analyses

All raw data supporting the study have been uploaded onto the Harvard Dataverse (https://doi.org/10.7910/DVN/H1TCLA).

For pairwise comparisons of numerical values, statistical significance was assessed with an unpaired, two-tailed Student's *t*-test. For multiple comparisons of numerical values, a one-way ANOVA with Tukey's posthoc comparison was used. To assess the significance of categorical variables between groups (fluorescein angiography), a chi-squared (χ^2) test was used. Data are expressed as means ± standard error of the means (S.E.M.). Statistical outliers were identified using the ROUT test (CI 90%) and were excluded from final analyses. Outlier calculations and data sets ± outliers can be found in supporting raw data files. For all analyses, $p \leq 0.05$ was considered statistically significant.

All procedures conformed to ARRIVE 2.0 principles, and animals were treated as the biological unit. All data are publicly available: https://dataverse.harvard.edu/dataset.xhtml?persistentId=doi:10.7910/DVN/H1TCLA

4.9. Cell Culture, Macrophage Skewing, and Experimental Treatments

Macrophage skewing experiments were conducted to test the hypothesis that estrogen could affect macrophage activation/phenotype using the readout of M1- and M2-like marker gene expression. in RAW 264.7 mouse macrophage-like cells, which are of female origin and express estrogen receptors [39]. Cells were obtained directly from ATCC, and all studies conducted on passages 10–30. Unless otherwise specified, reagents were purchased from Sigma. Cells were cultured in Dulbecco's Modified Eagle Medium (DMEM) supplemented with 10% fetal bovine serum and 1% antibiotic/antimycotic solution in a humidified 5% CO_2-95% air atmosphere at 37 °C.

M1 and M2 Skewing: Cells were seeded in 12-well plates (100,000 cells/well) and allowed to adhere overnight. Biological replicates (n = 3/group) were defined as separate wells with two repetitions, and technical replicates were defined as individual RT-PCR reactions (n = 4/biological replicate). All Cytokines were purchased from BioLegend. For M1 skewing, cells were treated with 100 ng/mL LPS (Isotype 0.111:B4) + 20 ng/mL mouse IFNγ in DMEM + 10% FBS for 8 h and harvested for mRNA extraction. For M2 skewing, cells were treated with a mouse cytokine cocktail (20 ng/mL IL-4 + 20 ng/mL IL-10 + 20 ng/mL IL-13) in DMEM + 10% FBS for 8 h and harvested for mRNA extraction. For both M1 and M2 experiments, skewed cells were co-treated with vehicle, 5 nM estrogen [39], or 1 μM propyl pyrazole triol (PPT) [57].

Preparation and treatment with 17β-Estradiol: 17β-Estradiol was purchased from Sigma (E8875) and dissolved in 100% ethanol to make a 1 mM stock, which was aliquoted and stored at −20 °C until use. Just prior to treatment, PCR water was warmed to 37 °C and used to make a 1 μM aqueous stock. Water was used in lieu of PBS to avoid salt precipitation. Solution was vortexed thoroughly to mix, and absence of precipitate confirmed prior to final dilution into experimental media (5 nM).

Preparation and treatment with PPT: PPT was purchased from Cayman (10008841) and resuspended in DMSO to produce a 10 mM stock, which was aliquoted and stored at -20 °C until use. Just prior to treatment, PCR water was warmed to 37 °C and used to make a 100 μM aqueous stock prior to final dilution in experimental media (1 μM).

4.10. Reverse Transcription and Quantitative Real-Time PCR

M1 and M2 marker mRNA levels were measured in RAW 264.7 cells as described previously [58]. Total RNA was extracted using an RNeasy kit (Qiagen; Hilden, DEU) according to manufacturer instructions. cDNA was reverse transcribed with 1 μg RNA using the iScript cDNA synthesis kit (Bio-Rad; Hercules, CA, USA) per manufacturer's instructions. Gene expression was measured by semi-quantitative PCR using iQ SYBR Supermix (BioRad) per manufacturer's instructions and a QuantStudio qPCR system. The PCR mixture was heated initially at 95 °C for 5 min, followed by 40 cycles of denaturation 95 °C 10 sec and combined annealing/extension at 60 °C for 30 sec. All reactions were performed in quadruplicate and normalized to *18s*. Gene expression data analysis was performed using the ΔΔCT (comparative threshold cycle) method. Primer sequences were as follows. *18s*-Fwd TGCTGCAGTTAAAAAGCTCGT, *18s*-Rev GGCCTGCTTTGAACACTCTAA; *inos*-Fwd CATTGGAAGTGAAGCGTTTCG *inos*-Rev; CAGCTGGGCTGTACAAACCTT *Il-6*-Fwd CTTCCATCCAGTTGCCTTCT, *Il-6*-Rev CTCCGACTTGTGAAGTGGTATAG; *Arg-1*-Fwd CAGAGGTCCAGAAGAATGGAAG, *Arg-1*-Rev TCCACCCAAATGACACATAGG; *Il-10*-Fwd GCTCTTACTGACTGGCATGAG, *Il-10*-Rev CGCAGCTCTAGGAGCATGTG.

5. Conclusions

In the present study, we newly report age-dependent sexual dimorphism in L-CNV, with increased disease severity in aged, but not young, female mice relative to age-matched males, which has significant rigor/reproducibility implications. We also provide mechanistic insight into AMD sexual dimorphism, suggesting a role for estrogenic M2-like macrophage polarization.

Supplementary Materials: The following supporting information can be downloaded at: https://www.mdpi.com/article/doi/s1.

Author Contributions: Conceptualization R.C., K.S., A.N., J.C., P.H.T., K.M.C. and E.A.P.; Methodology, R.C., K.S., A.N., J.C. and E.A.P.; Validation K.S. and D.A.; Formal Analysis, R.C., K.S., A.N., D.A. and E.A.P.; Investigation R.C., K.S., A.N., D.A., J.C. and E.A.P.; Resources E.A.P., J.C. and K.M.C.; Data Curation E.A.P.; Writing—Original Draft Preparation, E.A.P.; Writing—Review and Editing, R.C., K.S., D.A. and P.H.T.; Visualization, RC; Supervision, K.M.C. and E.A.P.; Project Administration, K.M.C. and E.A.P.; Funding Acquisition, J.C., K.M.C. and E.A.P. All authors have read and agreed to the published version of the manuscript.

Funding: This work was supported by NIH grants from the National Heart, Lung, and Blood Institute: F30HLI16055 (DA), and from the National Eye institute: R01EY034742 (JC); R01EY029269 (KMC); and R01EY034247, F32EY029962, SSBO7417 (EAP).

Institutional Review Board Statement: Animal studies were performed after approval by and under strict adherence to the following: Massachusetts Eye & Ear IACUC; Approval No. 11-011A; Approval dates: 8/25/17–6/30/2021. University of Oklahoma Health Sciences Center IACUC; Approval No. 24-071; Approval date: 7/21/2025. Medical University of South Carolina IACUC; Approval No. IACUC-2024-01804; Approval date: 9/4/2024.

Data Availability Statement: The data that support the findings of this study have been uploaded onto the Harvard Dataverse https://dataverse.harvard.edu/dataset.xhtml?persistentId=doi:10.7910/DVN/H1TCLA (accessed on November 11, 2025).

Conflicts of Interest: The authors declare no conflicts of interest.

Cell Line Statement: RAW264.7 cells were obtained from ATCC (stock no. TIB-71).

References

1. Bhutto, I.; Lutty, G. Understanding age-related macular degeneration (AMD): Relationships between the photoreceptor/retinal pigment epithelium/Bruch's membrane/choriocapillaris complex. *Mol. Aspects Med*. **2012**, *33*, 295–317. https://doi.org/10.1016/j.mam.2012.04.005.
2. Cohen, S.Y.; Dubois, L.; Grenet, T.; Nghiem-Buffet, S.; Jung, C.; Fajnkuchen, F.; Delahaye-Mazza, C.; Quentel, G.; Tadayoni, R. Peripapillary Retinal Pigment Epithelium Changes in Age-Related Macular Degeneration. *Retina* **2016**, *36*, 458–464. https://doi.org/10.1097/IAE.0000000000000741.
3. Schmidt-Erfurth, U.M.; Pruente, C. Management of neovascular age-related macular degeneration. *Prog. Retin. Eye Res*. **2007**, *26*, 437–451. https://doi.org/10.1016/j.preteyeres.2007.03.002.
4. Nowak, J.Z. Age-related macular degeneration (AMD): Pathogenesis and therapy. *Pharmacol. Rep*. **2006**, *58*, 353–363.
5. Chakravarthy, U.; Bailey, C.C.; Scanlon, P.H.; McKibbin, M.; Khan, R.S.; Mahmood, S.; Downey, L.; Dhingra, N.; Brand, C.; Brittain, C.J.; et al. Progression from Early/Intermediate to Advanced Forms of Age-Related Macular Degeneration in a Large UK Cohort: Rates and Risk Factors. *Ophthalmol. Retina* **2020**, *4*, 662–672. https://doi.org/10.1016/j.oret.2020.01.012.
6. Age-Related Eye Disease Study Research Group. Risk factors associated with age-related macular degeneration. A case-control study in the age-related eye disease study: Age-Related Eye Disease Study Report Number 3. *Ophthalmology* **2000**, *107*, 2224–2232. https://doi.org/10.1016/s0161-6420(00)00409-7.
7. de Carlo Forest, T.E.; Gill, Z.; Lisker-Cervantes, A.; Gnanaraj, R.; Grove, N.; Patnaik, J.L.; Lynch, A.M.; Palestine, A.G.; Mathias, M.; Manoharan, N.; etal. Association Between Quantitative and Qualitative Imaging Biomarkers and Geographic Atrophy Growth Rate. *Am. J. Ophthalmol*. **2024**, *264*, 168–177. https://doi.org/10.1016/j.ajo.2024.03.023.
8. Joachim, N.; Mitchell, P.; Rochtchina, E.; Tan, A.G.; Wang, J.J. Incidence and progression of reticular drusen in age-related macular degeneration: Findings from an older Australian cohort. *Ophthalmology* **2014**, *121*, 917–925. https://doi.org/10.1016/j.ophtha.2013.10.043.
9. Hallak, J.A.; de Sisternes, L.; Osborne, A.; Yaspan, B.; Rubin, D.L.; Leng, T. Imaging, Genetic, and Demographic Factors Associated with Conversion to Neovascular Age-Related Macular Degeneration: Secondary Analysis of a Randomized Clinical Trial. *JAMA Ophthalmol*. **2019**, *137*, 738–744. https://doi.org/10.1001/jamaophthalmol.2019.0868.
10. Clemons, T.E.; Milton, R.C.; Klein, R.; Seddon, J.M.; Ferris, F.L.; 3rd Age-Related Eye Disease Study Research Group. Risk factors for the incidence of Advanced Age-Related Macular Degeneration in the Age-Related Eye Disease Study (AREDS) AREDS report no. 19. *Ophthalmology* **2005**, *112*, 533–539. https://doi.org/10.1016/j.ophtha.2004.10.047.
11. Jonasson, F.; Fisher, D.E.; Eiriksdottir, G.; Sigurdsson, S.; Klein, R.; Launer, L.J.; Harris, T.; Gudnason, V.; Cotch, M.F. Five-year incidence, progression, and risk factors for age-related macular degeneration: The age, gene/environment susceptibility study. *Ophthalmology* **2014**, *121*, 1766–1772. https://doi.org/10.1016/j.ophtha.2014.03.013.
12. Parikh, R.; Avery, R.L.; Saroj, N.; Thompson, D.; Freund, K.B. Incidence of New Choroidal Neovascularization in Fellow Eyes of Patients with Age-Related Macular Degeneration Treated with Intravitreal Aflibercept or Ranibizumab. *JAMA Ophthalmol*. **2019**, *137*, 914–920. https://doi.org/10.1001/jamaophthalmol.2019.1947.
13. Grossniklaus, H.E.; Kang, S.J.; Berglin, L. Animal models of choroidal and retinal neovascularization. *Prog. Retin. Eye Res*. **2010**, *29*, 500–519. https://doi.org/10.1016/j.preteyeres.2010.05.003.
14. Liu, C.H.; Wang, Z.; Sun, Y.; Chen, J. Animal models of ocular angiogenesis: From development to pathologies. *FASEB J*. **2017**, *31*, 4665–4681. https://doi.org/10.1096/fj.201700336R.
15. Rastoin, O.; Pages, G.; Dufies, M. Experimental Models in Neovascular Age Related Macular Degeneration. *Int. J. Mol. Sci*. **2020**, *21*, 4627. https://doi.org/10.3390/ijms21134627.
16. Campa, C.; Kasman, I.; Ye, W.; Lee, W.P.; Fuh, G.; Ferrara, N. Effects of an anti-VEGF-A monoclonal antibody on laser-induced choroidal neovascularization in mice: Optimizing methods to quantify vascular changes. *Investig. Ophthalmol. Vis. Sci*. **2008**, *49*, 1178–1183. https://doi.org/10.1167/iovs.07-1194.
17. Hachana, S.; Fontaine, O.; Sapieha, P.; Lesk, M.; Couture, R.; Vaucher, E. The effects of anti-VEGF and kinin B(1) receptor blockade on retinal inflammation in laser-induced choroidal neovascularization. *Br. J. Pharmacol*. **2020**, *177*, 1949–1966. https://doi.org/10.1111/bph.14962.
18. Shah, R.S.; Soetikno, B.T.; Lajko, M.; Fawzi, A.A. A Mouse Model for Laser-induced Choroidal Neovascularization. *J. Vis. Exp*. **2015**, e53502. https://doi.org/10.3791/53502.
19. Gong, Y.; Li, J.; Sun, Y.; Fu, Z.; Liu, C.H.; Evans, L.; Tian, K.; Saba, N.; Fredrick, T.; Morss, P.; et al. Optimization of an Image-Guided Laser-Induced Choroidal Neovascularization Model in Mice. *PLoS ONE* **2015**, *10*, e0132643. https://doi.org/10.1371/journal.pone.0132643.

20. Espinosa-Heidmann, D.G.; Suner, I.; Hernandez, E.P.; Frazier, W.D.; Csaky, K.G.; Cousins, S.W. Age as an independent risk factor for severity of experimental choroidal neovascularization. *Investig. Ophthalmol. Vis. Sci*. **2002**, *43*, 1567–1573.
21. Marneros, A.G.; She, H.; Zambarakji, H.; Hashizume, H.; Connolly, E.J.; Kim, I.; Gragoudas, E.S.; Miller, J.W.; Olsen, B.R. Endogenous endostatin inhibits choroidal neovascularization. *FASEB J*. **2007**, *21*, 3809–3818. https://doi.org/10.1096/fj.07-8422com.
22. Giani, A.; Thanos, A.; Roh, M.I.; Connolly, E.; Trichonas, G.; Kim, I.; Gragoudas, E.; Vavvas, D.; Miller, J.W. In vivo evaluation of laser-induced choroidal neovascularization using spectral-domain optical coherence tomography. *Investig. Ophthalmol. Vis. Sci*. **2011**, *52*, 3880–3887. https://doi.org/10.1167/iovs.10-6266.
23. Hasegawa, E.; Inafuku, S.; Mulki, L.; Okunuki, Y.; Yanai, R.; Smith, K.E.; Kim, C.B.; Klokman, G.; Bielenberg, D.R.; Puli, N.; et al. Cytochrome P450 monooxygenase lipid metabolites are significant second messengers in the resolution of choroidal neovascularization. *Proc. Natl. Acad. Sci. USA* **2017**, *114*, E7545–E7553. https://doi.org/10.1073/pnas.1620898114.
24. Ambati, J.; Anand, A.; Fernandez, S.; Sakurai, E.; Lynn, B.C.; Kuziel, W.A.; Rollins, B.J.; Ambati, B.K. An animal model of age-related macular degeneration in senescent Ccl-2- or Ccr-2-deficient mice. *Nat. Med*. **2003**, *9*, 1390–1397. https://doi.org/10.1038/nm950.
25. Sakurai, E.; Anand, A.; Ambati, B.K.; van Rooijen, N.; Ambati, J. Macrophage depletion inhibits experimental choroidal neovascularization. *Investig. Ophthalmol. Vis. Sci*. **2003**, *44*, 3578–3585. https://doi.org/10.1167/iovs.03-0097.
26. Martinez, F.O.; Gordon, S. The M1 and M2 paradigm of macrophage activation: Time for reassessment. *F1000Prime Rep*. **2014**, *6*, 13. https://doi.org/10.12703/P6-13.
27. Ji, Z.Z.; Chan, M.K.; Chan, A.S.; Leung, K.T.; Jiang, X.; To, K.F.; Wu, Y.; Tang, P.M. Tumour-associated macrophages: Versatile players in the tumour microenvironment. *Front. Cell Dev. Biol*. **2023**, *11*, 1261749. https://doi.org/10.3389/fcell.2023.1261749.
28. Apte, R.S.; Richter, J.; Herndon, J.; Ferguson, T.A. Macrophages inhibit neovascularization in a murine model of age-related macular degeneration. *PLoS Med*. **2006**, *3*, e310. https://doi.org/10.1371/journal.pmed.0030310.
29. Liu, X.; Guo, A.; Tu, Y.; Li, W.; Li, L.; Liu, W.; Ju, Y.; Zhou, Y.; Sang, A.; Zhu, M. Fruquintinib inhibits VEGF/VEGFR2 axis of choroidal endothelial cells and M1-type macrophages to protect against mouse laser-induced choroidal neovascularization. *Cell Death Dis*. **2020**, *11*, 1016. https://doi.org/10.1038/s41419-020-03222-1.
30. Zandi, S.; Nakao, S.; Chun, K.H.; Fiorina, P.; Sun, D.; Arita, R.; Zhao, M.; Kim, E.; Schueller, O.; Campbell, S.; et al. ROCK-isoform-specific polarization of macrophages associated with age-related macular degeneration. *Cell Rep*. **2015**, *10*, 1173–1186. https://doi.org/10.1016/j.celrep.2015.01.050.
31. Yuan, X.; Wu, H.; Ren, H.; Jiang, B.; Liu, W.; Yao, Q.; Wu, J.; Liu, G.; Lu, P. B7-H3 Exacerbates Laser-induced Choroidal Neovascularization by Promoting Macrophage Recruitment and Polarization via S100A8/A9. *Ophthalmic Res*. **2025**, *68*, 400–418. https://doi.org/10.1159/000546556.
32. Grossniklaus, H.E.; Ling, J.X.; Wallace, T.M.; Dithmar, S.; Lawson, D.H.; Cohen, C.; Elner, V.M.; Elner, S.G.; Sternberg, P., Jr Macrophage and retinal pigment epithelium expression of angiogenic cytokines in choroidal neovascularization. *Mol. Vis*. **2002**, *8*, 119–126.
33. Nakamura, R.; Sene, A.; Santeford, A.; Gdoura, A.; Kubota, S.; Zapata, N.; Apte, R.S. IL10-driven STAT3 signalling in senescent macrophages promotes pathological eye angiogenesis. *Nat. Commun*. **2015**, *6*, 7847. https://doi.org/10.1038/ncomms8847.
34. Penfold, P.L.; Madigan, M.C.; Gillies, M.C.; Provis, J.M. Immunological and aetiological aspects of macular degeneration. *Prog. Retin. Eye Res*. **2001**, *20*, 385–414. https://doi.org/10.1016/s1350-9462(00)00025-2.
35. Shepherd, R.; Cheung, A.S.; Pang, K.; Saffery, R.; Novakovic, B. Sexual Dimorphism in Innate Immunity: The Role of Sex Hormones and Epigenetics. *Front. Immunol*. **2020**, *11*, 604000. https://doi.org/10.3389/fimmu.2020.604000.
36. Jacobson, D.L.; Gange, S.J.; Rose, N.R.; Graham, N.M. Epidemiology and estimated population burden of selected autoimmune diseases in the United States. *Clin. Immunol. Immunopathol*. **1997**, *84*, 223–243. https://doi.org/10.1006/clin.1997.4412.
37. Ghisletti, S.; Meda, C.; Maggi, A.; Vegeto, E. 17beta-estradiol inhibits inflammatory gene expression by controlling NF-kappaB intracellular localization. *Mol. Cell. Biol*. **2005**, *25*, 2957–2968. https://doi.org/10.1128/MCB.25.8.2957-2968.2005.
38. Pepe, G.; Locati, M.; Della Torre, S.; Mornata, F.; Cignarella, A.; Maggi, A.; Vegeto, E. The estrogen-macrophage interplay in the homeostasis of the female reproductive tract. *Hum. Reprod. Update* **2018**, *24*, 652–672. https://doi.org/10.1093/humupd/dmy026.
39. Villa, A.; Rizzi, N.; Vegeto, E.; Ciana, P.; Maggi, A. Estrogen accelerates the resolution of inflammation in macrophagic cells. *Sci. Rep*. **2015**, *5*, 15224. https://doi.org/10.1038/srep15224.
40. Pearsall, E.A. Evaluation of sex differences in laser-induced choroidal neovascularization severity, phenotype and disease progression. *bioRxiv* **2022**, 2022.04.20.488904. https://doi.org/10.1101/2022.04.20.488904.
41. Nelson, J.F.; Felicio, L.S.; Randall, P.K.; Sims, C.; Finch, C.E. A longitudinal study of estrous cyclicity in aging C57BL/6J mice: I. Cycle frequency, length and vaginal cytology. *Biol. Reprod*. **1982**, *27*, 327–339. https://doi.org/10.1095/biolreprod27.2.327.

42. Bresilla, D.; Habisch, H.; Pritisanac, I.; Zarse, K.; Parichatikanond, W.; Ristow, M.; Madl, T.; Madreiter-Sokolowski, C.T. The sex-specific metabolic signature of C57BL/6NRj mice during aging. *Sci. Rep*. **2022**, *12*, 21050. https://doi.org/10.1038/s41598-022-25396-8.
43. Gaytan, F.; Morales, C.; Leon, S.; Heras, V.; Barroso, A.; Avendano, M.S.; Vazquez, M.J.; Castellano, J.M.; Roa, J.; Tena-Sempere, M. Development and validation of a method for precise dating of female puberty in laboratory rodents: The puberty ovarian maturation score (Pub-Score). *Sci. Rep*. **2017**, *7*, 46381. https://doi.org/10.1038/srep46381.
44. Ingberg, E.; Theodorsson, A.; Theodorsson, E.; Strom, J.O. Methods for long-term 17beta-estradiol administration to mice. *Gen. Comp. Endocrinol*. **2012**, *175*, 188–193. https://doi.org/10.1016/j.ygcen.2011.11.014.
45. Caligioni, C.S. Assessing reproductive status/stages in mice. *Curr. Protoc. Neurosci*. **2009**, *48*, A.4I.1–A.4I.8. https://doi.org/10.1002/0471142301.nsa04is48.
46. Droho, S.; Thomson, B.R.; Makinde, H.M.; Cuda, C.M.; Perlman, H.; Lavine, J.A. Ocular macrophage origin and heterogeneity during steady state and experimental choroidal neovascularization. *J. Neuroinflammation* **2020**, *17*, 341. https://doi.org/10.1186/s12974-020-02010-0.
47. Espinosa-Heidmann, D.G.; Marin-Castano, M.E.; Pereira-Simon, S.; Hernandez, E.P.; Elliot, S.; Cousins, S.W. Gender and estrogen supplementation increases severity of experimental choroidal neovascularization. *Exp. Eye Res*. **2005**, *80*, 413–423. https://doi.org/10.1016/j.exer.2004.10.008.
48. Camelo, S. Potential Sources and Roles of Adaptive Immunity in Age-Related Macular Degeneration: Shall We Rename AMD into Autoimmune Macular Disease? *Autoimmune Dis*. **2014**, *2014*, 532487. https://doi.org/10.1155/2014/532487.
49. Haines, J.L.; Hauser, M.A.; Schmidt, S.; Scott, W.K.; Olson, L.M.; Gallins, P.; Spencer, K.L.; Kwan, S.Y.; Noureddine, M.; Gilbert, J.R.; et al. Complement factor H variant increases the risk of age-related macular degeneration. *Science* **2005**, *308*, 419–421. https://doi.org/10.1126/science.1110359.
50. Hooper, M.J.; Wang, J.; Browning, R.; Ash, J.D. Damage-associated molecular pattern recognition is required for induction of retinal neuroprotective pathways in a sex-dependent manner. *Sci. Rep*. **2018**, *8*, 9115. https://doi.org/10.1038/s41598-018-27479-x.
51. Berghofer, B.; Frommer, T.; Haley, G.; Fink, L.; Bein, G.; Hackstein, H. TLR7 ligands induce higher IFN-alpha production in females. *J. Immunol*. **2006**, *177*, 2088–2096. https://doi.org/10.4049/jimmunol.177.4.2088.
52. Ashcroft, G.S.; Ashworth, J.J. Potential role of estrogens in wound healing. *Am. J. Clin. Dermatol*. **2003**, *4*, 737–743. https://doi.org/10.2165/00128071-200304110-00002.
53. Droho, S.; Rajesh, A.; Cuda, C.M.; Perlman, H.; Lavine, J.A. CD11c+ macrophages are proangiogenic and necessary for experimental choroidal neovascularization. *JCI Insight* **2023**, *8*, e168142. https://doi.org/10.1172/jci.insight.168142.
54. Losordo, D.W.; Isner, J.M. Estrogen and angiogenesis: A review. *Arterioscler. Thromb. Vasc. Biol*. **2001**, *21*, 6–12. https://doi.org/10.1161/01.atv.21.1.6.
55. Yanai, R.; Mulki, L.; Hasegawa, E.; Takeuchi, K.; Sweigard, H.; Suzuki, J.; Gaissert, P.; Vavvas, D.G.; Sonoda, K.H.; Rothe, M.; et al. Cytochrome P450-generated metabolites derived from omega-3 fatty acids attenuate neovascularization. *Proc. Natl. Acad. Sci. USA* **2014**, *111*, 9603–9608. https://doi.org/10.1073/pnas.1401191111.
56. Dong, L.; Cheng, R.; Ma, X.; Liang, W.; Hong, Y.; Li, H.; Zhou, K.; Du, Y.; Takahashi, Y.; Zhang, X.; et al. Regulation of Monocyte Activation by PPARalpha Through Interaction with the cGAS-STING Pathway. *Diabetes* **2023**, *72*, 958–972. https://doi.org/10.2337/db22-0654.
57. Belboul, A.; Ashworth, J.; Fadel, A.; McLoughlin, J.; Mahmoud, A.; El Mohtadi, M. Estrogen induces the alternative activation of macrophages through binding to estrogen receptor-alpha. *Exp. Mol. Pathol*. **2025**, *143*, 104971. https://doi.org/10.1016/j.yexmp.2025.104971.
58. Sundararaj, K.; Rodgers, J.; Angel, P.; Wolf, B.; Nowling, T.K. The role of neuraminidase in TLR4-MAPK signalling and the release of cytokines by lupus serum-stimulated mesangial cells. *Immunology* **2021**, *162*, 418–433. https://doi.org/10.1111/imm.13294.

Disclaimer/Publisher's Note: The statements, opinions and data contained in all publications are solely those of the individual author(s) and contributor(s) and not of MDPI and/or the editor(s). MDPI and/or the editor(s) disclaim responsibility for any injury to people or property resulting from any ideas, methods, instructions or products referred to in the content.

Item	Recommendation	Experiment	Section/Line number for recommendation
Study Design	For each experiment, provide brief details of study design, including: a. The groups being compared, including control groups. If no control group has been used, the rationale should be stated. b. The experimental unit (e.g. a single animal, litter, or cage of animals).	FA	a. Sec. 4.3, Para 3, Lines 1-3
			b. Sec. 4.3, Para 3, Lines 3-12
		OCT	a. Sec. 4.4, Para 3, Lines 1-3
			b. Sec. 4.4, Para 3, Lines 3-11
		FM	a. Sec. 4.5, Para 3, Lines 1-2
			b. Sec. 4.5, Para 3, Lines 2-10
		IHC	a. Sec. 4.6, Para 1, Line 17
			b. Sec. 4.6, Para 1, Lines 13-15
Sample Size	a. Specify the exact number of experimental units allocated to each group, and the total number in each experiment. Also indicate the total number of animals used. b. Explain how the sample size was decided. Provide details of any a priori sample size calculation, if done.	FA	a. Table S1
			b. Section 4.7, lines 1-3, Table S4
		OCT	a. Table S2
			b. Section 4.7, lines 1-3, Table S4
		FM	a. Table S3
			b. Section 4.7, lines 1-3, Table S4
		IHC	a. Table S4
			b. Section 4.7, lines 1-3, Table S4
Inclusion/Exclusion Criteria	a. Describe any criteria used for including and excluding animals (or experimental units) during the experiment, and data points during the analysis. Specify if these criteria were established a priori. If no criteria were set, state this explicitly. b. For each experimental group, report any animals, experimental units or data points not included in the analysis and explain why. If there were no exclusions, state so. c. For each analysis, report the exact value of n in each experimental group.	FA	a. Sec. 4.3, Para. 2, Lines 6-10, Fig. S1
			b. Table S1
			c. Table S1
		OCT	a. Sec. 4.4, Para. 2, Lines 8-11
			b. Table S2
			c. Table S2
		FM	a. Sec. 4.5, Para. 2, Line 6-8
			b. Table S3
			c. Table S3
		IHC	a. Sec. 4.6, Lines 16-17
			b. Section 4.6, Lines 17-18
			c. Table S4
Randomization	a. State whether randomisation was used to allocate experimental units to control and treatment groups. If done, provide the method used to generate the randomisation sequence b. Describe the strategy used to minimise potential confounders such as the order of treatments and measurements, or animal/cage location. If confounders were not controlled, state this explicitly	All	a. Sec. 4.1, Lines 6-8
			b. Sec. 4.2, Para. 1, Lines 12-13; Para 2, Lines 3-4
Blinding	Describe who was aware of the group allocation at the different stages of the experiment during: (i) Allocation (ii) Conduct of the experiment (iii) Outcome assessment (iv) Data analysis	FA	(i) Sec. 4.1, Para. 1, Lines 6-8
			(ii) Sec. 4.1, Para. 1, Lines 14-16
			(iii) Sec. 4.3, Para. 2, Lines 1-5
			(iv) Sec 4.3, Para. 2, Lines 21-22
		OCT	(i) Sec. 4.1, Para. 1, Lines 6-8
			(ii) Sec. 4.1, Para. 1, Lines 14-16
			(iii) Sec. 4.4, Para. 2, Lines 1-11
			(iv) Sec. 4.4, Para. 2, Lines 12-13

		FM	(i) Sec. 4.1, Para. 1, Lines 6-8
			(ii) Sec. 4.5, Para 1, Lines 10-11
			(iii) Sec 4.5, Para. 2, Lines 1-8
			(iv) Sec 4.5, Para. 2, Lines 9-10
		IHC	(i) Sec. 4.1, Para. 1, Lines 6-8
			(ii) Sec. 4.6, Line 14
			(iii) Sec. 4.6, Lines 14-16
			(iv) Sec. 4.6, Lines 17-18
Outcome Measures	a. Clearly define all outcome measures assessed (e.g. cell death, molecular markers, or behavioural changes). b. For hypothesis-testing studies, specify the primary outcome measure, i.e. the outcome measure that was used to determine the sample size	FA	a. Sec. 4.3, Para. 2, Lines 11-21
			b. Sec. 4.3, Para. 1, Lines 1-2
		OCT	a. Sec. 4.4, Para. 2, Lines 5-8
			b. Sec. 4.4, Para. 1, Lines 1-2
		FM	a. Sec. 4.5, Para. 2, Lines 5-6
			b. Sec. 4.5, Para. 1, Lines 1-3
		IHC	a. Sec. 4.6, Lines 14-16
			b. Sec. 4.6, Lines 1-4
Statistical Methods	a. Provide details of the statistical methods used for each analysis, including software used. b. Describe any methods used to assess whether the data met the assumptions of the statistical approach, and what was done if the assumptions were not met. [NA for all]	FA	a. Sec. 4.3, Para 3, Lines 3-11
		OCT	a. Sec. 4.4, Para. 3, Lines 3-12
		FM	a. Sec. 4.5, Para. 3, Lines 2-11
		IHC	a. Sec. 4.6, Lines 15-19
Experimental Animals	a. Provide species-appropriate details of the animals used, including species, strain and substrain, sex, age or developmental stage, and, if relevant, weight. b. Provide further relevant information on the provenance of animals, health/immunestatus, genetic modification status, genotype, and any previous procedures.	All	a. Sec. 3.3 (all); Sec. 4.1, Lines 1-5
			b.NA
Experimental Procedures	For each experimental group, including controls, describe the procedures in enough detail to allow others to replicate them, including: a. What was done, how it was done and what was used. b. When and how often. c. Where (including detail of any acclimatisation periods). d. Why (provide rationale for procedures).	FA	a. Laser Photocoagulation (LPC): Sec. 4.1, Para. 1, Lines 3-10 FA Imaging: Sec. 4.3, Para. 1, Lines 2-9
			b. Sec. 4.3, Para 1, Lines 9-10
			c. Sec. 4.1, Para 1, Lines 2-4
			d. Sec. 1, Para 5 (all)
		OCT	a. LPC: Sec. 4.1, Para 1, Lines 3-10 OCT: Sec 4.4, Para 1, Lines 3-8
			b. Sec 4.4, Para 1, Line 9
			c. Sec. 4.1, Para 1, Lines 2-4
			d. Sec. 1, Para 5 (all)
		FM	a. LPC: Sec. 4.1, Para 1, Lines 3-10 FM: Sec. 4.5, Para 1, Lines 2-3
			b. Sec. 4.5, Para 1, Line 2
			c. Sec. 4.1, Para 1, Lines 2-4
			d. Sec. 1, Para 5 (all)
		IHC	a. LPC: Sec. 4.1, Para 1, Lines 3-10 FM: Sec. 4.6, Line 4
			b. Sec. 4.6, Line 4

			c. Sec. 4.1, Para 1, Lines 2-4
			d. Sec. 2.3, Para 1, Lines 1-2
Results	For each experiment conducted, including independent replications, report: Summary/descriptive statistics for each experimental group, with a measure of variability where applicable (e.g. mean and SD, or median and range).	FA	Table S1
		OCT	Table S2
		FM	Table S3
		IHC	Table S4

SUPPLEMENTARY TABLES

Experimental Conditions				Experimental Findings					Numbers		Exclusions	
Fig Panel	**Age (wk)**	**Sex**	**Post-CNV**	**Cohort M v F χ^2 (All Lesion Grades)**	**Cohort % 2B Lesions**	**Per-Mouse % 2B**	**Per-Mouse M v F t-test**	**Inter-batch χ^2**	**No. Mice**	**No. Lesions**	**Fused**	**Over-burnt**
1A	8	M	3D	0.71	44.9	42.13 ± 7.4	0.41	0.36	9	78	2	3
	8	F	3D		41.8	26.4 ± 7.1		0.59	10	67	1	1
1C	8	M	5D	0.68	44.3	42.2 ± 10	0.65	0.56	10	61	5	0
	8	F	5D		34.7	36.3 ± 7.8		0.53	10	72	2	3
2A	8	M	7D	0.30	43.6	42.1 ± 7.4	0.14	0.64	9	55	2	3
	8	F	7D		27.9	26.4 ± 7.1		0.70	10	68	4	3
3A	26	M	3D	< 0.0001	17.1	17.24 ± 5.8	< 0.0001	0.92	11	76	0	3
	26	F	3D		71.6	73.9 ± 8.5		0.69	11	81	0	2
3C	26	M	5D	0.01	41.2	38.15 ± 7.6	0.03	>0.99	10	68	0	2
	26	F	5D		62.1	62.9 ± 7.1		0.86	9	66	1	0
4A	26	M	7D	0.005	22.4	22.56 ± 6.3	0.089	0.91	10	67	2	3
	26	F	7D		43.9	40.95 ± 8.0		0.73	10	66	1	1

Supplementary Table 1: Fluorescein Angiography (FA) experimental conditions, findings, numbers, and exclusions**. Experimental Conditions: "**Fig. Panel" refers to the main-text figure panel in which data are presented. "Post-CNV" refers to the time in days (D) following CNV induction. **Experimental Findings: "**Cohort M v F χ^{2}" refers to the p-value from contingency testing of all lesion grades (0, 1, 2A, 2B) between M vs. F animals in each condition, with all lesions from each cohort combined and each lesion considered to be an independent variable. "Cohort %2B lesions" refers to the total lesions graded "2B" relative to total lesions assigned any other grade (0, 1, or 2A). This percentage represents combined lesions from all animals in the cohort. "Per mouse % 2B" refers to the percent of lesions graded as 2B within each experimental animal (% 2B lesions/mouse ± SEM). "Per-Mouse M v F t-test" refers to the p-value in male vs. female mice in each experimental condition. Each mouse is considered a biological replicate, and lesions within each mouse (averaged prior to statistical analyses) are considered technical replicates. Interbatch χ^2 refers to the contingency testing p-value (all lesion grades) between repetitions of the same treatment group (e.g. male batch 1 vs. batch 2, 8 weeks of age, Day 3 post-CNV). **Experimental Numbers:** "No. Mice" refers to the number of experimental animals (biological replicates) in each cohort. "No. Lesions" refers to the combined number of analyzed lesions for each cohort, including all lesion grades, prior to exclusions. **Exclusions:** Specifies number of lesions excluded from analyses, as defined by the pre-determined exclusion criteria described in Fig. S1.

Experimental Conditions				Experimental Findings					Experimental Numbers		Exclusions			
Fig Panel	**Age (Wk)**	**Sex**	**Post-CNV**	**Cohort Lesion Size**	**Cohort t-test**	**Mouse lesion size**	**Per-Mouse t-test**	**Interbatch t-test**	**No. Mice**	**No. Lesions**	**Over-burnt**	**Fused**	**Img. QC**	**Stat. Outlier**
1B	8	M	3D	18.54 ± 0.74	0.09	18.69 ± 1.2	0.46	0.20	8	43	1	1	0	0
	8	F	3D	17.00 ± 0.48		17.65 ± 0.48		0.52	7	38	3	0	0	2
1D	8	M	5D	13.41 ± 0.53	0.07	13.37 ± 0.56	0.11	0.45	10	49	3	1	2	0
	8	F	5D	15.13 ± 0.84		15.72 ± 1.32		0.12	9	35	3	1	8	0
2B	8	M	7D	12.08 ± 0.65	0.49	12.01 ± 0.90	0.60	0.22	10	33	2	1	5	1
	8	F	7D	12.70 ± 0.59		12.64 ± 0.76		0.18	10	43	1	3	5	1
3B	26	M	3D	12.60 ± 0.77	0.0052	12.48 ± 0.79	0.0043	0.55	10	40	3	0	4	0
	26	F	3D	15.69 ± 0.74		16.70 ± 1.02		0.33	10	50	2	0	4	3
3D	26	M	5D	17.74 ± 0.81	0.0001	17.95 ± 1.10	0.0004	0.62	10	43	3	1	8	1
	26	F	5D	22.27 ± 0.78		23.54 ± 0.66		0.88	10	53	2	0	6	0
4B	26	M	7D	14.59 ± 0.58	<0.0001	15.70 ± 1.04	<0.0001	0.99	9	34	3	0	5	4
	26	F	7D	21.49 ± 0.60		22.12 ± 0.68		0.94	10	44	1	0	9	2

Supplementary Table 2: Optical coherence tomography (OCT) experimental conditions, findings, numbers, and exclusions**. Experimental Findings:** "Cohort lesion size" refers to the mean lesion size of all lesions in the cohort, with all animals combined (Mean ± SEM, μm^2), and "Cohort t-test" refers the M v F t-test for each experimental condition, with each lesion considered an independent replicate. "Mouse Lesion Size" refers to the average size of all lesions within each separate mouse (Mean ± SEM, μm^2), while "Mouse t-test" refers to the M v F t-test for each experimental condition, with individual mice considered biological replicates, and individual lesions in each mouse (averaged for statistical analyses) considered technical replicates. "Interbatch t-test" refers to the p-value between repetitions of the same treatment group (e.g. Male Batch 1 vs. Male Batch 2, 8 weeks of age, Day 7 post-CNV). **Experimental Numbers: "**No. Mice" refers to the number of experimental animals (biological replicates) for each cohort. "No Lesions" refers to number of lesions quantified. Exclusions refer to the total number of lesions excluded from analysis according to pre-determined exclusion criteria described in Fig. S3.

Experimental Conditions				Experimental Findings					Numbers		Exclusions		
Fig. Panel	**Age (Wk)**	**Sex**	**Post-CNV**	**Cohort Lesion Size**	**Cohort t-test**	**Per-Mouse Lesion Size**	**Per-Mouse t-test**	**Interbatch t-test**	**No. Mice**	**No. Lesions**	**Over-burnt**	**Fused**	**Stat. Outlier**
2C	8	M	7D	18.26 ± 0.81	0.42	18.27 ± 0.69	0.65	0.33	10	33	2	7	0
	8	F	7D	19.28 ± 0.98		18.87 ± 1.19		0.43	8	24	5	4	2
4C	26	M	7D	13.7 ± 0.44	<0.0001	13.93 ± 0.49	<0.0001	0.18	10	59	11	5	0
	26	F	7D	21.64 ± 0.56		22.92 ± 0.86		0.43	10	63	7	2	7

Supplementary Table 3: Flat Mount experimental conditions, findings, numbers, and exclusions. **Experimental Findings:** "Cohort lesion size" refers to the mean size of all lesions in the cohort, with all animals combined (Mean ± SEM, μm^2), and "Cohort t-test" refers the M v F t-test for each experimental condition, with each lesion considered an independent replicate. "Per-Mouse Lesion Size" refers to the average size of all lesions within each separate mouse (Mean ± SEM, μm^2), while "Per-mouse t-test" refers to the M v F t-test for each experimental condition, with individual mice considered biological replicates, and individual lesions in each mouse (averaged prior to statistical analyses) considered technical replicates. "Interbatch t-test" refers to the p-value between repetitions of the same treatment group (e.g. Male Batch 1 vs. Male Batch 2, 8 weeks of age, Day 7 post-CNV). **Experimental Numbers: "**No. Mice" refers to the total number of experimental animals (biological replicates) for each cohort. "No Lesions" refers to the total number of lesions from each cohort. Exclusions refer to the total number of lesions excluded from analysis according to pre-determined exclusion criteria described in Fig. S5.

Experimental Conditions				Experimental Findings			Experimental Numbers		
Fig Panel	**Age (Weeks)**	**Sex**	**Day Post CNV**	**Marker**	**No. (+) Cells/Lesion**	**p-value**	**No. Mice**	**No. Lesions**	**Outliers**
5B	26	M	7	Iba1	37.5±2.91	<0.0001	4	8	0
	26	F	7		16.5±1.41		3	6	0
5C	26	M	7	CD86	33.9±2.88	<0.0001	5	10	0
	26	F	7		62.5±4.99		3	6	0

Supplementary Table 4: IHC experimental conditions, findings, numbers, and exclusions. “Marker” refers to the marker used to stain lesions for each experiment. “No (+) Cells/Lesion” refers to the number of cells per lesion that stained positive for the respective markers (mean ± SEM). p-value was calculated using an unpaired, two-tailed Student’s t-test. “Outliers” refers to the number of statistical outliers identified using a ROUT test (90% confidence interval) to identify outliers in cell counts per lesion.

Parameter	Ctrl Lesion Size (Mean ± SD, μm²)	Eylea Lesion Size (Mean ± SD, μm²)	Predicted No. Lesions/Group	Predicted No. Mice/Group
Day 3 OCT	19.66 ± 4.79	17.43 ± 5.83	86	11
Day 5 OCT	15.40 ± 5.71	13.51 ± 3.41	66	9
Day 7 OCT	14.69 ± 4.9	11.72 ± 3.84	71	9
Flat Mount	20.52 ± 4.99	16.10 ± 5.72	73	10

Supplementary Table 5. Power analysis for sample size prediction. To calculate approximate number of animals required for experiments, we use prior template data from CNV mice injected with 1 μl sham (sterile saline) or Eylea (40 mg/mL aflibercept) as optimized previously[1] (Power Value = 0.99, p = 0.01). Predicted sample size refers to the number of lesions, while the predicted number of mice assumes 8 total lesions/animal, with 4 lesions/eye.

1. Ichiyama Y, Matsumoto R, Obata S, Sawada O, Saishin Y, Kakinoki M, Sawada T, Ohji M. Assessment of mouse VEGF neutralization by ranibizumab and aflibercept. *PLoS One*. 2022;17:e0278951. doi: 10.1371/journal.pone.0278951

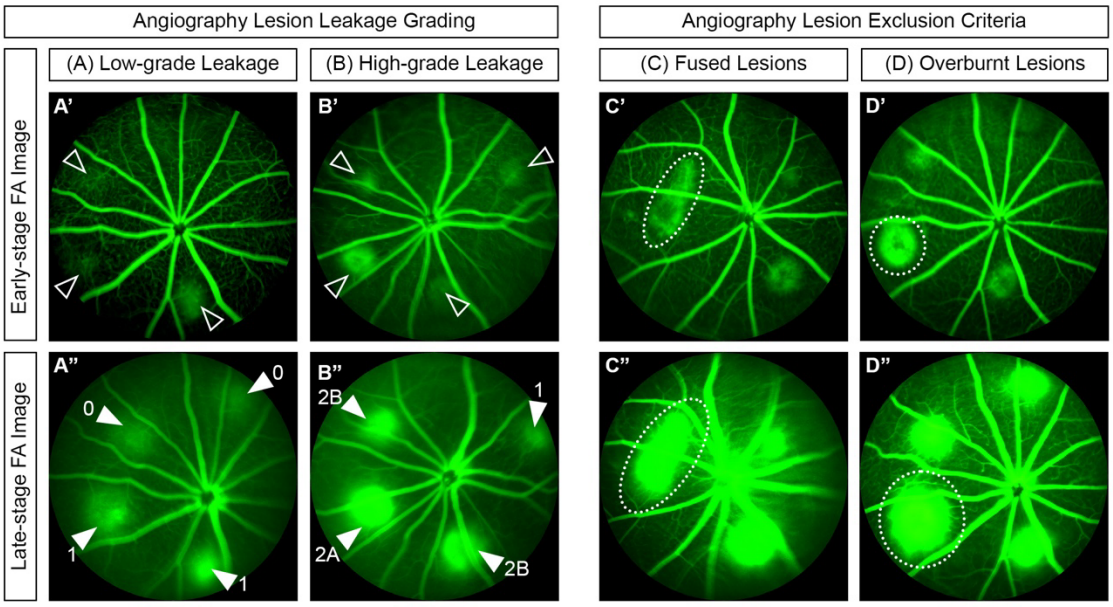

Supplementary Figure 1: Fluorescein Angiography (FA) lesion grading and exclusion criteria. Relevant to materials and methods. **(A)** Example lesion grading of low-grade leakage. Images graded "0" show little to no dye perfusion in early-stage FA images (A') and very faint fluorescence in late-stage FA images (A"). Images graded as "1" show faint dye perfusion in early-stage FA images (A') and modest fluorescence in late-stage FA lesions (A"). **(B)** Example lesion grading of high-grade leakage. Images graded as "2A" increase in fluorescence but not size between early-stage (B') and late-stage (B") FA images, and hyperfluorescence is present in late-stage images. Images graded as "2B" increase in fluorescence and size between early-stage (B') and late-stage (B") FA images. Hyperfluorescence is present. **(C)** Exclusion criteria: fused lesions. Fused lesions (indicated by ellipse) are easily visible in both early- and late-stage FA images, although in late-stage images, fused lesions can appear to be a single large lesion. **(D)** Exclusion criteria: overburnt lesions. Overburnt lesions (indicated by ellipse) exhibit hyperfluorescence in early-stage FA images (D'), and in late-stage images (D") have increased to a noticeably larger size than other high-grade lesions. Leakage sometimes perfuses unevenly at lesion borders.

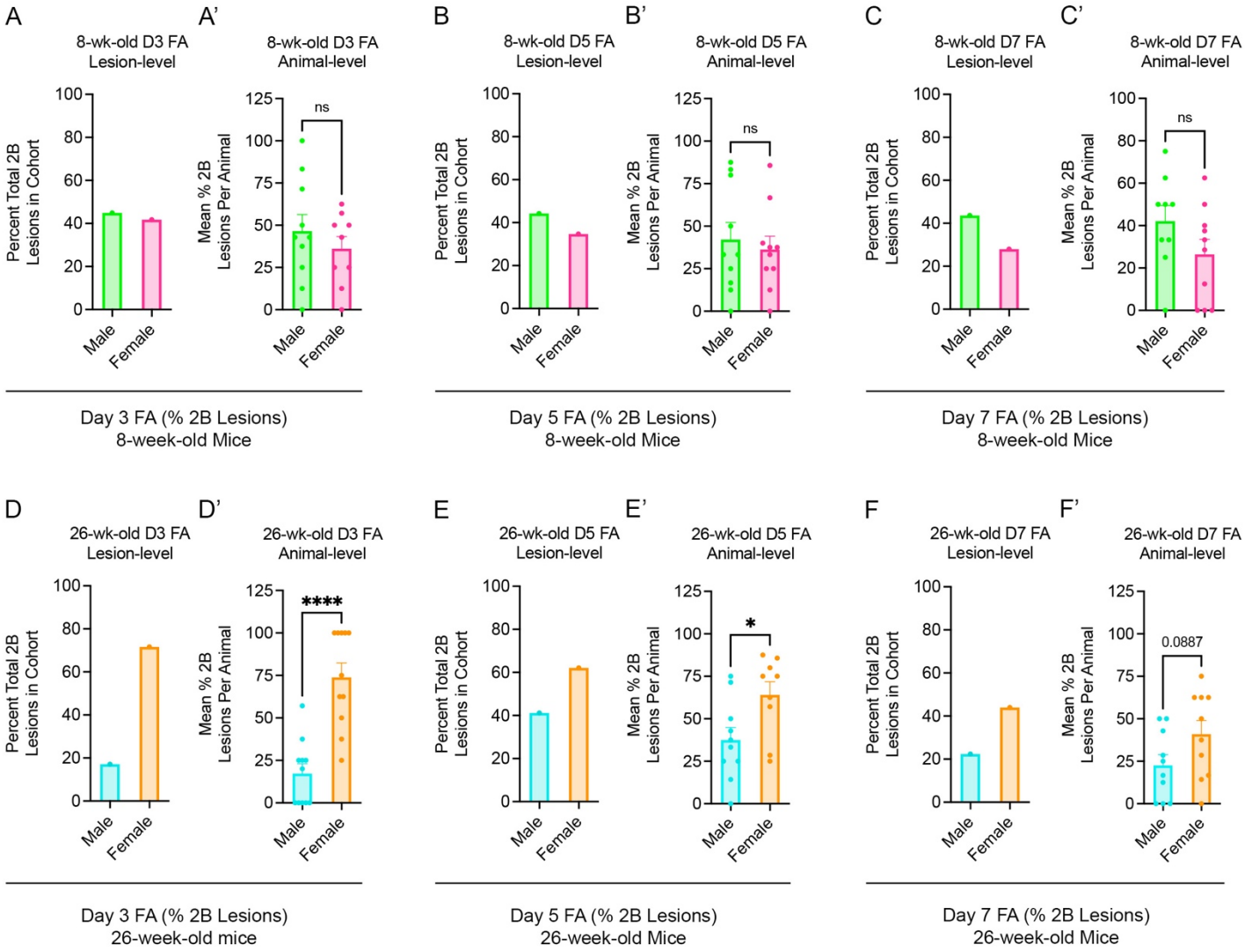

Supplementary Figure 2: Animal-level and Lesion-level fluorescein angiography analyses. Relevant to materials and methods, Figures 1-4. **(A)** Total percentage of clinically-significant 2B lesions from 8-week-old Day 3 L-CNV mice (Male n = 78, female n = 67 lesions/group). **(A')** Mean % 2B lesions per mouse in the same cohort. Individual mice are considered biological replicates, while individual lesions used to calculate % 2B lesions/mouse are considered technical replicates. (Male n = 9 mice, Female n = 10 mice). There was no significant difference between male and female mice (t-test $p = 0.41$) consistent with the contigency analysis of pooled lesion grades from the same cohort (χ^2 $p = 0.71$, shown in Fig. 1A). **(B)** Total percentage of 2B lesions from 8-week-old Day 5 L-CNV mice (Male n = 61, Female n = 72 lesions/group). **(B')** Mean % 2B lesions per mouse in the same cohort. (Male n = 10 mice, Female n = 10 mice). Statistical analyses of both mouse-level % 2B lesions/mouse (t-test $p = 0.65$) and a lesion-level contingency analysis (χ^2 $p = 0.68$, shown in Fig. 1C) did not detect significant differences between sexes. **(C)** Total percentage of 2B lesions from 8-week-old Day 7 L-CNV mice (Male n = 55, Female n = 68 lesions/group; χ^2 $p = 0.03$, shown in Figure 3A). **(C')** Mean % 2B lesions per mouse in the same cohort. (Male n = 9 mice, Female n = 10 mice; ns, $p = 0.14$). **(D)** Total percentage of 2B lesions from 26-week-old Day 3 L-CNV mice (Male n = 76, Female n = 81 lesions/group; (χ^2 $p < 0.0001$, shown in Fig. 3A). **(D')** Mean % 2B lesions per mouse in the same cohort. (Male n = 11 mice, Female n = 11 mice; **** $p <$ 0.0001). **(E)** Total percentage of 2B lesions from 26-week-old Day 5 L-CNV mice (Male n = 68, Female n = 66 lesions/group; (χ^2 p =0.01, shown in Fig. 3D). **(E')** Mean % 2B lesions per mouse in the same cohort. (Male n = 10 mice, Female n = 9 mice; * $p = 0.03$). **(F)** Total percentage of 2B lesions from 26-week-old Day 7 L-CNV

mice (Male $n = 67$, Female $n = 66$ lesions/group; (χ^2 $p = 0.005$, shown in Fig. 4A). **(F')** Mean % 2B lesions per mouse in the same cohort, which suggested leakage seerity was increased but did not reach statistical significance. (Male $n = 10$ mice, Female $n = 10$ mice; $p = 0.0887$).

‘

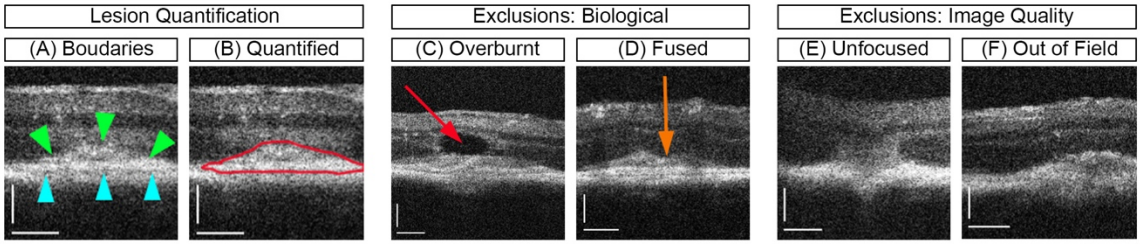

Supplementary Figure 3: Optical coherence tomography (OCT) image quantification and exclusion criteria. (A) Representative cross-sectional OCT image. In a normal OCT image, lesion boundaries are clearly defined and lesions are regularly shaped. The edge of the lesion’s protrusion into the retina is considered the anterior lesion border (green arrows), and the intraretinal space is considered the posterior lesion border (blue arrows). **(B)** Lesion shown in “A” quantified using the defined boundaries. **(C)** Exclusion criteria: overburnt lesions. Overburnt lesions are often significantly larger in size (note that image scaling differs between images; all scale bars are 100 μm) and exhibit signs of inflammation such as fluid accumulation around the lesion (red arrow). **(D)** Exclusion criteria: fused images. Although less visible on OCT than on FA, fused lesions can be spotted by fusion of lesion borders (orange area), especially when one lesion is higher-contrast (left), indicating differing distances from the focal plane. **(E)** Exclusion criteria: unfocused images. Images are not sufficiently focused to define lesion boundaries. **(F)** Exclusion criteria: lesion out of field. The entire lesion was not captured on the scan. All images: scale bars, 100 μm.

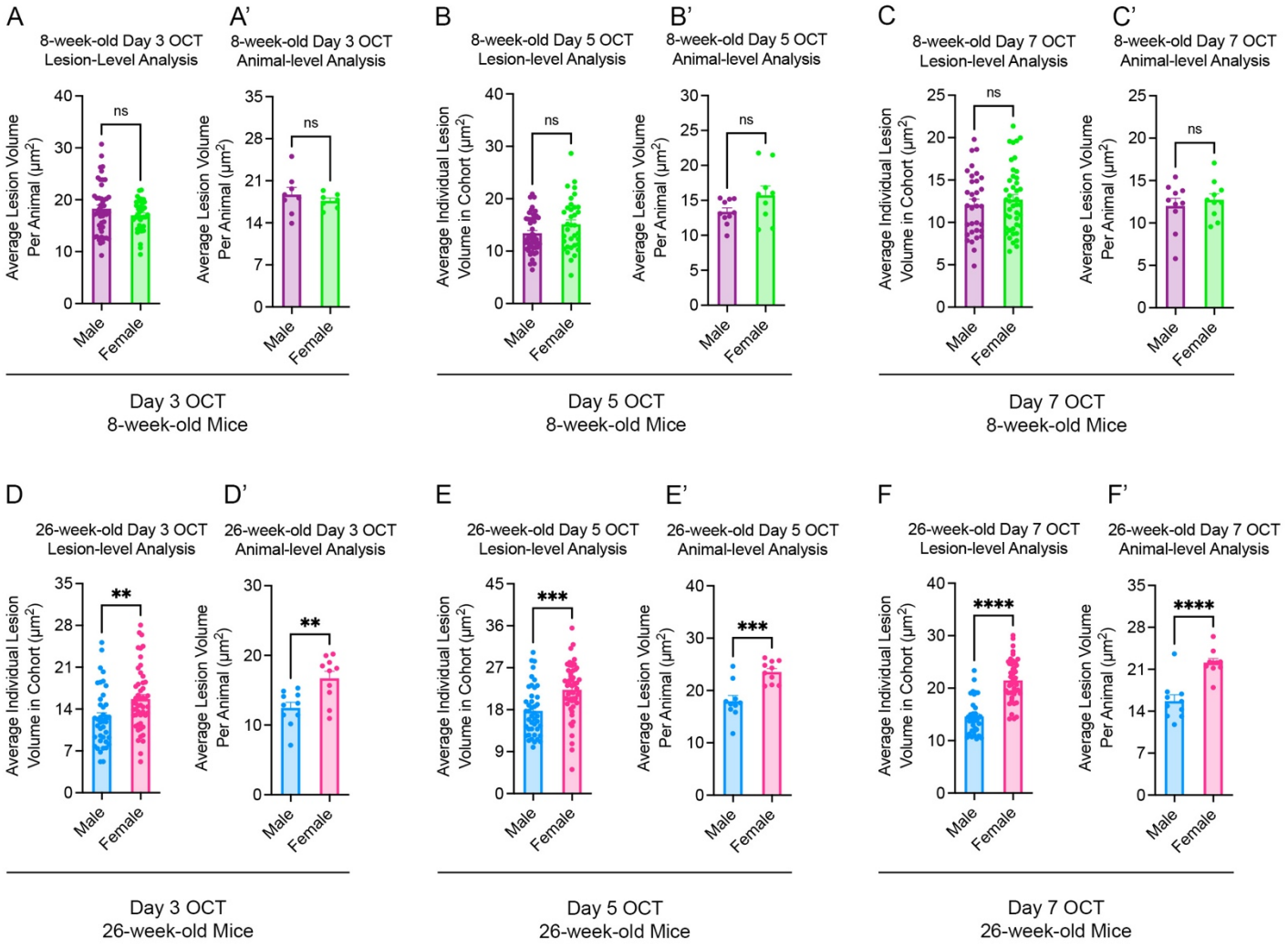

Supplementary Figure 4: Lesion-level and animal-level optical coherence tomography quantification. Relevant to materials and methods, figures 1-4. **(A)** Lesion-level quantification of OCT in 8-week-old Day 3 L-CNV mice, with lesions from all animals in each cohort pooled and considered independent replicates (Male n = 43, Female n = 38 lesions/group; ns, p = 0.09, unpaired two-tailed Student's t-test). **(A')** Animal-level quantification of OCT in the same cohort, with volumes of all lesions in each mouse averaged (serving as technical replicates), and data expressed as mean cross-sectional lesion volume per animal (biological replicate). (Male n = 8 mice, Female n = 7 mice; ns, p = 0.46, unpaired two-tailed Student's t-test). **(B)** Lesion-level quantification of OCT in 8-week-old Day 5 L-CNV mice (Male n = 49, Female n = 35 lesions/group; ns, p = 0.07). **(B')** Lesion-level quantification of the same cohort. (Male n = 10 mice, Female n = 9 mice; ns, p = 0.11). **(C)** Lesion-level quantification of OCT in 8-week-old Day 7 L-CNV mice (Male n = 33, Female n = 43 lesions/group; ns, p = 0.49). **(C')** Animal-level quantification in the same cohort (Male n = 10 mice, Female n = 10 mice; ns, p = 0.60). **(D)** Lesion-level quantification of OCT in 26-week-old Day 3 L-CNV mice, expressed as average volume of combined lesions in the cohort, with each lesion considered an independent replicate (Male n = 40, Female n = 50 lesions/group; ** p = 0.0052). **(D')** Animal-level quantification of the same cohort, expressed as mean of all lesions measured (technical replicates) in each mouse, which then represents an independent biological replicate. (Male n = 10 mice, Female n = 10 mice; ** p = 0.0043). **(E)** Lesion-level quantification of OCT in 26-week-old Day 5 L-CNV mice (Male n = 43, Female n = 53 lesions/group; *** p = 0.0001). **(E')** Animal-level quantification of the same cohort (Male n = 10 mice, Female n = 10 mice; *** p = 0.0004). **(F)** Lesion-level quantification of OCT in 26-week-old Day 7 L-CNV mice (Male n = 34, Female n = 44 lesions/group; **** $p < 0.0001$). **(E')** Animal-level analysis of the same cohort (Male n = 9 mice, Female n = 10 mice; **** $p < 0.0001$). Both analyses were consistent in the determination of significance, with similar sensitivities in detecting increased lesion volume in 26-week-old females.

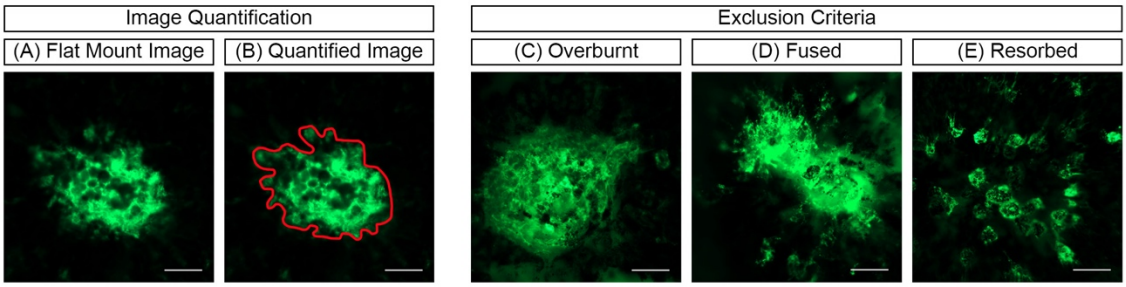

Supplementary Figure 5: Flat mount image quantification and exclusion criteria. Relevant to materials and methods. **(A)** Representative image of a normal flat-mount lesion with typical morphology and **(B)** Quantification of lesion area with typical definition of lesion boundaries. **(C)** Exclusion criteria: overburnt lesions. Overburnt lesions are generally noticeably larger in size, and have a rounded morphology that protrudes into the Z-axis. More mature capillary structures can frequently be observed. **(D)** Exclusion criteria: fused lesions. Fused lesions are indicated by fusion of two distinct lesions. **(E)** Exclusion criteria: resorbed images (Day 14 post-CNV only). After Day 7, lesions begin to regress and are ultimately resorbed into the subretinal space, where scar tissue is formed. Fully resorbed lesions are indicated by large phagocytic cells, with the lesion absent or very small.

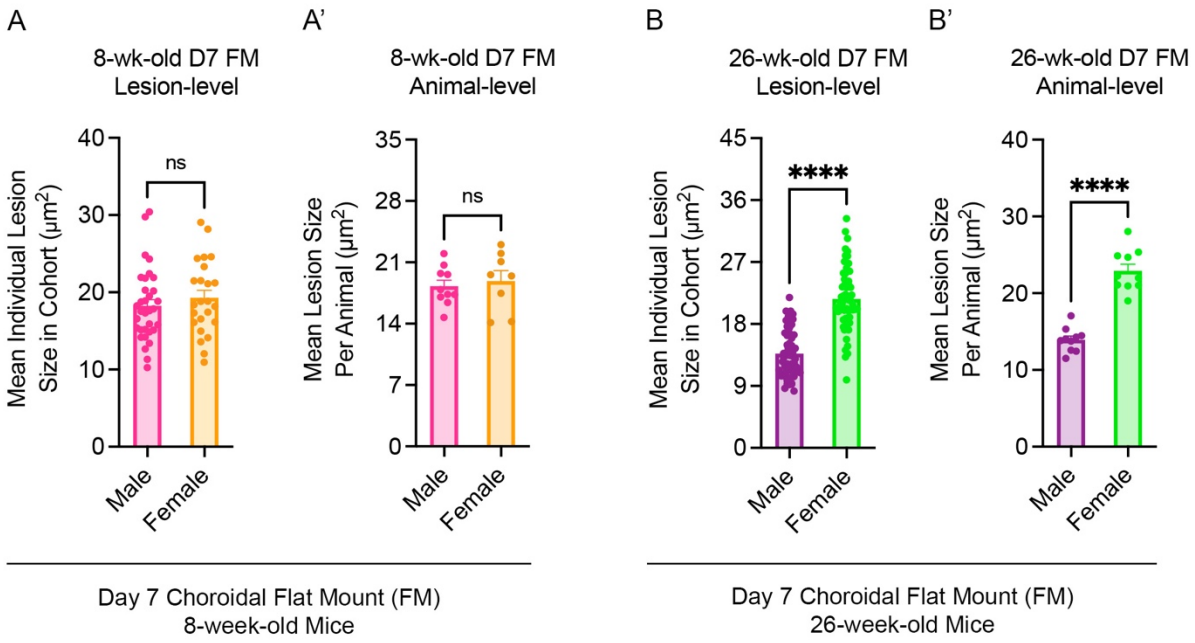

Supplementary Figure 6: Lesion- and Animal-level choroidal flat mount (FM) quantification. Relevant to materials and methods, Figure 2, Figure 4. **(A)** Lesion-level analysis of Day 7 FMs from 8-week-old L-CNV mice, with lesions from all animals in the experimental cohorts pooled and considered to be independent replicates in statistical analyses (Male n = 33, Female n = 24 lesions/group; ns, p = 0.42, unpaired two-tailed Student's t-test). **(A')** Animal-level analysis of the same cohorts, with sizes of all lesions in each mouse averaged (serving as technical replicates), and data expressed as mean lesion size per animal (biological replicate). (Male n = 10 mice, Female n = 8 mice, p = 0.65). **(B)** Lesion-level analysis of Day 7 FMs from 26-week-old L-CNV mice with each lesion considered an independent replicate (Male n = 59, Female n = 63 lesions/group; **** $p < 0.0001$). **(B')** Animal level analysis of Day 7 FMs from 26-week-old L-CNV mice, with sizes of all lesions in each mouse averaged (serving as technical replicates), and data expressed as mean lesion size per animal (biological replicate). (Male n = 10 mice, Female n = 10 mice,**** $p < 0.0001$). An unpaired, two-tailed student's t-test was used to determine statistical significance for both analysis platforms, with the same detectable sensitivity in aged females.

Author's Note:

After receiving the decision of accept pending minor revisions on November 7, we submitted the final files with requested minor revisions on November 15, 2025.

However, on November 17, 2025 the EiC issued a new decision requiring major revisions, despite no change in the referenced data below:

Your RT-qPCR methodology requires substantial revision. Key experimental details are missing or incomplete, and the current description does not meet accepted standards for transparency, reproducibility or MIQE compliance. • RNA quality control is insufficient: No evidence of RNA integrity assessment (Bioanalyzer/RIN or gel), no inhibition checks, and no confirmation of DNA-free RNA. • Reverse transcription is undefined: Priming strategy (random hexamers, oligo-dT, gene-specific), input RNA amount and RT conditions are not reported; no-RT controls are not mentioned. • Primer design and validation absent: Primer sequences, amplicon lengths, GC content, melting curves, or any specificity checks are not provided. • Amplification efficiency not measured: No standard curves, no efficiency values, no R^2, and no statement on re-optimisation of suboptimal assays. • Reference gene selection unsupported: The choice and number of reference genes are not stated; no evidence of stability analysis (geNorm/NormFinder/BestKeeper). • Replicate structure is unclear: Technical replicates appear to be treated as independent. It is not stated how many biological replicates were used or whether technical replicates were averaged. • Quantification method unspecified: No description of ΔCq/ΔΔCq, Pfaffl efficiency correction, or any normalisation procedure. • No description of controls: No-template controls, no-RT controls, or contamination checks are not reported. • Cycling conditions incomplete: Reaction volumes, reagent concentrations, and cycling parameters are missing or inadequately described. Figure 6 • The figure appears to present technical replicate scatter rather than summarised biological data. • There is no indication of efficiency correction, baseline selection, or Cq processing. • Reference gene instability is likely, but cannot be evaluated because no stability analysis is provided. • Without primer specificity or melt curves, the validity of each amplicon is unknown. • The interpretation of fold changes is not meaningful without verified efficiencies and validated reference genes. Figure 6 should be withdrawn until the qPCR dataset is fully re-analysed using validated MIQE-compliant methods. Required replacement text RNA extraction and quality control Total RNA was extracted from [tissue/cells] using [kit/method]. RNA purity was assessed by A260/280 and A260/230 ratios, and RNA integrity was evaluated using [Bioanalyzer/RIN scores or agarose electrophoresis]. Genomic DNA contamination was removed using on-column DNase treatment. Reverse transcription For each sample, [X] ng RNA was reverse-transcribed using [enzyme/kit] with [priming strategy: random hexamers/oligo-dT/gene-specific primers] in a [X µl] reaction. No-RT controls were included for every biological replicate. qPCR assay design and validation Primer sequences, amplicon lengths, GC content and accession numbers are provided in Supplementary Table X. Amplicon specificity was confirmed by melt-curve analysis or gel electrophoresis. Amplification efficiencies were determined using 5-point, 10-fold dilution series; only assays with 90–110 percent efficiency and $R^2 \geq 0.99$ were used. Reference gene evaluation Candidate reference genes were tested for stability using [geNorm/NormFinder/BestKeeper]. Only the two or three most stable genes were used for normalisation. qPCR conditions Reactions (10–20 µl) contained [2×] master mix, [X] nM primers, and [X] ng cDNA. Cycling: 95°C X min; 40 cycles of 95°C X s, 60°C X s. Melt curves were run for all SYBR Green assays. NTCs remained negative. Data processing Technical replicates were averaged. Only biological replicates were used for statistical analysis. Relative quantities were calculated using the efficiency-corrected ΔCq method (Pfaffl). Cq values, efficiencies and normalisation factors are provided in Supplementary Data. Please revise your Methods and Figure 6 accordingly and consult the MIQE and MIQE 2.0 guidelines before resubmission.

We determined that this was not a reasonable request, and submitted the below response letter.

MUSC Health
Medical University of South Carolina

Storm Eye Institute
Ophthalmology
167 Ashley Avenue, MSC 611
Charleston, SC 29425
Office 843-792-2020
Fax 843-792-1166
MUSChealth.org/eyes

Livia Hu, MS
Managing Editor, IJMS

RE: ijms-3802232

November 29, 2025

Dear Ms. Hu,

We are writing in response to the Editor-in-Chief's additional feedback following the decision to accept pending minor revisions. The EiC has now requested that RT-qPCR data in Figure 6 be significantly revised to meet MIQE standards.

Below, we propose to withdraw these data based on (i) infeasibility of this request and (ii) new experimental findings that suggest the role of estrogen remains uncertain in our disease model, so scientifically support the decision. Based on the below-provided information, we propose that:

1. All RT-qPCR data in Fig. 6 be removed from the manuscript
2. The manuscript text be revised to de-emphasize the specific role of estrogen and state that the molecular underpinnings of in vivo phenotypes will be investigated in future studies currently underway in the laboratory

We have now undergone an extensive revisions process, with an initial submission in July and five subsequent rounds of revision. The Editor-in-Chief has now had the chance to (a) review the appeal and issue an arbitration in our favor, (b) review the rest of the manuscript's contents, identifying problems in the qRT-PCR findings, and (c) consider our suggestion to withdraw this figure.

Considering the substantial time already invested, we respectfully ask in earnest that the EiC issue a final decision to either accept or reject the manuscript, allowing us to either publish the work or submit it to another journal.

Sincerely,

Elizabeth Pearsall, PhD
Assistant Professor of Ophthalmology
843-792-5469
pearsale@musc.edu
167 Ashley Ave HA613 Charleston SC 29425

RESPONSE TO EDITOR-IN CHIEF

The EiC has asked for extensive revisions to RT-qPCR data presented in Figure 6, ensuring data meet MIQE standards. Although this would improve scientific rigor, it would also necessitate extensive additional wet lab work that could require 1-2 additional months to complete:

- We have used up all our original samples, so would be required to repeat all in vitro studies in triplicate to generate new RNA/cDNA needed to run additional loading controls and gels of PCR products as requested
- The staff scientist who conducted these studies (K. Sundararaj) is no longer in the lab, so we would need to re-allocate effort of other lab personnel to conduct this work.

These data show that in RAW 294.6 macrophagic cells, estrogen suppresses M1-like inflammatory skewing and promotes M2-like anti-inflammatory skewing, which we propose as a putative mechanism for in vivo phenotypes. We are confident in the validity and repeatability of these findings, which are consistent with the literature.[1] However, as outlined below, new findings from the lab suggest that these in vitro data might not be as directly applicable to our experimental system as we had originally concluded.

Hormone receptor expression in choroidal immune cells

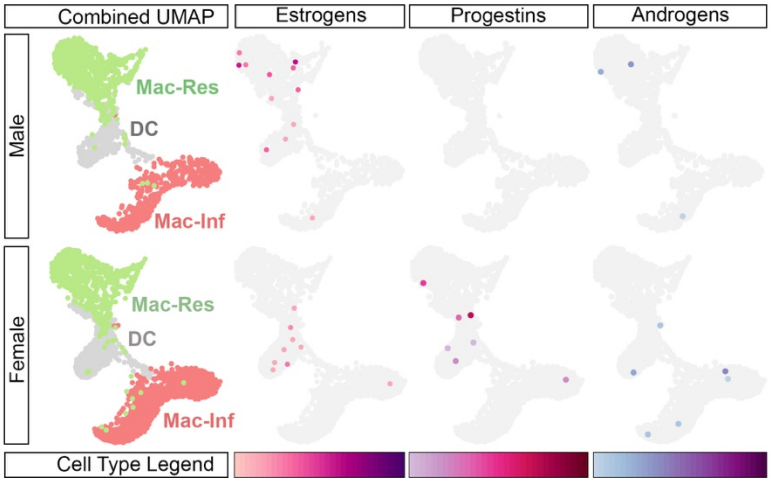

Fig. 1: scRNA-seq analysis of hormone receptor expression in human choroidal mononuclear phagocytes. **Left:** Combined UMAPs of male and female samples showing cell types: anti-inflammatory macrophages (Mac-Res), dendritic cells (DC) and inflammatory macrophages (Mac-Inf). **Right:** UMAP plots and corresponding Log2 scales (0–4) for hormone receptors, including estrogens (combined *erα*, *erβ*, *gper1*), progestins (*pgr)* and androgens (*ar).*

We are presently writing a grant proposal that will follow up on these studies, and as a part of this work, have re-interrogated a human single-cell RNA-sequencing (scRNRA-seq) database.[2] On 11/19/25, after our most recent resubmission to the EiC, we examined expression of hormone receptors in choroidal immune cells from human AMD donors and age-matched controls.

Very few macrophages expressed hormone receptors, including the estrogen receptors ERα, ERβ, and Gper1 **(Fig. 1)**. This was unaffected by disease, and further confirmed in the Human Atlas, verifying that lack of receptor expression was not age-related. These findings suggest hormone-independent factors could contribute to sex differences in immunomodulation of AMD, or at minimum that the role of sex hormones is more nuanced than originally anticipated. For example, monocytic macrophages, which are short-lived, could express estrogen receptors in the circulation and be phenotypically responsive to estrogen via similar mechanisms to our in vitro findings, but lose message-level receptor expression prior to their recruitment to the choroid. However, this is uncertain, and the underlying molecular mechanisms require further investigation before any conclusions can be made. This will require extensive studies and is the topic of our three-year proposal.

Unfortunately, the cell numbers in the above scRNA-seq dataset are too small to be statistically rigorous, so we do not deem these data worthy of publication. However, they do provide sufficient evidence that removing in vitro estrogen findings from the present manuscript would be scientifically appropriate.

We propose that RT-qPCR data from estrogen skewing experiments be removed, and that the manuscript be revised to state that although we have demonstrated that the immune response is sexually dimorphic in L-CNV, the precise molecular underpinnings are yet to be determined.

REFERENCES

1. Villa A, Rizzi N, Vegeto E, Ciana P, Maggi A. Estrogen accelerates the resolution of inflammation in macrophagic cells. *Sci Rep*. 2015;5:15224. doi: 10.1038/srep15224
2. Voigt AP, Mullin NK, Mulfaul K, Lozano LP, Wiley LA, Flamme-Wiese MJ, Boese EA, Han IC, Scheetz TE, Stone EM, et al. Choroidal endothelial and macrophage gene expression in atrophic and neovascular macular degeneration. *Hum Mol Genet*. 2022;31:2406-2423. doi: 10.1093/hmg/ddac043

Final Author's Note

On December 4 2025, we were issued the decision of "Declined for Publication - Encourage Resubmission after Revisions" or alternatively to submit our work for consideration by another MDPI journal, as described below by the editorial office:

Your paper could be transferred to another of our SCIE-indexed journals, Current Issues in Molecular Biology. We believe your manuscript aligns well with the scope of this journal and would reach a suitable readership. CIMB is an SCIE-indexed open-access journal with an Impact Factor of 2.081. The article processing charge is CHF 1600 per paper. Manuscripts undergo peer review, with a median time to first decision of approximately 17.8 days and a median acceptance-to-publication period of 2.7 days.

If you agree, you may resubmit your manuscript directly to CIMB. Upon receipt, processing will begin immediately. Reviews will be collected within *two weeks* at the latest, and provided revisions proceed smoothly, publication can be expected *within one month* This approach should help minimize any disadvantage resulting from the earlier delay.

We greatly value the time and scholarly contributions of every researcher, and we sincerely appreciate the effort you have invested in this work. Should you wish to proceed with resubmission, please let me know at your earliest convenience.

We advised that we would not be submitting the work for any further consideration by either journal.